MIMO EQUALIZATION

JERRY GEORGE MATHEW

Submitted in fulfillment of the academic requirements
for the degree of MSc Eng
in the School of Electrical, Electronic and Computer Engineering
at the University of Kwazulu Natal, Durban, South Africa

25 November 2005

ABSTRACT

In recent years, space-time block codes (STBC) for multi-antenna wireless systems have emerged as attractive encoding schemes for wireless communications. These codes provide full diversity gain and achieve good performance with simple receiver structures without the additional increase in bandwidth or power requirements. When implemented over broadband channels, STBCs can be combined with orthogonal frequency division multiplexing (OFDM) or single carrier frequency domain (SC-FD) transmission schemes to achieve multi-path diversity and to decouple the broadband frequency selective channel into independent flat fading channels.

This dissertation focuses on the SC-FD transmission schemes that exploit the STBC structure to provide computationally cost efficient receivers in terms of equalization and channel estimation. The main contributions in this dissertation are as follows:

- The original SC-FD STBC receiver that bench marks STBC in a frequency selective channel is limited to coherent detection where the knowledge of the channel state information (CSI) is assumed at the receiver. We extend this receiver to a multiple access system. Through analysis and simulations we prove that the extended system does not incur any performance penalty. This key result implies that the SC-FD STBC scheme is suitable for multiple-user systems where higher data rates are possible.

- The problem of channel estimation is considered in a time and frequency selective environment. The existing receiver is based on a recursive least squares (RLS) adaptive algorithm and provides joint equalization and interference suppression. We utilize a system with perfect channel state information (CSI) to show from simulations how various design parameters for the RLS algorithm can be selected in order to get near perfect CSI performance.

- The RLS receiver has two modes of operation viz. training mode and direct decision mode. In training mode, a block of known symbols is used to make the initial estimate. To ensure convergence of the algorithm a re-training interval must be predefined. This results in an increase in the system overhead. A linear predictor

that utilizes the knowledge of the autocorrelation function for a Rayleigh fading channel is developed. The predictor is combined with the adaptive receiver to provide a bandwidth efficient receiver by decreasing the training block size. The simulation results show that the performance penalty for the new system is negligible.

- Finally, a new Q-R based receiver is developed to provide a more robust solution to the RLS adaptive receiver. The simulation results clearly show that the new receiver outperforms the RLS based receiver at higher Doppler frequencies, where rapid channel variations result in numerical instability of the RLS algorithm. The linear predictor is also added to the new receiver which results in a more robust and bandwidth efficient receiver.

PREFACE

The research work presented in this dissertation was performed by Jerry George Mathew, under the supervision of Dr. H. Xu, at the University of Kwazulu Natal's School of Electrical, Electronic and Computer Engineering, in the Centre of Radio Access Technologies. This work was partially sponsored by Telkom South Africa Ltd and Alcatel as part of the Centre of Excellence programme.

Parts of this dissertation have been presented at the ICT and SATNAC conferences and submitted to the IEE Proceedings on Communications.

The entire dissertation, unless otherwise indicated, is the author's work and has not been submitted in part, or in whole, to any other Universities for degree purposes.

ACKNOWLEDGEMENTS

I would like to thank my supervisor, Dr. H. Xu, for his excellent supervision and support throughout the course of my research work. His patience, advice and guidance are very much appreciated and have directly contributed to the completion of this dissertation. I would also like to thank Prof. F. Takawira for his guidance and helpful discussions.

I am greatly indebted to my parents and my brother for their constant support and encouragement. They are the source of my inspiration and have been instrumental in my pursuit of higher education.

I am also grateful for the financial support received from Telkom SA Ltd and Alcatel S.A. during my M.Sc. I would like to thank all my friends for making my stay at university a truly memorable one. Finally I would like to thank the one would taught me the best and most beautiful things in the world can not be seen, nor touched but are felt in the heart. No matter what happens in the future, I will not cry because it is over but rather smile because it happened. What happened is that I met you and I will cherish this forever.

TABLE OF CONTENTS

Abstract i

Preface iii

Acknowledgements iv

Table of Contents v

List of Figures viii

List of Acronyms ix

1. Introduction 1

1.1 General 1

1.2 Notations 4

1.3 Data Transmission Model 4

1.4 Channel Model 5

1.5 Space Time Block Codes 6

1.5.1 Maximum Likelihood Detector 8

1.5.2 Minimum Mean-Square Error Detector 9

1.5.3 Advantages of the Alamouti Code 9

1.6 Channel Estimation 9

1.7 Overview of Equalization Schemes for Space Time Block Codes in Frequency Selective Channels 11

1.7.1 Time reversal Space Time Block Code 11

1.7.2 Orthogonal Frequency Division Multiplexed Space Time Block Code . 12

1.7.3 Single Carrier Frequency Domain Equalized Space Time Block Code . 13

1.8 Motivation for Research 13

1.9 Outline 16

1.10 Original Contribution 16

2. Single-carrier Space time block codes in Multiple Access Systems 19

2.1 Introduction 19

2.2 Cyclic Prefix Transmission 20

2.3 Input-Output Model for the Multiple Access System 22

2.4 Overview of Single Carrier Schemes in Rich Scattering Environments 26

2.4.1 CP-Only Transmission 26

2.4.2 Linearly Precoded Cyclic Prefix (LP-CP) 26

2.4.3 Affine Precoded Cyclic Prefix (AP-CP) 27

2.4.4 Zero Padding Only 27
2.5 Equalization and Decoding 27
2.6 Performance Analysis 30
2.7 Simulation Results 32
2.8 Concluding Remarks 34
3. RLS Based Adaptive Reciever for Joint Equalization and Interference Suppression 35
3.1 Introduction 35
3.2 Single User Transmission 37
3.3 Adaptive Implementation 39
3.4 Simulation Environment 43
3.5 Simulation Results 44
3.5.1 The Effect of Doppler Frequency 45
3.5.2 The Effect of Re-training Interval and Block Size 46
3.5.3 The Effect of the Forgetting Factor 47
3.6 Concluding Remarks 48
4. A New Linear Prediction Based RLS Receiver for Better Performance 49
4.1 Introduction 49
4.2 Overview of Prediction Algorithms 50
4.3 Overview of Linear Prediction 51
4.3.1 Preliminary Definitions 51
4.3.2 Optimal MMSE Forward Linear Prediction 53
4.4 Continuous Time Channel Model 53
4.5 Applying Linear Prediction to the RLS Algorithm 54
4.6 Simulation Results 57
4.6.1 Performance Penalty 57
4.6.2 Performance Using Equivalent Pilot Symbols 58
4.7 Concluding Remarks 59
5. QR-based receiver with Linear prediction for more Robust and Improved Performance 60
5.1 Introduction 60
5.2 Overview of Adaptive Algorithms 62
5.3 Important Properties of QR Decomposition 64
5.4 The Givens Rotation Algorithm 65

5.5 Modified QRD-based receiver 68
5.5.1 QRD receiver 68
5.5.2 QRD receiver with LP 71
5.6 Simulation Results 73
5.6.1 Performance at High Doppler Frequency 73
5.6.2 Tracking and Estimation Error Performance 74
5.6.3 Performance of the QRD-LP 75
5.7 Concluding Remarks 77
6. Conclusion 78
6.1 Concluding Remarks 78
6.2 Future work 80
Appendix A Circulant Matrices Properties 82
Appendix B An Example of the Givens Rotation 83
References 85

LIST OF FIGURES

Fig. 1.1 Data transmission model 4
Fig. 1.2 Equivalent baseband model 5
Fig. 1.3 Tap delay line model for a frequency selective channel 6
Fig. 1.4 Two transmit and one receive antenna system 7
Fig. 1.5 Block diagram for the Alamouti scheme 8
Fig. 1.6 Blind Channel estimation problem 10
Fig. 2.1 Overall single-carrier STBC transceiver model for a single user 23
Fig. 2.2 Cyclic prefix Transmission 24
Fig. 2.3 Two-user system configuration 25
Fig. 2.4 Performance comparison for the single user and two user scenarios 33
Fig. 3.1 Block diagram for the single user adaptive receiver with two-transmit one-receive antennas 39
Fig. 3.2 Equivalent CIR for a TU channel with GMSK pulse shaping 43
Fig. 3.3 Effect of Doppler frequency on the performance of RLS algorithm. 45
Fig. 3.4 Effect of block size and re-training interval 46
Fig. 3.5 Effect of forgetting factor 47
Fig. 4.1 Comparison of performance penalty with the linear predictor 57
Fig. 4.2 Performance of the linear predictor with equivalent number of pilot symbols. 58
Fig. 5.1 Equivalent receiver model with the QRD 71
Fig. 5.2 Equivalent receiver model with the QRD and LP 72
Fig. 5.3 Simulation results to verify the robust property of the QRD algorithm 73
Fig. 5.4 Simulation results of the QRD and RLS algorithms for different Doppler frequencies 74
Fig. 5.5 Comparison of QRD and QRD with LP at 60 Hz 76
Fig. 5.6 Overall modified QRD-LP receiver versus RLS receiver 77

LIST OF ACRONYMS

2G	Second Generation
3G	Third Generation
AP-CP	Affine Precoded Cyclic Prefix
ASK	Amplitude Shift Keying
AWGN	Additive White Gaussian Noise
BER	Bit Error Rate
CDMA	Code Division Multiple Access
CIBS CDMA	Chip Interleaved Block Spread Code Division Multiple Access
CIR	Channel Impulse Response
CORDIAC	Coordinate Rotation Digital Computation
CP	Cyclic Prefix
CSI	Channel State Information
DS CDMA	Direct Sequence Code Division Multiple Access
EDGE	Enhanced Data rates for Global Evolution
ERLS	Extended Recursive Least Squares algorithm
FDMA	Frequency Division Multiple Access
FER	Frame Error Rate
FFT	Fast Fourier Transform
FIR	Finite Impulse Response
FSK	Frequency Shift Keying

GMSK	Gaussian Minimum Shift Keying
GSM	Global System for Mobile Communication
IBI	Inter-Block Interference
ICI	Inter-Chip Interference
i.i.d.	Independent and Identically Distributed
IFFT	Inverse Fast Fourier Transform
IEEE	Institute of Electrical and Electronic Engineers
ISI	Inter-Symbol Interference
LMS	Least Mean Square
LP	Linear Prediction
LP-CP	Linearly Precoded Cyclic Prefix
MC-CDMA	Multi-Carrier Code Division Multiple Access
MIMO	Multiple Input Multiple Output
ML	Maximum likelihood
MMSE	Minimum Mean Squared Error
MUI	Multiple User Interference
OFDM	Orthogonal Frequency Division Multiplexing
OFDMA	Orthogonal Frequency Division Multiple Access
PAR	Peak to Average Power Ratio
PN	Pseudo-random Codes
PSK	Phase Shift Keying
QOS	Quality Of Service

QRD	QR based Decomposition
QRDLP	QR Decomposition with Linear Prediction
QR-RLS	QR based Recursive Least Squares Algorithm
RLS	Recursive Least Squares
SC FDE	Single Carrier Frequency Domain Equalizer
SISO	Soft-Input Soft-Output
SNR	Signal to Noise Ratio
STBC	Space Time Block Coding
SVD	Singular Value Decompostion
TDMA	Time Division Multiple Access
TR	Time Reversal
TU	Typical Urban
UMTS	Universal Mobile Telecommunications System
WCDMA	Wideband Code Division Multiple Access
WLAN	Wireless Local Area Network
ZP	Zero Padding

CHAPTER 1

INTRODUCTION

1.1 General

Wireless communication has emerged as one of the most active areas in research for the simple reason that today it covers a wide array of applications. Some of these include wireless sensor networks, high speed wireless internet and video transmission over wireless channels. The demand for higher information capacity in these and other similar applications has motivated the use of broadband wireless channels in order to provide wider bandwidth and higher data rates. In addition, multi-user communication schemes are also employed in order to allow users to share the same physical channel thereby contributing to even higher data rates.

The main areas of research that have been involved in increasing the data rate of a communications system are:

- Coding
- Multi-user detection
- Space-time processing

The recent 3rd generation (3G) standard provides support for a number of these new techniques. These include the following:

- Turbo codes: These error correcting codes [45] use the idea of parallel concatenation of simple codes to define powerful error correction mechanisms. The performance improves as one repeatedly iterates the decoder.

- Multi-user detection: This is theoretically superior to co-channel suppression or cancellation techniques [14], and can increase capacity considerably. In particular, the pilot signals on the code division multiple access (CDMA) uplink enable fairly sophisticated multi-user detection at the base-station.

- Space-time processing: Various techniques include spatial multiplexing [47], the use of the so called smart antennas [46] and space time coding, have been developed.

This dissertation focuses on the use of space time coding to improve the data rate of the communication systems. Space time coding is a key part of research that involves the development of efficient signal transmission techniques and advanced receiver structures that result in an increase in wireless capacity without the additional increase in bandwidth or power requirements. The challenge that limits the performance of such multi-user communication systems is the distortion that is introduced by the coupled communication channels in the form of fading conditions, inter-symbol interference (ISI), inter-user interference, and noise. Another challenge is the increasing complexity of the receiver due to the large number of users and the long impulse response of wideband or frequency selective channels. Hence the previous flat or narrowband channel model does not hold for many current and next generation wireless applications.

Direct sequence code division multiple access (DS-CDMA) has emerged as the dominant multiple access technique in 3G cellular networks. During DS-CDMA downlink, the frequency selective channel may destroy the orthogonality of user signals and hence induce severe multi-user interference (MUI). Space time block code (STBC) [1] has been introduced in the wideband CDMA (WCDMA) and CDMA2000 standards. However, these codes were designed assuming a narrowband channel model. Therefore, space-time equalization becomes imperative in order to combat the ISI and MUI that results from the frequency selective channel.

Two good examples where multi-user MIMO communications are used are wireless local area networks (WLANs) and cellular telephony, where a single base station must communicate with many users simultaneously. WLANs are well suited for MIMO technology because of the rich multipath environment in which they are usually deployed. This is an important criterion for achieving high capacity. In such applications, the user mobility may be regarded as very slow, and the channel may be regarded as quasi-static. However, cellular telephone applications are more challenging due to the high user mobility and restrictions on the cost and size of the mobile device.

Hence, in addition, the mobility of the users may cause the channel impulse response (CIR) to vary rapidly. The channel in this case becomes a time-selective channel and the equalization problem becomes an even more challenging one. In effect, joint channel estimation, equalization and interference suppression is required at the receiver.

Under such conditions, transmission schemes that exploit spatial diversity and enable reliable transmission at high data rates become desirable. Among the promising encoding schemes for such scenarios are space-time block codes (STBC) [1] for multi-antenna wireless systems. These codes provide full diversity gains and achieve good performance with simple receiver structures without the additional increase in bandwidth or power requirements.

When implemented over broadband channels, STBCs can be combined with orthogonal frequency division multiplexing (OFDM) or single carrier frequency domain (SC-FD) transmission schemes to achieve multi-path diversity and to decouple the broadband frequency selective channel into independent flat channels. Although OFDM has become the technique of choice for many high-data rate wireless applications, OFDM systems are multi-carrier systems and hence have several disadvantages such as sensitivity to carrier frequency offset and higher computational complexity, as opposed to its single carrier counter part. In this dissertation we focus on the SC-FD scheme combined with STBC in order to provide a transmission scheme that exploits the unique STBC structure to preserve orthogonality and suppress ISI and MUI.

The rest of this chapter is organized as follows. Sections 1.3 and 1.4 provide a brief description of the data transmission model and channel model for the communications link that are used throughout this dissertation. We then cover the basics of STBC (Alamouti scheme) for narrowband channels in section 1.4. A key assumption made in most multi-user systems is the availability of the channel state information (CSI) at the receiver. An overview of various channel estimation techniques used to estimate the CSI is given in section 1.6. An overview of the different equalization techniques used for STBC in frequency selective channels is given in section 1.7. Finally we provide the motivation for our research and outline in sections 1.8 and 1.9, respectively.

1.2 Notations

The following notations are used for the rest of this dissertation. Upper case letters denote matrices, lower case letters stand for column vectors; $(\cdot)^*$, $(\cdot)^T$ and $(\cdot)^H$ represent conjugate, transpose and Hermitian, respectively; $E[\cdot]$ stands for expectation and $\mathbf{I}_N$ denotes an identity matrix of size $N \times N$. $\mathbf{F}_N$ is for an $N \times N$ discrete fourier transform (DFT) matrix. $\|\bullet\|$ denotes the Euclidean norm and cond$(\cdot)$ stands for condition number. $O(n)$ denotes the order of n multiplications. $\mathrm{Re}\{\bullet\}$ stands for the real part of the term.

1.3 Data Transmission Model

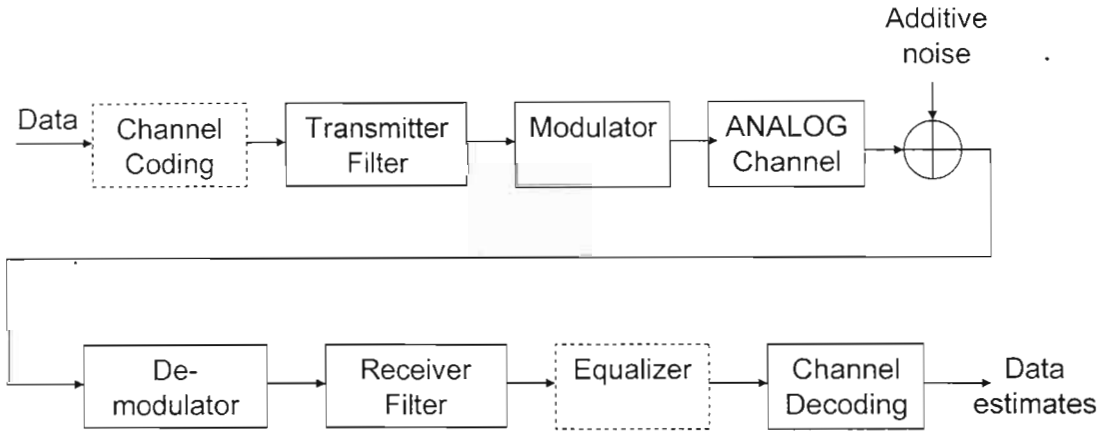

Fig. 1.1 Data transmission model

Some basic elements that are found in a data transmission system is shown in Fig. 1.1. To ensure reliable transmission, channel coding which introduces some controlled redundancy to the data, is performed on the data sequence. The coded data is then fed into the transmit filter to yield an analog signal for baseband transmission. The modulator moves the signal to a desired pass band using a predefined constellation. These include amplitude shift keying (ASK), phase shift keying (PSK) and frequency shift keying (FSK).

The passband signal is then transmitted over the channel. In wireless channels, typical problems include multipath propagation and both frequency and time selective fading, with rapid time-varying characteristics. More details of the channel model are given in

the next section. At the receiver, after demodulation and matched filtering, the channel decoder is used to provide estimates of the data sent.

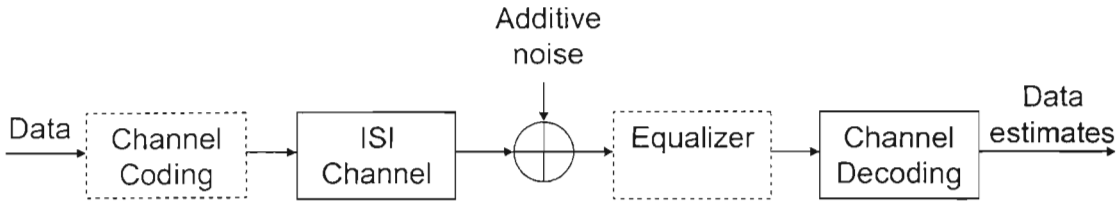

Fig. 1.2 Equivalent baseband model

For the remainder of this thesis, the discrete time baseband representation, shown in Fig. 1.2 is used. The channel coding and decoding blocks are taken without change from the analog scheme. The remaining blocks are combined into a equivalent, discrete-time, baseband ISI channel specified by a discrete-time impulse response.

1.4 Channel Model

When the doppler spread between multi-paths of a channel exceed the symbol duration of the data, the channel experiences time selective fading. The channel experiences frequency selective fading when the coherent bandwidth of the channel is smaller than the symbol bandwidth. Inter-symbol interference (ISI) is the distortion that results from frequency selective fading while rapid variation of channel conditions is the result of time-selective fading. Throughout this thesis, the time selective fading is modelled using the well known Jakes model [18]. The fading process $x[n]$ using the sum of sinusoids method is represented as [18,26]

$$x[n] = \sum_{i=1}^{N_s} c_i e^{-j(2\pi f_{D_i} n + \theta_i)}, \tag{1.1}$$

where $1 \le i \le N_s$, N_s is the total number of sinusoids, f_{D_i} is the normalized Doppler frequency and θ_i is the phase offset.

The ISI channel is modelled as a finite impulse response (FIR) filter. The received sequence , r_n , is given by

$$r_n = \sum_{k=0}^{L-1} h_k y_{n-k} + w_n. \tag{1.2}$$

In (1.2), h_k are the tap coefficients, L is the channel memory (length of the FIR), y_{n-k} is the transmitted sequence and w_n is the additive white Gaussian noise (AWGN). The above expression clearly shows that the received symbol at time n is a linear combination of $L+1$ transmitted symbols which represent the ISI effect. Hence ISI results when the channel is frequency selective.

The overall tap delay line model is shown is Fig. 1.3. The D elements represent the delay components of the channel. In the 2.5G (EDGE) standard, the transmit filter shown in Fig.1.1 is essentially a Gaussian minimum shift key (GMSK) filter. In order to model the channel for this standard, the overall channel impulse response is pulse shaped with the GMSK filter. This model is described in chapter 3, section 3.4.

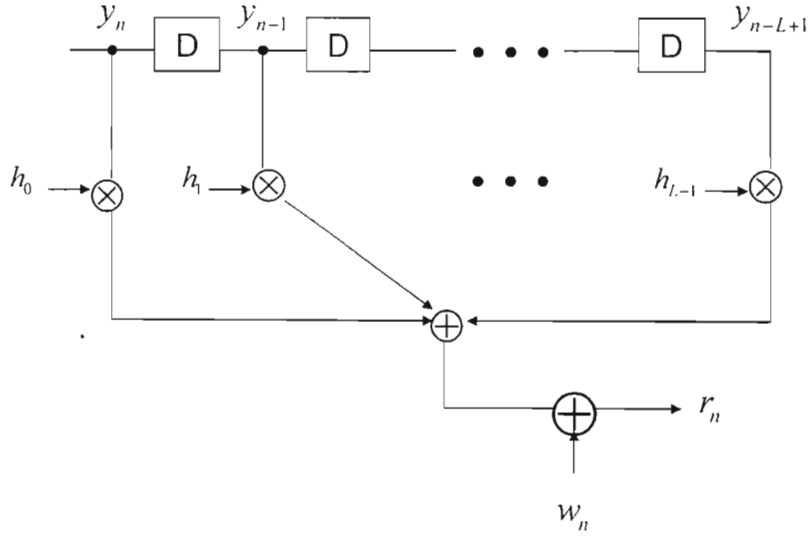

Fig. 1.3 Tap delay line model for a frequency selective channel

1.5 Space Time Block Codes

Consider the block transmission defined for K symbols $x = (x_1 \quad x_2 \quad \cdots \quad x_K)^T$. The column vector x is fed into a predefined block encoder that generates a matrix X containing the coded symbols. Hence, in general the size of X is $M_t \times N$ which means that the K symbols are transmitted over N time intervals from M_t transmit antennas. The code rate is defined as

$$R = \frac{K}{N} \tag{1.3}$$

Smaller code rate implies increased system overhead and hence reduced overall transmission rate. When $K = N$, we have a full-rate code. The Alamouti code [1] is a full rate code.

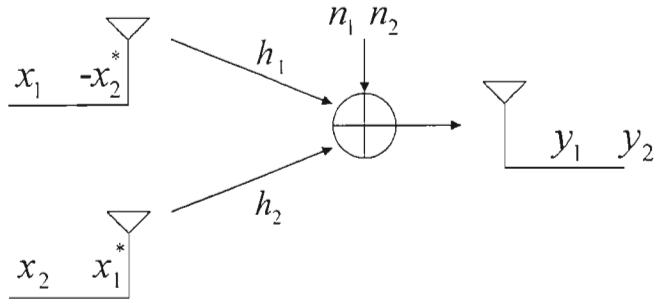

Fig. 1.4 Two transmit and one receive antenna system

An instance of this code is shown in in Fig. 1.4. The transmitter is equipped with two antennas and the receiver has one antenna. For this case, the Alamouti scheme is defined as

$$\begin{bmatrix} x_1 & -x_2^* \\ x_2 & x_1^* \end{bmatrix}_{\rightarrow Time}^{\downarrow Antenna} . \tag{1.4}$$

Under the assumption that the channel is quasi-static (i.e it is fixed for two consecutive symbol periods) the received sequence is given by

$$y = \begin{bmatrix} y_1 \\ y_2 \end{bmatrix} = \begin{bmatrix} x_1 & x_2 \\ -x_2^* & x_1^* \end{bmatrix} \begin{bmatrix} h_1 \\ h_2 \end{bmatrix} + \begin{bmatrix} n_1 \\ n_2 \end{bmatrix} = Xh + n, \tag{1.5}$$

where $X = \begin{bmatrix} x_1 & x_2 ; -x_2^* & x_1^* \end{bmatrix}$, $h = \begin{bmatrix} h_1 & h_2 \end{bmatrix}^T$, and $n = \begin{bmatrix} n_1 & n_2 \end{bmatrix}^T$. By conjugating the second term we can write the received sequence in terms of the data vector. Hence we have

$$\bar{y} = \begin{bmatrix} y_1 \\ -y_2^* \end{bmatrix} = \begin{bmatrix} h_1 & h_2 \\ -h_2^* & h_1^* \end{bmatrix} \begin{bmatrix} x_1 \\ x_2 \end{bmatrix} + \begin{bmatrix} n_1 \\ n_2^* \end{bmatrix} = Hx + \bar{n}, \tag{1.6}$$

where $H = \begin{bmatrix} h_1 & h_2 ; -h_2^* & h_1^* \end{bmatrix}$, $x = \begin{bmatrix} x_1 & x_2 \end{bmatrix}^T$ and $\bar{n} = \begin{bmatrix} n_1 & n_2 \end{bmatrix}^T$.

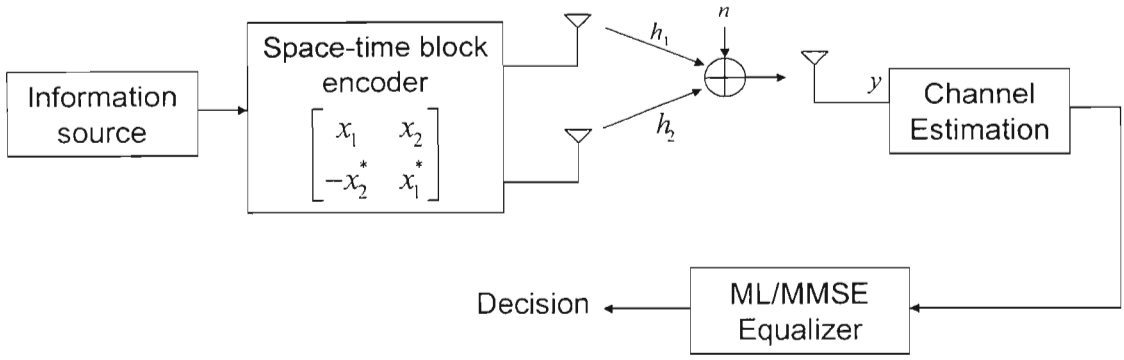

Fig. 1.5 Block diagram for the Alamouti scheme

The overall block diagram for the Alamouti scheme is shown in Fig. 1.5. The availability of the channel knowledge is assumed by the equalizer. The equalizer uses this knowledge to estimate the transmitted symbols. A brief overview of the various channel estimation techniques is given in the section 1.6. Two commonly used single input single out (SISO) equalizers are described next.

1.5.1 Maximum Likelihood Detector

Multiplying the received vector $\bar{y}$ in (1.6) by H^H from the left results in

$$\begin{aligned} z &= \begin{bmatrix} z_1 \\ z_2 \end{bmatrix} = H^H \bar{y} \\ &= \begin{bmatrix} |h_1|^2 + |h_2|^2 & 0 \\ 0 & |h_1|^2 + |h_2|^2 \end{bmatrix} x + H^H \bar{n} \\ &= \alpha x + n', \end{aligned} \tag{1.7}$$

where we let $\alpha = \left[|h_1|^2 + |h_2|^2 \quad 0;0 \quad |h_1|^2 + |h_2|^2 \right]$ and $n' = H^H \bar{n}$. From [1], the maximum likelihood (ML) detector with constant energy per symbol (PSK transmission) is given by

$$\begin{aligned} \tilde{x}_1 &= \min_{x_1} \left\{ |z_1 + x_1|^2 \right\}, \\ \tilde{x}_2 &= \min_{x_2} \left\{ |z_2 + x_2|^2 \right\}. \end{aligned} \tag{1.8}$$

1.5.2 Minimum Mean-Square Error Detector

Using the linearly combined version of the received sequence in (1.6), the mean square error estimates of x are given by [24]

$$\begin{aligned}\hat{x} &= \left(H^* H + \frac{1}{SNR}\mathbf{I}_2 \right)^{-1} H^* \tilde{y}, \\ &= \frac{1}{|h_1|^2 + |h_2|^2 + 1/SNR}\mathbf{I}_2 H^* \tilde{y},\end{aligned} \tag{1.9}$$

where SNR denotes the signal to noise ratio defined as σ_w / σ_s with σ_w and σ_s representing the noise and signal covariance, respectively. The output is then applied to a slicer that maps the output of minimum mean square error (MMSE) detector to the closest constellation point.

1.5.3 Advantages of the Alamouti Code

The key advantages of the Alamouti scheme are as follows:

- It achieves full spatial diversity at full transmission rate.
- This scheme does not require the knowledge of the channel state information (CSI) at the transmitter.
- The Alamouti scheme caters for ML or MMSE equalization which requires only simple linear processing at the receiver due to the orthogonal structure. This makes this scheme ideal for implementation in mobile terminals of wireless networks.

One drawback of that the Alamouti scheme has over schemes such as space time trellis coding (STTC) is that it does not provide any coding gain due to the absence of memory in these codes.

1.6 Channel Estimation

Channel estimation is defined as the process of characterising the effect that the physical channel has on the input sequence. The channel estimation algorithms that

have been proposed in the literature can be classified into three main categories: training, semi-blind and blind methods.

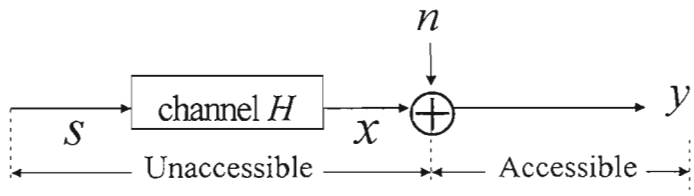

Fig. 1.6 Blind Channel estimation problem

Blind channel estimation implies that the problem only has the observation signal, y, available for processing and estimation of channel H. This is shown in Fig. 1.6. Blind techniques do not use training data, but instead they use certain prior information that is inherent in the original strings of the data symbols. The process of blindly estimating the channel rests on the exploitation of structures of the channel and properties of the input. The typical assumption made in blind techniques is that the input has known probabilistic description such as distribution and moments [39].

Conventional receivers use training sequences embedded in each block to estimate the CSI. The common pilot channel (CPICH) in 3G systems is an example of this [40,13]. However, the addition of training sequences decreases the overall throughput.

Pure blind channel estimation algorithms that are proposed [41,42,43] have high complexity and the performance penalty compared to training based receivers is significant.

Semi-blind methods are a combination of existing training and blind methods that aim to estimate the channel using not only the known data in the transmitted signal and its corresponding observation, but also the observation of the unknown transmitted signal. Semi-blind channel estimation is motivated by the fact that in modern communication systems there are known pilot symbols that can be used to improve the performance of the channel estimation algorithm. Semi-blind channel estimation has also attracted attention due to the need for fast and efficient channel estimation algorithms. In most cases, a weighted linear combination of the cost function for the blind and training-based channel estimation algorithms are used to form the optimisation function of the

semi-blind method. Examples of semi-blind adaptive algorithms include least mean squares (LMS), recursive least squares (RLS) and lattice based algorithms. We will now give a survey of the various equalization schemes that are available for STBC in frequency selective channels.

1.7 Overview of Equalization Schemes for Space Time Block Codes in Frequency Selective Channels

There are three main joint equalization and decoding schemes. These are

- Time reversal STBC (TR-STBC).
- Orthogonal frequency division multiplexed STBC (OFDM-STBC).
- Single carrier frequency domain equalized based STBC (SC-FDE-STBC)

A detailed overview of various equalization schemes for space-time coded signals is presented in [17]. For the descriptions to follow, we consider the case of two transmit antennas and one receive antenna.

1.7.1 Time reversal Space Time Block Code

TR-STBC, introduced in [3], is effectively an extension of the Alamouti STBC scheme to frequency selective channels by imposing the orthogonal structure at a block level and not symbol level. The transmitted blocks from antenna 1 and 2 at time $k+1$ is generated by the following encoding rule.

$$\begin{aligned} x_1^{(k+1)} &= -J \cdot x_2^{*(K)}, \\ x_2^{(k+1)} &= -J \cdot x_1^{*(K)}. \end{aligned} \tag{1.10}$$

J is the time reversal matrix that consists of ones in its main anti-diagonal and zeros everywhere else. To eliminate inter-block interference (IBI), adjacent blocks are guarded by the all-zero guard sequence with length equal to the length of the channel. At the receiver end, TR-STBC employs linear combination techniques to eliminate the mutual interference between the two transmit antennas.

Essentially, TR-STBC uses complex conjugate, time reversal and matched filtering operations to convert the two input single output channel into two equivalent SISO channels. The equivalent SISO channel is given by

$$h_{eq} = h_1(D)h_1^*(D^{-1}) + h_2(D)h_2^*(D^{-1}). \tag{1.11}$$

Standard SISO equalization techniques can now be applied. The major disadvantages of this scheme are as follows:

- Maximum multipath diversity is not ensured.
- This scheme does not handle the IBI at the beginning and end of each block burst.

We will now describe two other alternative schemes.

1.7.2 Orthogonal Frequency Division Multiplexed Space Time Block Code

In OFDM, the high-rate input stream is demultiplexed and transmitted over N low-rate independent frequency sub carriers, with N representing the block size of the transmitted data.

In order to eliminate IBI, a guard sequence that is equal to the length of the channel is added. This ensures that the individual subcarriers are isolated at the receiver. The most commonly used guard sequence is the cyclic prefix (CP) which reduces the channel matrix to a circulant channel matrix [46]. The circulant matrix can be diagonalized by the DFT operation. OFDM possesses the advantage of having flexibility since multiple signals at different rates and quality of service (QOS) requirements can be transmitted over parallel frequency sub carriers.

However, there are two main drawbacks of OFDM, namely:

- A high peak to average rate (PAR) which results in large backoff with non-linear amplifiers.
- High sensitivity to frequency offset and phase noise.

1.7.3 Single Carrier Frequency Domain Equalized Space Time Block Code

The main difference between the SC-FDE and its OFDM counter part is that the IDFT block is moved to the receiver end and placed before the decision device. This causes the deep nulls in the channel frequency response to spread out over all symbol periods, hence improving the overall performance. Due to this added advantage, the SC-FDE is pursued as the option for equalization in this dissertation. Furthermore, when combined with CP transmission, the IBI is effectively removed. In [5], it is proven that the SC-FDE STBC achieves maximum diversity order. Detailed description of the SC-FDE is given in chapter 2.

1.8 Motivation for Research

Code Division Multiple Access (CDMA) was established as a promising alternative to Time and Frequency Division Multiple Access (TDMA, FDMA) [32]. On the other hand in the case of high performance CDMA systems, there are major challenges that limit the bit error rate (BER) performance, capacity and throughput. These include multi-user interference (MUI), time-selective and frequency-selective fading and multi-path propagation.

The current CDMA systems rely on long a-periodic pseudo-random (PN) codes with strict power control to restrict MUI. The MUI suppression capability of these systems is limited by the number of interfering users. However, in the case of Direct-Sequence (DS) CDMA, proposals with symbol-periodic short spreading codes relax the need for strict power control. The disadvantage with this is the requirement of high-complexity MUI cancellers that are less affordable at the mobile unit downlink. Hence, unless bandwidth is sacrificed, performance degradation is experienced by high-mobility and high data transmission users due to time and frequency selective fading.

Multistage demodulators [34], decision-feedback receivers [35], and adaptive detectors [36] offer useful alternatives to the highly complex ML receivers in the absence of multipath. At higher frequencies, the accentuated frequency-selectivity induces inter-chip interference (ICI).

Initial efforts in trying to solve this problem were proposed in [37], [38] and [39]. However these schemes require the knowledge of the multipath channels for all users and suppress MUI statically even when the prefect channel state information (CSI) is available at the receiver.

Multi-carrier (MC-CDMA) multi-user schemes (Orthogonal Frequency Division Multiple Access (OFDMA) systems) [40, 41] suppress MUI due to the user specific orthogonal sub-carrier codes that retain their orthogonality regardless of the multipath. However, symbol recovery is not assured due to the sensitivity to phase and carrier offset. Furthermore, MC-CDMA schemes are not power-efficient because their transmissions are not constant modulus.

Due to the limitations of the existing DS and MC multi-user transmission schemes, a new multiple access scheme over frequency-selective and time-selective channels that arises at high date rates and high mobility, respectively, is desired.

The chip-interleaved block-spread (CIBS) CDMA proposed in [33] relies on spreading a block of symbols with long yet structured and deterministic user codes. This can be viewed as block-spread transmissions with chip-interleaved symbols spread by short codes. This scheme is simple with transceivers involving interleavers and low-complexity matched filters. Furthermore it offers flexibility as it can revert to DS-CDMA, TDMA and FDMA.

The CIBS-CDMA can be enhanced with advanced space-time coding to benefit from the extra spatial diversity gains offered by multiple transmit antennas. This becomes particularly useful during downlink were multiple antennas are deployed at the base station instead of the low cost mobile unit.

Space time block code (STBC), which was first introduced in [1] and later generalized in [2], has been an attractive MIMO technique due to its simple linear processing at the receiver. The scheme in [1] is designed for frequency flat channels. STBC DS-CDMA downlink schemes have been proposed for UMTS and IS-2000 W-CDMA standards. However these schemes do not enable the maximum multi-antenna and multi-path diversity [39].

In order to extend STBC to broad-band wireless applications, such a scheme had to be designed in the presence of frequency-selective multi-path channels. Improved versions of this scheme are developed with the time reversal space time block code (TR-STBC) in [3], and the single carrier space time block-coded transmission (SC-STBC) in [4], [5] and [7]. In [5] the proposed SC-STBC achieves full antenna and multipath diversity while handling edge effects by zero post-fix unlike the schemes provided in [3] and [7]. The scheme in [7] provides a novel transmission format that , for a single user system, achieves a maximum diversity order $N_t N_r (L+1)$ in rich scattering environments, where $N_t (N_r)$ is the number of transmit (receive) antennas and L is the order of the finite impulse response (FIR) channel. This scheme therefore bench marks performance and capacity over space time (ST) frequency-selective channels

In [38], [37] and [13], the DS-CDMA downlink scheme is combined with the SC-STBC scheme to enable maximum antenna and spatial diversity. The results in [13] show that the new proposed receiver out performs the Rake receiver that is currently deployed in the DS-CDMA systems.

Given the limited spectrum resource, multiple users sharing a common frequency selective channel becomes a very important option in order to efficiently use this resource. Therefore extending [7] for multiple users become an important task. Furthermore, the performance penalty of such an extension is an important issue.

The system presented in [7] assumes perfect knowledge of the channel. The case when the time and frequency selective channel is not available at the receiver is not discussed. Hence although [7] benchmarks STBC for frequency selective channels, performance with high-mobility and high data transmission users that results in time and frequency selective fading has not been properly evaluated.

Therefore conservation of bandwidth and the performance of the STBC system when the receiver does not have perfect channel state information are two key issues that must be resolved for such a receiver.

1.9 Outline

The focus of this thesis is on the SC-FD transmission schemes that exploit the STBC structure to provide computationally cost efficient receivers in terms of equalization and channel estimation. More specifically, in chapter 2 the original SC-FD STBC receiver is extended to a multiple access system. Through analysis and simulations we prove that the extended system does not incur any performance penalty. This key result therefore implies that this scheme is suitable for multiple-user systems with higher data rates.

In chapter 3, we look at the problem of channel estimation in a time and frequency selective environment. The existing receiver is based on a recursive least squares (RLS) adaptive algorithm that provides joint equalization and interference suppression [8]. Through computer simulations, we replicate the same results presented in [8] for various Doppler frequencies. We then utilize a system with perfect channel state information (CSI) and show from simulations how various design parameters for the RLS algorithm can be selected in order to get near perfect CSI performance. In Chapter 4, a linear predictor that uses the knowledge of the autocorrelation function of the channel is developed and combined with the adaptive receiver to provide a bandwidth efficient receiver. The simulation results provided shows that there is no performance loss.

Finally in chapter 5, a new Q-R based receiver is developed to provide a more numerically stable solution than the RLS adaptive receiver. The simulation results clearly show that the new receiver outperforms the RLS based receiver at higher Doppler frequencies.

1.10 Original Contribution

- The original SC-FD STBC receiver [7] is extended to a multiple access system in chapter 2, section 2.3. In the same chapter, through analysis in section 2.6 and simulations in section 2.7 we prove that the extended system does not incur any performance penalty.

- The problem of channel estimation is treated in a time and frequency selective environment. The existing receiver is based on a recursive least squares (RLS) adaptive algorithm and provides joint equalization and interference suppression. In chapter 3, section 3.5, we utilize a system with perfect channel state information (CSI) and show from simulations how various design parameters for the RLS algorithm can be selected in order to get near perfect CSI performance.

- The RLS receiver has two modes of operation viz. training mode and direct decision mode. In training mode, a block of known symbols is used to make the initial estimate. To prevent convergence of the algorithm a re-training interval must be predefined. This results in an increase in the system overhead. A linear predictor that utilizes the knowledge of the autocorrelation function for a Rayleigh fading channel is developed. In chapter 4, section 4.5, the predictor is combined with the adaptive receiver to provide a bandwidth efficient receiver by decreasing the training block size. In section 4.6.1 of the same chapter, the simulation results provided shows that the performance loss for the new system is negligible.

- Finally, a new Q-R based receiver is developed to provide a more robust solution to the RLS adaptive receiver in chapter 5, section 5.5.1. The simulation results in section 5.6 clearly show that the new receiver outperforms the RLS based receiver at higher Doppler frequencies, where rapid channel variations result in numerical instability of the RLS algorithm. The linear predictor is also added to the new receiver in section 5.5.2 which results in a more robust and bandwidth efficient receiver.

Parts of this research have been presented and submitted in the following conferences and journal:

- J. G. Mathew, H. Xu, F. Takawira, "Single Carrier Space Time Block Coded Transmission over frequency selective channels", in *Proc.* International Conference in Telecommunications (ICT), Capetown, 2005.

- J. G. Mathew, H. Xu, F. Takawira, "Low Complexity Adaptive Receivers for Joint Equalization and Interference Cancellation in Space-Time Block-Coded

Systems" in *Proc. SATNAC 2005*, Champagne Sports, Drakensberg, South Africa, Sept. 2005.

- J. G. Mathew, H. Xu, F. Takawira, "An Adaptive Receiver for STBC in Frequency Selective Channel with Improved Robustness and Pilot Requirements" submitted to IEEE Transactions on Vehicular Technology, 2006.

CHAPTER 2

SINGLE-CARRIER SPACE TIME BLOCK CODES IN MULTIPLE ACCESS SYSTEMS

2.1 Introduction

In an attempt to increase the data rate of communication systems, the bandwidth requirements have also increased. The frequency spectrum has become a scarce resource and hence efficient utilization of this resource is imperative. Given this limited resource, multiple users sharing a common frequency selective channel are considered in this chapter.

Multiple-input multiple-output (MIMO) systems have been proven to significantly increase the system capacity in rich scattering environments. Space time block code (STBC), which was first introduced in [1] and later generalized in [2], has been an attractive MIMO technique due to its simple linear processing at the receiver. The scheme proposed in [1] was designed for frequency flat channels. In order to extend STBC to broad-band wireless applications, such a scheme had to be designed in the presence of frequency-selective multipath channels. Therefore improved versions of this scheme were developed with the time reversal space time block code (TR-STBC) in [3], and the single carrier space time block-coded transmission (SC-STBC) in [4], [5] and [7]. In [5] the proposed SC-STBC achieves full antenna and multipath diversity while handling edge effects by zero post-fix unlike the schemes provided in [3] and [7]. This scheme therefore benchmarks performance and capacity over space time (ST) frequency-selective channels.

Extensions of the systems, described in [3] and [7] for multi-user transmission, are provided in [6] and [10], respectively. No performance analysis for the multi-user TR-STBC is given in [10]. It is shown in [6] that the multi-user system achieves the same diversity order as the single-user system. But the question left unanswered is "does any performance penalty in terms of signal-to-noise-ratio (SNR) incur due to multi-user interference?" Motivated by this question, we will derive the SNR for the SC-ST transmitter and receiver techniques over multi-user environments for the system

provided in [5]. The approach followed is similar to that shown in [6] for the time-reversed space-time technique. In a multi-user system each user is equipped with multiple transmit and receive antennas over a common multiple access channel. Such a system configuration is motivated by the need of efficient bandwidth utilization.

This chapter is organized as follows. Section 2.2 discusses the cyclic prefix (CP) transmission which eliminates the inter-symbol-interference (ISI) effect and induces a circulant channel structure. The circulant structure can be exploited at the receiver to great advantage as will be shown in the rest of the dissertation. In section 2.3 the input-output model for the single and multi-user scenarios are presented. Section 2.4 looks at the different single carrier transmission schemes that are available as shown in [5]. Section 2.5 details the equalization and decoding designs in an MMSE sense. In section 2.6, we show that the multiple user system incurs no performance penalty in terms of diversity and SNR when compared to the single user case. The simulation results are presented in section 2.6, while conclusions are drawn in Section 2.7.

2.2 Cyclic Prefix Transmission

The long impulse response sequence associated with frequency-selective channels results in ISI and hence degrades the system performance. To combat the ISI effects, equalization and extra symbols, known as cyclic prefix (CP), are used to decompose the frequency selective channel into independent flat channels. This reduces the required complexity of the equalizer.

Consider the data sequence $x(n)$ that is transmitted over a frequency selective channel $h=[h(0)\cdots h(L)]^T$, where L denotes the channel length. The received sequence $y(n)$ is given by the convolution sum

$$y(n)=\sum_{k=0}^{L} h(k)x(n-k)+w(n), \tag{2.1}$$

where $w(n)$ are the noise samples which are assumed zero mean Gaussian with white power spectrum. The above expression clearly shows that the received symbol at time n is a linear combination of $L+1$ transmitted symbols which represent the ISI effect. In

order to combat the ISI, the frequency-selective channel h is converted into parallel flat channels. By collecting R samples of the received sequence and ignoring the noise component, (2.1) can be re-written as

$$\begin{pmatrix} y(0) \\ \vdots \\ y(R-2) \\ y(R-1) \end{pmatrix} = \underbrace{\begin{pmatrix} h(L) & \cdots & h(0) & & & \\ & \ddots & \ddots & \ddots & & \\ & & h(L) & \cdots & h(0) & \\ & & & h(L) & \cdots & h(0) \end{pmatrix}}_{\mathrm{H}_T} \cdot \begin{pmatrix} x(-L) \\ \vdots \\ x(-1) \\ \hline x(0) \\ \vdots \\ x(R-2) \\ x(R-1) \end{pmatrix}, \tag{2.2}$$

where H_T, defined in (2.2), is the Toeplitz channel matrix of dimensions $R \times (R+L)$. We will now proceed to convert this Toeplitz structure to a circulant structure as the latter has very useful mathematical properties. If the symbols $\{x(-L), \cdots, x(-1)\}$ are replaced by $\{x(R-L), \cdots x(R-1)\}$, which represents CP insertion, then (2.2) reduces to

$$\begin{pmatrix} y(0) \\ \vdots \\ y(R-2) \\ y(R-1) \end{pmatrix} = \begin{pmatrix} h(0) & 0 & \cdots & h(L) & \cdots & h(1) \\ \vdots & \ddots & \ddots & \ddots & \ddots & \vdots \\ 0 & 0 & h(L) & \cdots & h(0) & 0 \\ 0 & 0 & 0 & h(L) & \cdots & h(0) \end{pmatrix} \cdot \begin{pmatrix} x(0) \\ \vdots \\ x(R-2) \\ x(R-1) \end{pmatrix}. \tag{2.3}$$

The CP given above falls under a special class known as linearly precoded CP only (LP – CP). The different types of CP insertions are discussed in section 2.4. The important result to be observed is that the channel matrix is now a $R \times R$ circulant matrix. We define this channel matrix as,

$$\tilde{\mathrm{H}} = \begin{pmatrix} h(0) & 0 & \cdots & h(L) & \cdots & h(1) \\ \vdots & \ddots & \ddots & \ddots & \ddots & \vdots \\ 0 & 0 & h(L) & \cdots & h(0) & 0 \\ 0 & 0 & 0 & h(L) & \cdots & h(0) \end{pmatrix}, \tag{2.4}$$

where the $\sim$ emphasizes the circulant structure. $\tilde{\mathrm{H}}$ can be diagonalized through the following decomposition [5]:

$$\tilde{\mathrm{H}}=\mathbf{F}_R^H \cdot \Lambda \cdot \mathbf{F}_R, \tag{2.5}$$

where $\mathbf{F}_R$ is the $R \times R$ unitary discrete Fourier transform (DFT) matrix with the $(i,k)^{th}$ element defined as

$$\left[\mathrm{F}_R\right]_{i,k} \triangleq \frac{1}{\sqrt{R}} e^{-j\frac{2\pi}{R}ik}, \quad j=\sqrt{-1},\ i,k=1,2,\cdots,R-1. \tag{2.6}$$

Furthermore, Λ is the diagonal matrix with the entries given by the R-point DFT of the channel impulse response vector h. Next we define $\mathbf{y} \triangleq \mathbf{F}_R \cdot y$ and $\mathbf{x} \triangleq \mathbf{F}_R \cdot x$, where $y=\left[y(0)\, y(1) \quad \cdots \quad y(R-1)\right]^T$ and $x=\left[x(0)\, x(1) \quad \cdots \quad x(R-1)\right]^T$. By applying the DFT matrix to the received data block in (2.3) and using the unitary property $\mathbf{F}_R \cdot \mathbf{F}_R^H = I_R$ we get

$$\begin{aligned} \mathbf{F}_R \cdot y &= \mathbf{F}_R \cdot \tilde{\mathrm{H}} \cdot x, \\ &= \mathbf{F}_R \cdot \tilde{\mathrm{H}} \cdot \mathbf{F}_R^H \cdot \mathbf{F}_R \cdot x, \\ \mathbf{y} &= \Lambda \cdot \mathbf{x}. \end{aligned} \tag{2.7}$$

Therefore the original sequence y in (2.3) which suffers from the ISI effect is now decomposed into a sequence $\mathbf{y}$ in which each entry is equivalent to transmitting symbols over a flat channel Λ. Hence, standard single input single out (SISO) equalization techniques can now be applied. This forms the basis of SC transmission. In the next section, the STBC structure is combined with the SC transmission to provide the capacity achieving scheme presented in [5]. The system is then extended to the multi-user case.

2.3 Input-Output Model for the Multiple Access System

The overall SC-STBC transceiver for the case of single user equipped with two transmit antennas and one receive antenna is shown is Fig. 2.1. The explanation to follow is based on this special case. The derivation for the general case of more than two transmit antennas and multiple receive antennas is given in [5].

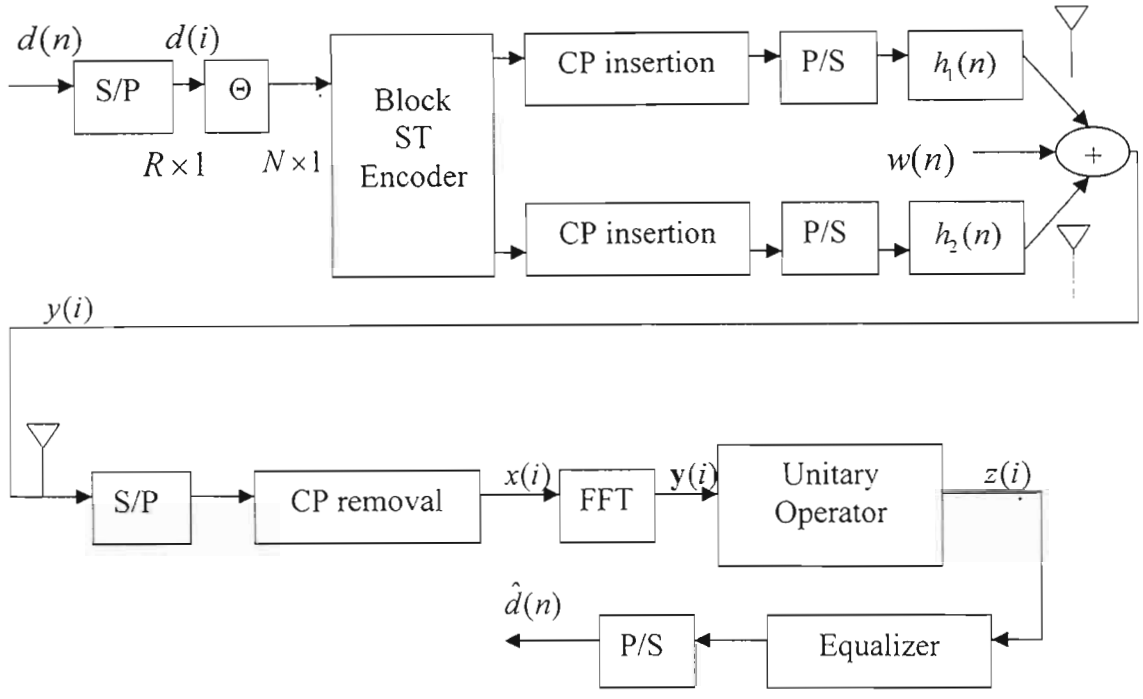

Fig. 2.1 Overall single-carrier STBC transceiver model for a single user

The information bearing data symbols $d(n)$, which belongs to a fixed constellation, are initially converted to $R\times 1$ blocks:

$$d(n)\xrightarrow{S/P}\mathbf{d}(i)\triangleq\left[d(iR),\ \cdots\ ,d(iR+R-1)\right]^{T}. \tag{2.8}$$

The serial index n is related to the block index i by $n=iR+q,\ q\in[0,R-1]$. Two consecutive blocks of $\mathbf{d}(i)$, denoted by $2i$ and $2i+1$, are multiplied by the $R\times N$ precoder matrix Θ to give the following $N\times 1$ output.

$$\Theta\times\left[\mathbf{d}(2i)\quad\mathbf{d}(2i+1)\right]^{T}=\left[x(2i)\quad x(2i+1)\right]^{T}\triangleq\left[x_1\quad x_2\right]^{T}. \tag{2.9}$$

The ST encoder is defined as

$$\begin{bmatrix} x_1 & x_2 \\ -\mathbf{P}x_2^{*} & \mathbf{P}x_1^{*}\end{bmatrix}\begin{matrix}\rightarrow space\\ \downarrow time\end{matrix}, \tag{2.10}$$

where $\mathbf{P}$ is the permutation matrix drawn from a set of permutation matrices $\left\{\mathbf{P}_N^{(n)}\right\}_{n=0}^{N-1}$.

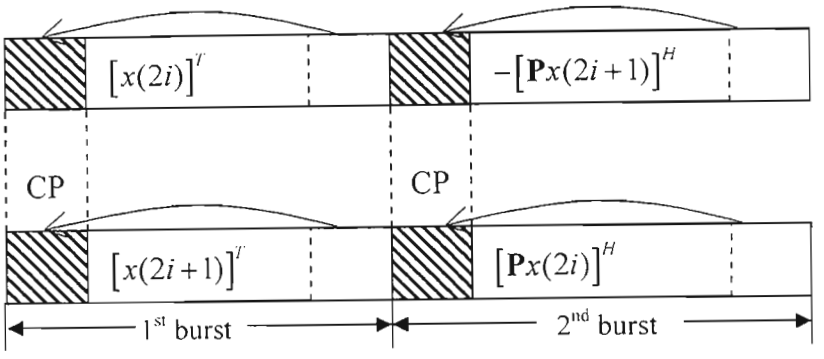

Fig. 2.2 Cyclic prefix Transmission

The overall transmission format is depicted in Fig. 2.2. The addition of cyclic prefix (CP) at the transmitter together with the removal of CP at the receiver, as shown in Fig. 2.1, gives the following channel input-output relationship:

$$y(i) = \sum_{\mu=1}^{2} \tilde{\mathbf{H}}_{\mu} x(i) + \mathbf{w}(i), \tag{2.11}$$

where $x(i)$ is the received i^{th} block sequence, $\tilde{\mathbf{H}}_{\mu}$ is the circulant channel matrix and $\mathbf{w}(i)$ is the noise term which is assumed to be zero-mean Gaussian with variance N_0. The index for the two different channels is denoted by μ. Using (2.10), the received sequence for the first and second sub-blocks, is given by

$$\begin{aligned} y(2i) &= \tilde{\mathbf{H}}_1 x_1 + \tilde{\mathbf{H}}_2 x_2 + \mathbf{w}(2i), \\ y(2i+1) &= -\tilde{\mathbf{H}}_1 \mathbf{P} x_2^* + \tilde{\mathbf{H}}_2 \mathbf{P} x_1^* + \mathbf{w}(2i+1). \end{aligned} \tag{2.12}$$

In the steps to follow the reader is referred to properties **P.1** and **P.2** [5] that are relegated to Appendix A. Pre-multiplying the second expression above by **P** and taking conjugate results in the following expression.

$$\mathbf{P} y^*(2i+1) = -\tilde{\mathbf{H}}_1^H x_2 + \tilde{\mathbf{H}}_2^H x_1 + \mathbf{P}\mathbf{w}^*(2i+1). \tag{2.13}$$

The resultant hermitian channel matrix is due to property **P.2** in Appendix A. Next we define $\mathbf{y}(i) \triangleq \mathbf{F}_N y(i)$, $\eta(i) \triangleq \mathbf{F}_N w(i)$ and $\mathbf{x}_{\mu} \triangleq \mathbf{F}_N x_{\mu}$ $\forall$ μ=1,2, where $\mathbf{F}_N$ is defined as in (2.6). Using property **P.1** in Appendix A (also see (2.5)) the output after the DFT operation can be written as follows.

$$\begin{aligned}\mathbf{y}(2i) &= \Lambda_1\mathbf{x}_1 + \Lambda_2\mathbf{x}_2 + \eta(2i),\\ \mathbf{y}(2i+1) &= -\Lambda_1^*\mathbf{x}_2 + \Lambda_2^*\mathbf{x}_1 + \eta(2i+1).\end{aligned} \tag{2.14}$$

The matrix Λ_μ represents the diagonalized channel matrix of $\mathbf{H}_\mu$. As proven in [5], it should be noted that the resulting noise term after the DFT operation is still white with variance N_0. It is important to note that pre and post-multiplying the channel matrix by $\mathbf{P}$ in (2.13) results in the hermitian channel matrix. This in turn, using property **P.1,** results in the preservation of the Alamouti structure after the DFT operation as shown in (2.14). This expression can be re-written as follows:

$$\begin{bmatrix}\mathbf{y}(2i)\\ \mathbf{y}(2i+1)\end{bmatrix} = \underbrace{\begin{bmatrix}\Lambda_1 & \Lambda_2\\ \Lambda_2^* & -\Lambda_1^*\end{bmatrix}}_{\mathbf{D}_1}\cdot\begin{bmatrix}\mathbf{x}_1\\ \mathbf{x}_2\end{bmatrix} + \begin{bmatrix}\eta(2i)\\ \eta(2i+1)\end{bmatrix}. \tag{2.15}$$

Defining $\mathbf{y}_1 \triangleq [\mathbf{y}(2i) \quad \mathbf{y}(2i+1)]^T$, $\mathbf{s} \triangleq [\mathbf{x}_1 \quad \mathbf{x}_2]^T$ and $\eta_1 \triangleq [\eta(2i) \quad \eta(2i+1)]^T$, and using $\mathbf{D}_1$ as defined in (2.15), we get

$$\mathbf{y}_1 \triangleq \mathbf{D}_1 \cdot \mathbf{s} + \eta_1. \tag{2.16}$$

We can now extend this model to the two receive antenna case. By defining

$$\begin{bmatrix}\mathbf{y}_1\\ \mathbf{y}_2\end{bmatrix} = \begin{bmatrix}\mathbf{D}_1\\ \mathbf{D}_2\end{bmatrix}[\mathbf{s}] + \begin{bmatrix}\eta_1\\ \eta_2\end{bmatrix}, \tag{2.17}$$

where $\mathbf{D}_2$ is similarly defined as $\mathbf{D}_1$ for the second receive antenna.

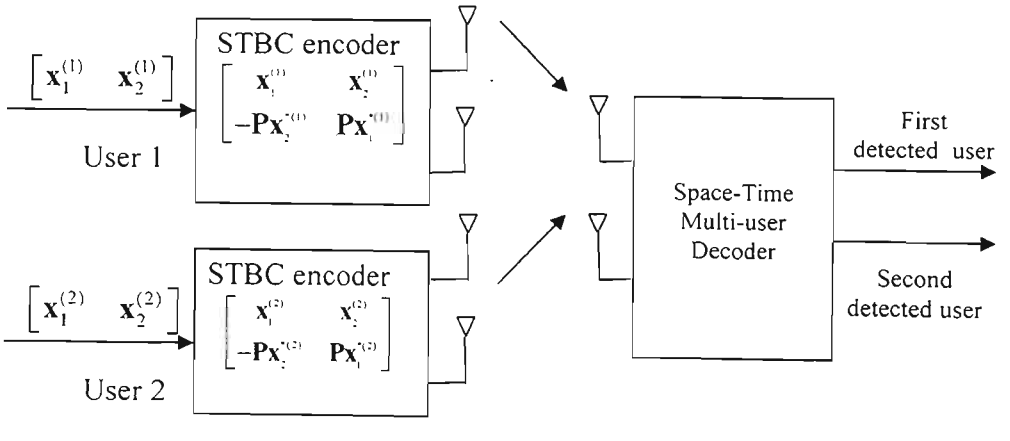

Fig. 2.3 Two-user system configuration

Fig. 2.3 shows the system configuration we are about to describe for the two user scenario. As shown, each user is equipped with two transmit and one receive antennas. By introducing the corresponding channel and data matrices for user one and user two, (2.17) is modified to

$$\begin{bmatrix} \mathbf{y}_1 \\ \mathbf{y}_2 \end{bmatrix} = \begin{bmatrix} \mathbf{D}_1^{(1)} & \mathbf{D}_1^{(2)} \\ \mathbf{D}_2^{(1)} & \mathbf{D}_2^{(2)} \end{bmatrix} \begin{bmatrix} \mathbf{s}^{(1)} \\ \mathbf{s}^{(2)} \end{bmatrix} + \begin{bmatrix} \eta_1 \\ \eta_2 \end{bmatrix}, \tag{2.18}$$

where the superscript indicates the corresponding user. Generalizing this for M_r receive antennas and K users, each equipped with two transmit antennas, we finally get

$$\begin{bmatrix} \mathbf{y}_1(D) \\ \vdots \\ \mathbf{y}_{M_r}(D) \end{bmatrix} = \begin{bmatrix} \mathbf{D}_1^{(1)}(D) & \cdots & \mathbf{D}_1^{(K)}(D) \\ \vdots & \ddots & \vdots \\ \mathbf{D}_{M_r}^{(1)}(D) & \cdots & \mathbf{D}_{M_r}^{(K)}(D) \end{bmatrix} \begin{bmatrix} \mathbf{s}^{(1)}(D) \\ \vdots \\ \mathbf{s}^{(K)}(D) \end{bmatrix} + \begin{bmatrix} \eta_1(D) \\ \vdots \\ \eta_{M_r}(D) \end{bmatrix}, \tag{2.19}$$

which concludes the derivation for the general multi-user case. A brief overview of the different single carrier schemes given in [5] is discussed next. These schemes vary by the selection of the precoder matrix, Θ. The equalization and unitary combining steps are explained thereafter.

2.4 Overview of Single Carrier Schemes in Rich Scattering Environments

2.4.1 CP-Only Transmission

CP only transmission refers to the class of block transmission where there is no precoding i.e. $\Theta = \mathbf{I}_R$ and $x(i) = \mathbf{d}(i)$. It was proven is [5] that such a system achieves a diversity order of $G_d = 2$ for the two transmit and one receive antenna case. This is nothing but antenna diversity and hence such a system is said to suffer from loss of multipath diversity. The system presented in [7] is an example of this.

2.4.2 Linearly Precoded Cyclic Prefix (LP-CP)

When $x(i) = \Theta\mathbf{d}(i)$, and $\Theta \neq \mathbf{I}_K$, this type of transmission is termed LP-CP. The two variations are referred to as redundant LP-CP, when $N = R$, and non-redundant, when $N = R + L$. It is established in [5] that both these schemes achieve the maximum

diversity order of $N_t N_R(L+1)$, with N_R and N_T denoting the number of receive and transmit antennas, respectively.

2.4.3 Affine Precoded Cyclic Prefix (AP-CP)

This class of precoding is governed by the following equation:

$$x(i) = \Theta \mathbf{d}(i) + \Theta' \mathbf{b}(i). \tag{2.20}$$

The term $\mathbf{b}(i)$ is a known symbol vector.

This can also be written as

$$\mathbf{P}_N^{(R)} x(i) = \left[\left(\mathbf{P}_R^{(0)} \mathbf{d}(i) \right)^T, \left(\mathbf{P}_L^{(0)} \mathbf{b}(i) \right)^T \right],$$

given a specific choice of the permutation matrix $\mathbf{P} = \mathbf{P}_N^{(R)} = \left[\mathbf{P}_R^{(0)} \quad \mathbf{P}_L^{(0)} \right]^T$. This choice implies that the data blocks and the known symbol blocks are both time reversed. As shown in [5], this format of transmission has the data block surrounded by a pre-amble and a post-amble of known symbols. This results in an increase in the overhead.

2.4.4 Zero Padding Only

If we let $\mathbf{b}(i) = 0$ then two adjacent blocks are surrounded by two zero blocks of length L each. For a channel of length L, a padding of length L is only required. This corresponds to the removal of the CP insertion operation at the transmitter. The ZP-only system therefore not only saves the transmitted power occupied by CP but also increases the overall rate of the system by decreasing the overhead requirements. It is proven in [5] that this scheme also achieves full diversity order. The equalization and decoding steps are described next.

2.5 Equalization and Decoding

The initial part of this section details the derivation of the decoupled data for the single user case. The extension for the two user case follows this. From (2.15), we define the diagonal matrix as

$$\mathbf{D}_{12} = \left[\Lambda_1^* \cdot \Lambda_1 + \Lambda_2^* \cdot \Lambda_2 \right]^{1/2}, \tag{2.21}$$

then the unitary operator as defined in [5] (also see **P.3** in Appendix A) is given by

$$\mathbf{U} \triangleq \mathbf{D}_1 \cdot (\mathbf{I}_2 \otimes (\mathbf{D}_{12})^{-1}), \tag{2.22}$$

where $\otimes$ stands for the kronecker product. The unitary operator, $\mathbf{U}$, has the following two properties [5]:

$$\begin{aligned} \mathbf{U}^{\mathrm{H}} \cdot \mathbf{U} &= \mathbf{I}_{2N}, \\ \mathbf{U}^{\mathrm{H}} \cdot \mathbf{D}_1 &= \mathbf{I}_2 \otimes \mathrm{D}_{12}. \end{aligned} \tag{2.23}$$

Combining (2.15) with the unitary operator yields the following output:

$$\mathrm{z}(i) \triangleq \mathrm{U}^{\mathrm{H}} \cdot \begin{bmatrix} \mathbf{y}(2i) \\ \mathbf{y}(2i+1) \end{bmatrix} = \mathrm{U}^{\mathrm{H}} \cdot \begin{bmatrix} \mathbf{x}_1 \\ \mathbf{x}_2 \end{bmatrix} + \mathrm{U}^{\mathrm{H}} \cdot \begin{bmatrix} \eta(2i) \\ \eta(2i+1) \end{bmatrix}. \tag{2.24}$$

The resultant noise term, $\bar{\eta}(i) \triangleq \mathbf{U}^{\mathrm{H}} \left[\eta(2i) \quad \eta(2i+1)\right]^{\mathrm{T}}$, is still white with each entry having variance N_0. Recall that $\mathbf{x}_\mu \triangleq \mathbf{F}_N x_\mu \ \forall\ \mu$=1,2 and using (2.9), the unitary output equation (2.24) can be re-written as

$$\mathrm{z}(i) = \mathbf{D}_{12}\mathbf{F}_N x(i) + \bar{\eta}(i) = \mathbf{D}_{12}\mathbf{F}_N \Theta \mathbf{d}(i) + \bar{\eta}(i). \tag{2.25}$$

Next we define the matrix $\mathbf{A} \triangleq \mathbf{D}_{12}\mathbf{F}_N\Theta$. Since the focus of this system is simple linear processing with minimal receiver complexity, the linear zero-forcing (ZF) equalizer and the block minimum mean square (MMSE) equalizer that provides low complexity alternatives are considered. From [5], the MMSE block equalizer is given by

$$\gamma_{MMSE} \triangleq \left(\mathbf{A}^H \mathbf{A} + {\sigma_w}/{\sigma_s} \right)^{-1} \mathbf{A}^H, \tag{2.26}$$

where σ_w is the covariance of noise, σ_s is signal covariance and γ_{MMSE} is the MMSE equalizer coefficients. The symbol vectors are assumed to be white with covariance matrix $\mathbf{R}_s \triangleq E\left[x(i)x^H(i)\right] = \sigma_s^2 \mathbf{I}_N$. With $\sigma_w = 0$, (2.26) reduces to the ZF solution. Finally the estimates of the decoupled data for the two blocks can be written as

$$\gamma_{MMSE} \cdot z(i) = \begin{cases} \hat{\mathbf{d}}(2i) \ \forall\ i = 2i, \\ \hat{\mathbf{d}}(2i+1) \ \forall\ i = 2i+1. \end{cases} \tag{2.27}$$

We will now turn our attention to the two user case. In order to decouple the data for the different users, a new unitary operator has to be defined. To derive the solution for this term, the method of back substitution is used. Firstly, a new unitary operator is defined as:

$$\mathbf{W} \triangleq \begin{bmatrix} \mathbf{M} & \mathbf{J} \\ \mathbf{K} & \mathbf{L} \end{bmatrix}. \tag{2.28}$$

For the derivations to follow, the diagonal matrix given in (2.21) is re-defined for user one and user two as $\mathbf{D}_{12}^{(1)}$ and $\mathbf{D}_{12}^{(2)}$, respectively.

The entries **M, J, K** and **L** of the unitary operator in (2.28) are chosen such that after multiplying (2.18) with the unitary operator the following equation holds:

$$\mathbf{W}\begin{bmatrix} \mathbf{y}_1 \\ \mathbf{y}_2 \end{bmatrix} = \begin{bmatrix} \mathbf{D}_{12}^{(1)} & 0 \\ 0 & \mathbf{D}_{12}^{(2)} \end{bmatrix} \cdot \begin{bmatrix} \mathbf{F}_N x^{(1)} \\ \mathbf{F}_N x^{(2)} \end{bmatrix} + \mathbf{W}\begin{bmatrix} \eta_1 \\ \eta_2 \end{bmatrix}. \tag{2.29}$$

Note that $\mathbf{F}_N x^{(\mu)} = \begin{bmatrix} \mathbf{F}_N x_1^{(\mu)} & \mathbf{F}_N x_2^{(\mu)} \end{bmatrix}^T \ \forall\ \mu$=1,2 . From (2.18) and (2.29), it is easy to see that the solutions for the unitary operator entries **J** and **K** are given as

$$\begin{aligned} \mathbf{J} &= -\mathbf{M}\mathbf{D}_1^{(2)}\left(\mathbf{D}_2^{(2)}\right)^{-1}, \\ \mathbf{K} &= -\mathbf{L}\mathbf{D}_2^{(1)}\left(\mathbf{D}_1^{(1)}\right)^{-1}. \end{aligned} \tag{2.30}$$

If we let the unitary entries $\mathbf{L} = \mathbf{M} = \mathbf{I}_{2N}$, then plugging into the expression for the unitary operator and ignoring the noise term in (2.29), we get

$$\begin{aligned} \mathbf{W}\begin{bmatrix} \mathbf{y}_1 \\ \mathbf{y}_2 \end{bmatrix} &= \begin{bmatrix} \mathbf{I}_{2N} & -\mathbf{D}_1^{(2)}\left(\mathbf{D}_2^{(2)}\right)^{-1} \\ -\mathbf{D}_2^{(1)}\left(\mathbf{D}_1^{(1)}\right)^{-1} & \mathbf{I}_{2N} \end{bmatrix} \cdot \begin{bmatrix} \mathbf{D}_1^{(1)} & \mathbf{D}_1^{(2)} \\ \mathbf{D}_2^{(1)} & \mathbf{D}_2^{(2)} \end{bmatrix} \cdot \begin{bmatrix} \mathbf{F}_N x^{(1)} \\ \mathbf{F}_N x^{(2)} \end{bmatrix} \\ &= \begin{bmatrix} \mathbf{D}_{12}^{(1)} & 0 \\ 0 & \mathbf{D}_{12}^{(2)} \end{bmatrix} \cdot \begin{bmatrix} \mathbf{F}_N x^{(1)} \\ \mathbf{F}_N x^{(2)} \end{bmatrix}. \end{aligned} \tag{2.31}$$

The solutions for the diagonal matrices are given as

$$\begin{aligned}\mathbf{D}_{12}^{(1)}\mathbf{F}_N x^{(1)} &= \mathbf{M}\mathbf{y}_1 + \mathbf{J}\mathbf{y}_2,\\ \mathbf{D}_{12}^{(2)}\mathbf{F}_N x^{(2)} &= \mathbf{K}\mathbf{y}_1 + \mathbf{L}\mathbf{y}_2.\end{aligned} \tag{2.32}$$

Using this result, the data for the two users can finally be decoupled as follows:

$$\begin{aligned}\left(\mathbf{D}_1^{(1)} - \mathbf{D}_1^{(2)}\left(\mathbf{D}_2^{(2)}\right)^{-1}\mathbf{D}_2^{(1)}\right)\mathbf{F}_N\Theta\mathbf{d}^{(1)} &= \mathbf{y}_1 - \mathbf{D}_1^{(2)}\left(\mathbf{D}_2^{(2)}\right)^{-1}\mathbf{y}_2,\\ \left(\mathbf{D}_2^{(2)} - \mathbf{D}_2^{(1)}\left(\mathbf{D}_1^{(1)}\right)^{-1}\mathbf{D}_1^{(2)}\right)\mathbf{F}_N\Theta\mathbf{d}^{(2)} &= -\mathbf{D}_2^{(1)}\left(\mathbf{D}_1^{(1)}\right)^{-1}\mathbf{y}_1 + \mathbf{y}_2.\end{aligned} \tag{2.33}$$

The derivation for the MMSE equalizer is straight forward. For example, using the first equation in (2.33), the data for user 1 can be estimated by defining the matrix

$$\mathbf{B} \triangleq \left(\mathbf{D}_1^{(1)} - \mathbf{D}_1^{(2)}\left(\mathbf{D}_2^{(2)}\right)^{-1}\mathbf{D}_2^{(1)}\right)\mathbf{F}_N\Theta \tag{2.34},$$

and defining the MMSE equalizer as

$$\gamma_{MMSE2} = \left(\mathbf{B}^H\mathbf{B} + {}^{\sigma_w}\!/_{\sigma_s}\right)^{-1}\mathbf{B}^H. \tag{2.35}$$

Finally the decoupled data for user 1 is estimated as

$$\gamma_{MMSE2}\cdot\mathbf{y}_1(i) - \mathbf{D}_1^{(2)}\left(\mathbf{D}_2^{(2)}\right)^{-1}\mathbf{y}_2(i) = \begin{cases}\hat{\mathbf{d}}^{(1)}(2i) & \forall\ i = 2i\\ \hat{\mathbf{d}}^{(1)}(2i+1) & \forall\ i = 2i+1\end{cases}. \tag{2.36}$$

2.6 Performance Analysis

The purpose of this section is to prove, in terms of SNR, that the multi-user system does not have any performance loss with respect to the single user system. The reader is directed to [6] which details the proof of the diversity for the multi-user system. It is shown in [6] that the multi-user system achieves the same diversity order as the single-user system.

The expression for the single user case after unitary combining is given in (2.24). Using $\left[\bar{\eta}_1 \quad \bar{\eta}_2\right] \triangleq \mathbf{U}^{\mathbf{H}}\left[n(2i) \quad n(2i+1)\right]$ and $\mathbf{x}_\mu \triangleq \mathbf{F}_N x_\mu \ \forall\ \mu$=1,2 , (2.24) can be written as

$$z(i) = \mathbf{U}^H \begin{bmatrix} \mathbf{y}(2i) \\ \mathbf{y}(2i+1) \end{bmatrix} = \begin{bmatrix} \mathbf{D}_{12} & 0 \\ 0 & \mathbf{D}_{12} \end{bmatrix} \begin{bmatrix} \mathbf{F}_N x_1 \\ \mathbf{F}_N x_2 \end{bmatrix} + \begin{bmatrix} \bar{\eta}_1 \\ \bar{\eta}_2 \end{bmatrix}. \tag{2.37}$$

By recalling that $x(i) = \Theta d(i)$ and using the definition $\mathbf{A} \triangleq \mathbf{D}_{12}\mathbf{F}_N\Theta$, the decoupled expression for the i^{th} received block after the zero forcing equalizer reduces [5] to

$$\left[\left(\mathbf{A}^{\mathrm{H}}\mathbf{A}\right)^{-1}\mathbf{A}^{\mathrm{H}}\right]\cdot z(i) = d(i) + \left[\left(\mathbf{A}^{\mathrm{H}}\mathbf{A}\right)^{-1}\mathbf{A}^{\mathrm{H}}\right]\cdot\bar{\eta}(i). \tag{2.38}$$

Let us define the zero forcing equalizer as $\tilde{\mathbf{A}} \triangleq \left(\mathbf{A}^{\mathrm{H}}\mathbf{A}\right)^{-1}\mathbf{A}^{\mathrm{H}}$. By considering only a single data bit, $d(n)$, we can write

$$\tilde{\mathbf{A}}(n)\bullet z(i) = d(n) + \tilde{\mathbf{A}}(n)\bar{\eta}(i) \tag{2.39}$$

where the index $\tilde{\mathbf{A}}(n)$ represents the entire n^{th} row of the matrix $\tilde{\mathbf{A}}$. If we define the new noise term as $\bar{\bar{\eta}}(n) = \tilde{\mathbf{A}}(n)\bar{\eta}(i)$, then expectation of the signal to noise ratio expression is given by

$$E[SNR] = \frac{E\left[|d(n)|^2\right]}{E\left[\bar{\bar{\eta}}(n)\bar{\bar{\eta}}(n)^*\right]}$$

$$= \frac{E\left[|d(n)|^2\right]}{E\left[|\bar{\bar{\eta}}(n)|^2\right]}. \tag{2.40}$$

For the multi-user case, the overall expression after unitary combining is given by (2.31). The properties of a unitary operator are given in **P.3** of Appendix A. The following two expressions can be easily verified.

$$\mathbf{W}^H\mathbf{W} = \mathbf{I}_{4N}, \tag{2.41}$$

$$\mathbf{W}\begin{bmatrix} \mathbf{D}_1^{(1)} & \mathbf{D}_1^{(2)} \\ \mathbf{D}_2^{(1)} & \mathbf{D}_2^{(2)} \end{bmatrix} = \mathbf{I}_2 \otimes \begin{bmatrix} \mathbf{D}_{11} \\ \mathbf{D}_{22} \end{bmatrix}. \tag{2.42}$$

This implies that $\mathbf{W}$ is unitary. The multi-user output after unitary combining is given by (2.29). defining $\mathbf{A}^{(1)} \triangleq \mathbf{D}_{12}^{(1)}\mathbf{F}_N\Theta$, we get the decoupled expression for user 1 as

$$d(i)+\left(\mathbf{A}^{(1)\mathbf{H}}\mathbf{A}^{(1)}\right)^{-1}\mathbf{A}^{(1)\mathbf{H}}\overline{\eta}_1(i)$$

Again, by considering a single data bit for user 1, and defining $\tilde{\mathbf{A}}^{(1)} \triangleq \left(\mathbf{A}^{(1)\mathbf{H}}\mathbf{A}^{(1)}\right)^{-1}\mathbf{A}^{(1)\mathbf{H}}$ and $\overline{\overline{\eta}}^{(1)}(n) = \tilde{\mathbf{A}}^{(1)}(n)\overline{\eta}^{(1)}(i)$, it can be shown that expectation of the SNR expression is given by

$$\begin{aligned} E_{2\,\text{users}}\left[SNR\right] &= \frac{E\left[\left|d^{(1)}(n)\right|^2\right]}{E\left[\overline{\overline{\eta}}_1(n)\overline{\overline{\eta}}_1(n)^*\right]} \\ &= \frac{E\left[\left|d^{(1)}(n)\right|^2\right]}{E\left[\left|\overline{\overline{\eta}}_1(n)\right|^2\right]} \end{aligned} \tag{2.43}$$

Equations (2.40) and (2.43) are equivalent. Using this result and derivation for the overall diversity gain given in [6] it can be concluded there is no performance loss that occurs in terms of diversity and SNR when extending to the multiple- access system for sub-optimal zero forcing receiver. In the next section, through simulation results, it is proven that this property still holds for the sub-optimal MMSE receiver derived in section 2.6 and no performance loss is incurred for the multi-user case.

2.7 Simulation Results

In this section we compare the single and multi-user MMSE systems. The single user system is the same as in [5] with two transmit antennas and a single receive antenna. The block length of $R = 14$ is used. The channel length is set to $L = 2$, with the channels between the transmitter and receiver assumed to be independent and identically distributed (i.i.d), Gaussian, with covariance matrix $\mathbf{I}_{L+1}/(L+1)$. The receiver assumes knowledge of the channel state information (CSI). We also assume quasi static fading. QPSK constellation is employed. The zero padding cyclic prefix described in section 2.4.4 is used. All the above mentioned simulation parameter are the same as that used in [5]. This is done so that a comparison of the computer simulation can be done to verify that our results are the same as that in [5]. For the multi-user case, the system consists of two users each equipped with two transmit antennas and one receive antenna as shown in Fig. 2.2 is used. The SNR is defined as the average symbol to energy ratio at the

receiver. Since we are dealing with block transmission, we use frame error rate (FER). Fig. 2.4 shows the FER performance of the MMSE based receiver for both one and two user systems. The results for the single user system are exactly the same as in [5] which verifies our simulation model. Although the proofs given in section 2.6 and [6] were derived for the optimal receiver, the results shown in Fig 2.4 clearly show that sub-optimal MMSE receiver does not incur any performance loss. This important result is not provided in [5].

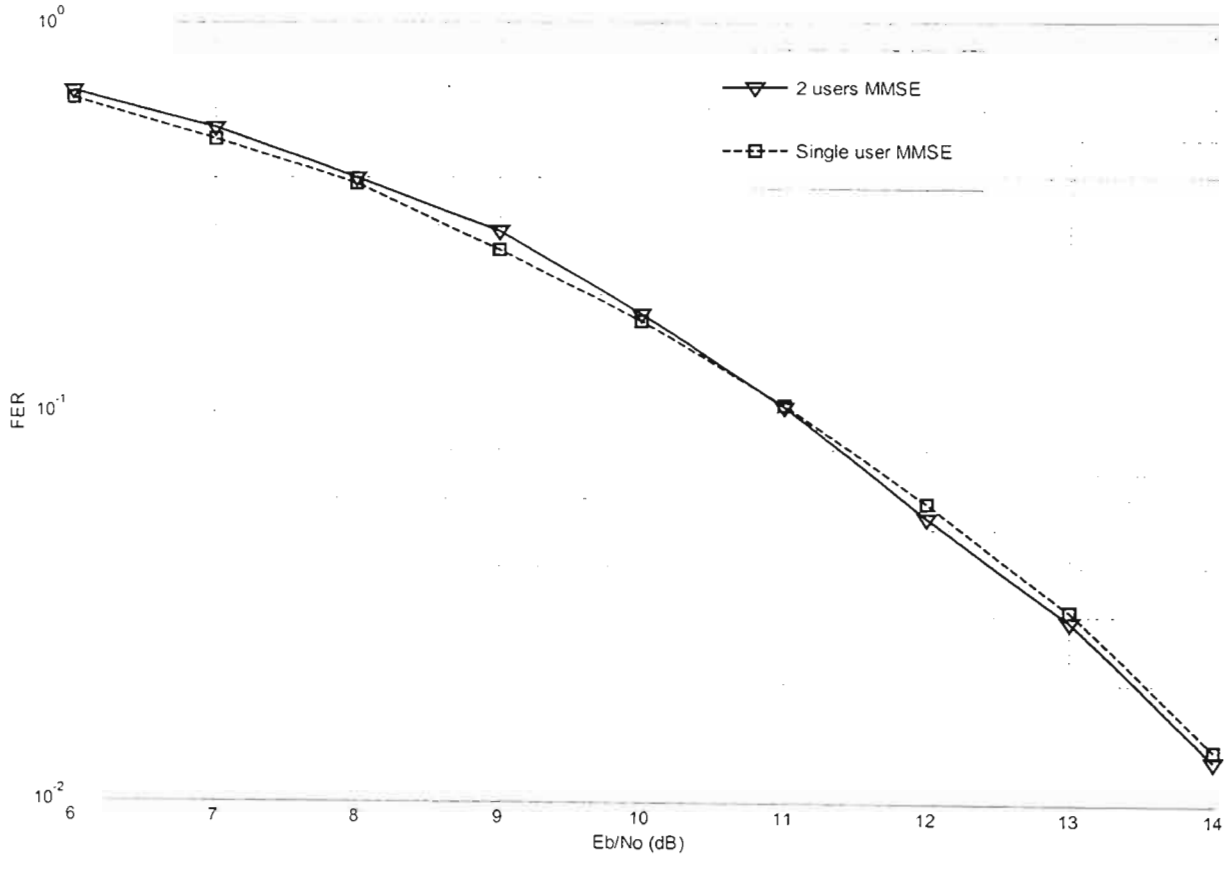

Fig. 2.4 Performance comparison for the single user and two user scenarios

Concluding Remarks

We have derived the single carrier block transmission for a multiple access channel. In section 2.7, it was proven that the multi-user system does not incur any performance loss in terms of diversity and SNR. The simulation results provided shows that this is valid for a sub-optimal algorithm such as the MMSE. Although, for most of this chapter, the example of two receive antennas and two users was used, the technique can be extended to any number of users and receive antennas. Throughout this chapter we assumed the case where the receiver has perfect knowledge of the channel conditions. In the next section we will look at non-coherent detection where, due to the mobility of the user, the channel condition is selective in both frequency and time. The receiver has to perform equalization/decoding without the knowledge of the CSI.

CHAPTER 3

RLS BASED ADAPTIVE RECEIVER FOR JOINT EQUALIZATION AND INTERFERENCE SUPPRESSION

3.1 Introduction

This chapter describes the low-complexity adaptive receiver, based on the recursive least squares (RLS) algorithm, that has been designed for space-time block-coded (STBC) transmissions over frequency–selective fading channels with rapid variations [8], [9]. The space-time block coded structure is exploited to reduce the complexity of the RLS algorithm to that of a least mean squares (LMS) algorithm. The performance of the adaptive receiver is compared to the system with perfect channel state information (CSI) to give a measure of the penalty associated with this receiver. In addition, the effect of the forgetting factor in the RLS algorithm is provided in the simulation results. These two aspects are not covered in [8] and [9].

Next generation broadband wireless channels are expected to provide users with high-speed data transmission capabilities to bring the dreams of wireless internet access, multimedia services and mobile computing features much closer to reality. Increasing the system capacity without requiring additional power and bandwidth has become a major tool in ensuring the availability of the scarce spectral resource.

In this respect, multiple-input multiple-output (MIMO) systems have been proven to significantly increase the capacity in rich scattering environments. In particular, STBC, which was first introduced in [1] and later generalized in [2], is an attractive MIMO technique due to its simple linear processing and lack of additional bandwidth and transmission power requirements. The Alamouti scheme, which is a special case full rate STBC with two transmit antennas and one receive antenna, is in-fact adopted in WCDMA and CDMA2000 standards. However, broadband wireless channels introduce random attenuations and delays to the transmitted signals and, due to the increased data rates, cause inter-symbol-interference (ISI) at the receiver. Such channels are termed frequency-selective or broadband channels. The Alamouti scheme was originally designed for narrow band flat fading channels. The first extension of STBC to

broadband channels was presented in [3] with the so-called time-reversal (TR) STBC. This scheme does not handle the ISI problem at the start and end of each block burst. To cater for the ISI in the start and end of each burst, the single carrier frequency domain equalizer (SC-FDE) schemes with zero post-fix [4] and cyclic prefix [7] were developed. These schemes are generalized in [5], which bench marks the single carrier STBC in frequency-selective channels. The SC-FDE has two main advantages over the orthogonal frequency division multiplexing (OFDM) counterpart, namely, lower peak-to-average ratio (PAR) and reduced sensitivity to carrier frequency errors.

All the above mentioned receivers require channel state information (CSI) at the receiver. One approach is to use training sequences embedded in each block to estimate the CSI. This, however, results in increased system overhead. In addition to this, the mobility of the users may cause the channel impulse response to vary rapidly and hence the quasi-static assumption of the channel becomes void. The use of longer blocks, which is required to reduce the system overhead in such training based schemes, can not be practical in such cases. This motivates the development of an effective low-complexity adaptive receiver with fast tracking abilities [8], [9].

The results in [8] show the performance of the algorithm for various Doppler frequencies. However a proper method for designing various parameters for the receiver, such as block size, forgetting factor and re-training interval, are not presented. By comparing the system performance to a system with perfect CSI we give a measure of the actual tracking performance of the adaptive receiver. Motivated by this, we provide simulation results when varying various parameters of the algorithm and compare the results to the system with perfect CSI. This provides a tool to design all the above mentioned parameters. Furthermore, an indication of how various parameters can be adjusted to achieve near "perfect CSI performance", which is the best case performance, can be determined.

A high data rate channel with high mobility users must be modelled in order to test the performance of such a receiver. The third generation TDMA cellular standard is known as enhanced data rates for global evolution (EDGE). EDGE results in a challenging equalization problem due to the use of 8-PSK modulation and general non minimum-phase characteristics of the typical urban (TU) channel. The Gaussian minimum shift

keying (GMSK) filter at the transmitter also adds additional ISI. Furthermore, when in the presence of high mobility users, the channel becomes selective in both frequency and time. Such a channel is widely used in many journals and papers [5,6,8,17] in order test the performance of various receivers. The model used to represent this channel, which is not comprehensively explained in literature, is also provided in this chapter.

The rest of this chapter is organized as follows. Section 3.2 details the SC-FDE in terms of cyclic prefix used and decoding designs in an MMSE sense. Section 3.3 describes the adaptive receiver for training and tracking mode developed in [8]. The simulation results are provided in section 3.4, while conclusions are drawn in Section 3.5. It should be noted that the same parameters and simulation environment as [8,9] are used in section 3.4 to verify that the results are the same, hence giving integrity to the simulations.

3.2 Single User Transmission

In the description to follow, it is assumed that each user is equipped with two transmit antennas and the receiver has a single antenna. Let the N-symbol block including cyclic prefix (CP) transmitted from the first and second antennas at block time $2i$ be given by x_1 and x_2, respectively. At block time $2i+1$, permuted conjugate versions, $-\mathbf{P}x_2^*$ and $\mathbf{P}x_1^*$, are sent from the first and second antennas, respectively. This is given by (2.12) in chapter 2. Assuming the original data sequence length and channel length is R and L, respectively, the permutation matrix $\mathbf{P}$ is a circular reversal matrix given by

$$\mathbf{P}=\begin{pmatrix}\mathbf{P}_R\\ \mathbf{P}_L\end{pmatrix}=\left(\begin{array}{cccc}1 & 0 & \cdots & 0\\ & \ddots & & \\ 0 & 0 & \cdots & 1\\ \hline 0 & \cdots & 1 & 0\\ & \iddots & & \\ 0 & 1 & \cdots & 0\end{array}\right). \tag{3.1}$$

Note that this is a special case of the AP-CP transmission described in section 2.4.3 and that $N=R+L$. The $k^{(\text{th})}$ received blocks, $\forall\, k=2i,2i+1$, in the presence of noise is given by

$$\mathrm{y}(k)=\mathrm{H}_1(k)x_1(k)+\mathrm{H}_2(k)x_2(k)+\mathrm{n}(k), \tag{3.2}$$

where $n(k)$ is the noise term which is assumed zero mean Gaussian with white power spectrum, and $H_1(k)$ and $H_2(k)$ are the circulant channel matrices from antenna one and two, respectively, to the receive antenna. Note that the index k for the channels is a key difference between (3.2) and (2.16) in chapter 2. This implies that the channels are not assumed to be quasi-static. The circulant channel results from the addition of the cyclic prefix of length L described in section 2.2.

Next, applying the $N \times N$ DFT matrix $\mathbf{F}_N$, given by (2.6), to the received sequence we get

$$Y(k) \triangleq \mathbf{F}_N \cdot y(k) = \Lambda_1(k)X_1(k) + \Lambda_2(k)X_2(k) + N(k), \tag{3.3}$$

where $X(k) \triangleq \mathbf{F}_N \cdot x(k)$, $N(k) \triangleq \mathbf{F}_N \cdot n(k)$ and $\Lambda_1(k)$ and $\Lambda_2(k)$ are the diagonal matrices of $H_1(k)$ and $H_2(k)$, respectively. Using the properties of DFT, the terms for the $2i+1$ block can be written as

$$\begin{aligned} X_1(2i+1) &= -X_2^*(2i), \\ X_2(2i+1) &= X_1^*(2i). \end{aligned} \tag{3.4}$$

Combining (3.3) and (3.4), we get

$$\mathbf{Y} = \begin{pmatrix} Y(2i) \\ Y^*(2i+1) \end{pmatrix} = \underbrace{\begin{pmatrix} \Lambda_1 & \Lambda_2 \\ \Lambda_2^* & -\Lambda_1^* \end{pmatrix}}_{\text{quatrionic structure}} \cdot \begin{pmatrix} X_1(2i) \\ X_2(2i) \end{pmatrix} + \begin{pmatrix} N(2i) \\ N^*(2i+1) \end{pmatrix}. \tag{3.5}$$

It should be noted that the choice of the permutation matrix in (3.1) alleviates the need of post multiplying the received sequence by $\mathbf{P}$ as in [5] (also see (2.15)). It is clear, from the Alamouti-like diagonal channel matrix in (3.5), that by forming the unitary matrix ,

$$\Lambda^H \triangleq \begin{pmatrix} \Lambda_1 & \Lambda_2 \\ \Lambda_2^* & -\Lambda_1^* \end{pmatrix}^H, \tag{3.6}$$

the data sequence can be decoupled by the following unitary operation,

$$\tilde{\mathbf{Y}} \triangleq \Lambda^H \mathbf{Y} = \begin{pmatrix} \Lambda_0 & 0 \\ 0 & \Lambda_0 \end{pmatrix} \cdot \begin{pmatrix} \mathrm{X}_1(2i) \\ \mathrm{X}_2(2i+1) \end{pmatrix} + \tilde{\mathrm{N}}, \tag{3.7}$$

where $\Lambda_0 \triangleq (\Lambda_1 \Lambda_1^* + \Lambda_2 \Lambda_2^*)$ and $\tilde{\mathrm{N}} \triangleq \Lambda^H \left[\mathrm{N}(2i) \quad \mathrm{N}^*(2i+1) \right]^T$. Next we define the minimum mean square estimator (MMSE) equalizer [8] as

$$\tilde{\Lambda} \triangleq \left(\Lambda^H \Lambda + \frac{1}{\mathrm{SNR}} \mathbf{I}_{2N} \right)^{-1}. \tag{3.8}$$

The SNR at the receiver is given by $\mathrm{SNR}=\sigma_x^2 / \sigma_w^2$, where σ_w is the covariance of noise, σ_x is signal covariance. The MMSE estimate of X is then given as

$$\hat{\mathrm{X}} = \begin{bmatrix} \hat{\mathrm{X}}_1(2i) \\ \hat{\mathrm{X}}_2(2i) \end{bmatrix} = \tilde{\Lambda} \Lambda^H \mathbf{Y} = \left(\Lambda^H \Lambda + \frac{1}{\mathrm{SNR}} \mathbf{I}_{2N} \right)^{-1} \Lambda^H \mathbf{Y}. \tag{3.9}$$

3.3 Adaptive Implementation

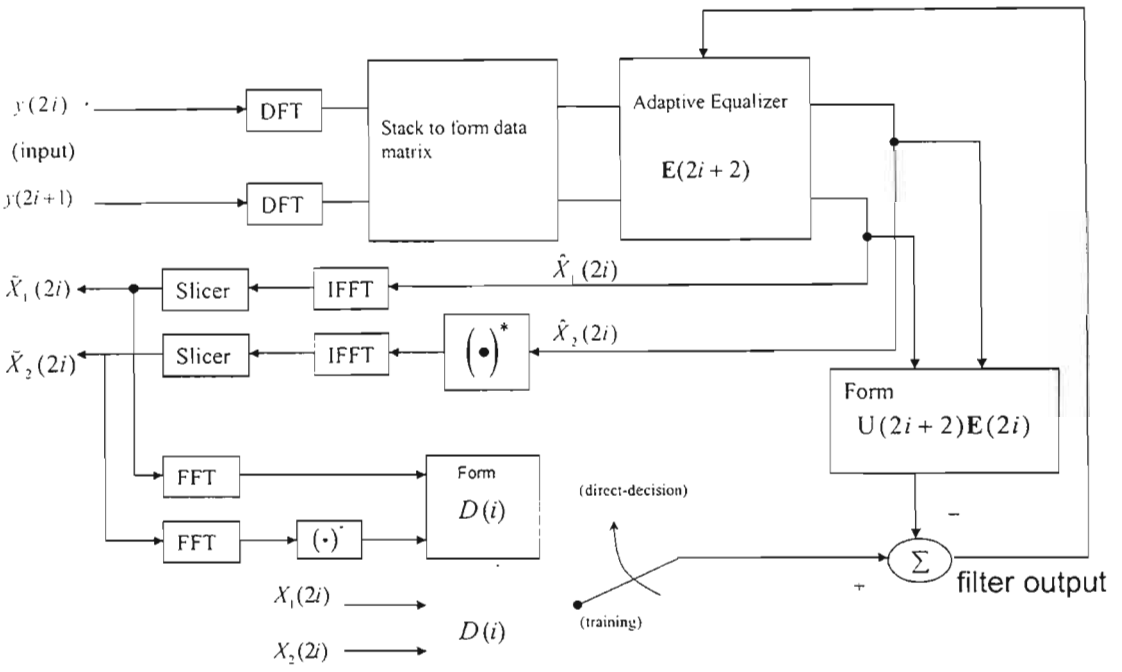

Fig. 3.1 Block diagram for the single user adaptive receiver with two-transmit one-receive antennas

The interference cancellation and equalization technique described in the previous section requires the knowledge of the channel state information (CSI) at the receiver. This is usually accomplished by the addition of training (pilot) sequence to each transmitted block in order to estimate the channel, at the expense of addition bandwidth

requirement. In order to decrease the overhead requirements, such pilot aided schemes will require longer blocks which become impractical in channels with fast variations.

Furthermore blind channel estimation based on second [11] and higher order statistics results in higher complexity and is not suitable for online implementation.

Hence the need of an online adaptive receiver under such conditions becomes imperative. The RLS algorithm provides fast tracking and, due to the special quadtronic structure of space- time block codes, the complexity can be reduce to that of an LMS algorithm. The overall adaptive receiver is shown in Fig. 3.1.

Defining the combined matrix of the MMSE in (3.9) as $\mathbf{B} \triangleq \tilde{\Lambda}\Lambda^{H}$, it can be shown that this matrix has an Alamouti (quadtronic) structure i.e.

$$\mathbf{B}=\begin{pmatrix} B_1 & B_2 \\ B_2^* & -B_1^* \end{pmatrix}, \tag{3.10}$$

where the entries of $\mathbf{B}$, the block size N ,are given by

$$\begin{aligned} B_1 &= \operatorname{diag}\left\{\frac{1}{\Lambda_0(n,n)+1/\mathrm{SNR}}\right\}_{n=0}^{N-1}\cdot\Lambda_1^*, \\ B_2 &= \operatorname{diag}\left\{\frac{1}{\Lambda_0(n,n)+1/\mathrm{SNR}}\right\}_{n=0}^{N-1}\cdot\Lambda_2. \end{aligned} \tag{3.11}$$

Hence (3.9) can be written as

$$\begin{pmatrix} \hat{X}_1(2i) \\ \hat{X}_2(2i) \end{pmatrix}=\begin{pmatrix} B_1 & B_2 \\ B_2^* & -B_1^* \end{pmatrix}\mathbf{Y}. \tag{3.12}$$

This can be rearranged into the following form.

$$\begin{pmatrix} \hat{X}_1(2i) \\ \hat{X}_2^*(2i) \end{pmatrix}=\underbrace{\begin{pmatrix} \operatorname{diag}(Y(2i)) & \operatorname{diag}(Y^*(2i+1)) \\ -\operatorname{diag}(Y(2i+1)) & \operatorname{diag}(Y^*(2i)) \end{pmatrix}}_{\text{quadtronic structure}}\cdot\begin{pmatrix} E_1 \\ E_2 \end{pmatrix}\triangleq U(i)\mathbf{E}. \tag{3.13}$$

The vectors E_1 and E_2 contain the diagonal entries of B_1 and B_2, respectively. The key point is the manner in which the quadtronic structure is maintained in the derivation (3.13), which is in the form of the RLS problem [15,16]. The adaptive RLS solution is now applied. The equalizer coefficients $\mathbf{E}$ are adaptively updated for every two blocks using the following recursion:

$$\mathbf{E}(2i+2) = \mathbf{E}(2i) + Q(2i+2)\mathrm{U}^H(2i+2)\left[\mathrm{D}(2i+2) - \mathrm{U}(2i+2)\mathbf{E}(2i)\right], \qquad (3.14)$$

where

$$\begin{aligned} &Q(2i+2) = \lambda^{-1}[Q(2i) - \lambda^{-1}Q(2i)\mathrm{U}(2i+2), \\ &\times\left(\mathrm{I}_{2N} + \lambda^{-1}\mathrm{U}(2i+2)Q(2i)\mathrm{U}^H(2i+2)\right)^{-1}\mathrm{U}^H(2i+2)Q(2i)]. \end{aligned} \qquad (3.15)$$

It is easy to see that the inverse term in (3.15) is given by a diagonal matrix

$$\left(\mathrm{I}_{2N} + \lambda^{-1}\mathrm{U}(2i+2)Q(2i)\mathrm{U}^H(2i+2)\right)^{-1} = \begin{pmatrix} \Theta(2i+2) & 0 \\ 0 & \Theta(2i+2) \end{pmatrix}. \qquad (3.16)$$

$\mathrm{D}(i)$ is referred to as the desired response and is given by,

$$\mathrm{D}(2i+2) = \begin{cases} \begin{pmatrix} \mathrm{X}_1(2i+2) \\ \mathrm{X}_2^*(2i+2) \end{pmatrix}, \text{for training} \\ \begin{pmatrix} \tilde{\mathrm{X}}_1(2i+2) \\ \tilde{\mathrm{X}}_2^*(2i+2) \end{pmatrix}, \text{for decision-direct tracking.} \end{cases} \qquad (3.17)$$

The parameters of the algorithm are initialized as follows: $\mathbf{E}(0) = 0$ and $Q(0) = \delta \mathrm{I}_{2N}$, with δ being a large number (usually $\approx 10^6$ [15]). λ is called the forgetting factor and can be in the range $[0,1]$. Using a smaller forgetting factor will result in faster convergence of the RLS algorithm. However this may result in numerical instability when dealing with systems with higher channel variations. It therefore becomes obvious that careful selection of λ is required and is further discussed in the next section.

The adaptive receiver operates in two modes. $\left[\mathrm{X}_1(2i+2) \quad \mathrm{X}_2^*(2i+2)\right]^T$ denotes the pilot block during training mode and $\left[\mathrm{X}_1(2i+2) \quad \mathrm{X}_2^*(2i+2)\right]^T$ denotes the slicer output of the received data during the decision direct mode as shown in Fig. 3.1.

$Q(2i+2)$ has the following diagonal structure.

$$Q(2i+2)=\begin{pmatrix} T(2i+2) & 0 \\ 0 & T(2i+2) \end{pmatrix}. \tag{3.18}$$

The recursive updates of $T(2i+2)$ is given by

$$T(2i+2)=\lambda^{-1}\left(T(2i)-\lambda^{-1}T(2i)\Omega(2i+2)T(2i)\right), \tag{3.19}$$

where

$$\Omega(2i+2)=\Theta(2i+2)\mathrm{diag}\left(\left|\mathrm{Y}(2i)\right|^2+\left|\mathrm{Y}(2i+1)\right|^2\right). \tag{3.20}$$

The diagonal matrix $\Theta(2i+2)$ in (3.16) is given by

$$\Theta(2i+2)=\left(\mathrm{I}_N+\lambda^{-1}T(2i)\mathrm{diag}\left(\left|Y(2i)\right|^2+\left|Y(2i+1)\right|^2\right)\right)^{-1}. \tag{3.21}$$

Hence we get

$$\Omega(2i+2)=\left[\mathrm{diag}\left(\left|\mathrm{Y}(2i)\right|^2+\left|\mathrm{Y}(2i+1)\right|^2\right)^{-1}+\lambda^{-1}T(2i)\right]^{-1}. \tag{3.22}$$

Finally the RLS equalizer is then given by

$$\begin{aligned}\mathbf{E}(2i+2)=\mathbf{E}(2i)+&\begin{pmatrix} T(2i+2) & 0 \\ 0 & T(2i+2) \end{pmatrix}\mathrm{U}^H(2i+2)\times \\ &\left[\mathrm{D}(2i+2)-\mathrm{U}(2i+2)\mathbf{E}(2i)\right].\end{aligned} \tag{3.23}$$

At first glance the RLS algorithm may appear computationally complex, due to the number of matrix inversions required in the algorithm. However, due to the quadtronic

structure of $Y(i)$ and the diagonal structure of $T(i)$, the matrix inversions in (3.21) and (3.22) are in fact scalar inversions. This results in the algorithm giving an LMS complexity. The EDGE simulation environment is used to test the performance of this adaptive receiver. The EDGE environment poses a challenging equalization problem due to the increase in data rate from the previous 2G and the presence of additional ISI due to the GMSK filter at the transmitter. However, proper documentation for this model is not provided in [5,6,8,17]. We provide the description of the EDGE simulation environment in terms of the TU channel next.

3.4 Simulation Environment

Table 3.1 A typical urban (TU) channel model

Delay (μsec)	0.0	0.2	0.5	1.6	2.3	5.0
Strength (dB)	-3.0	0.0	-2.0	-6.0	-8.0	-10

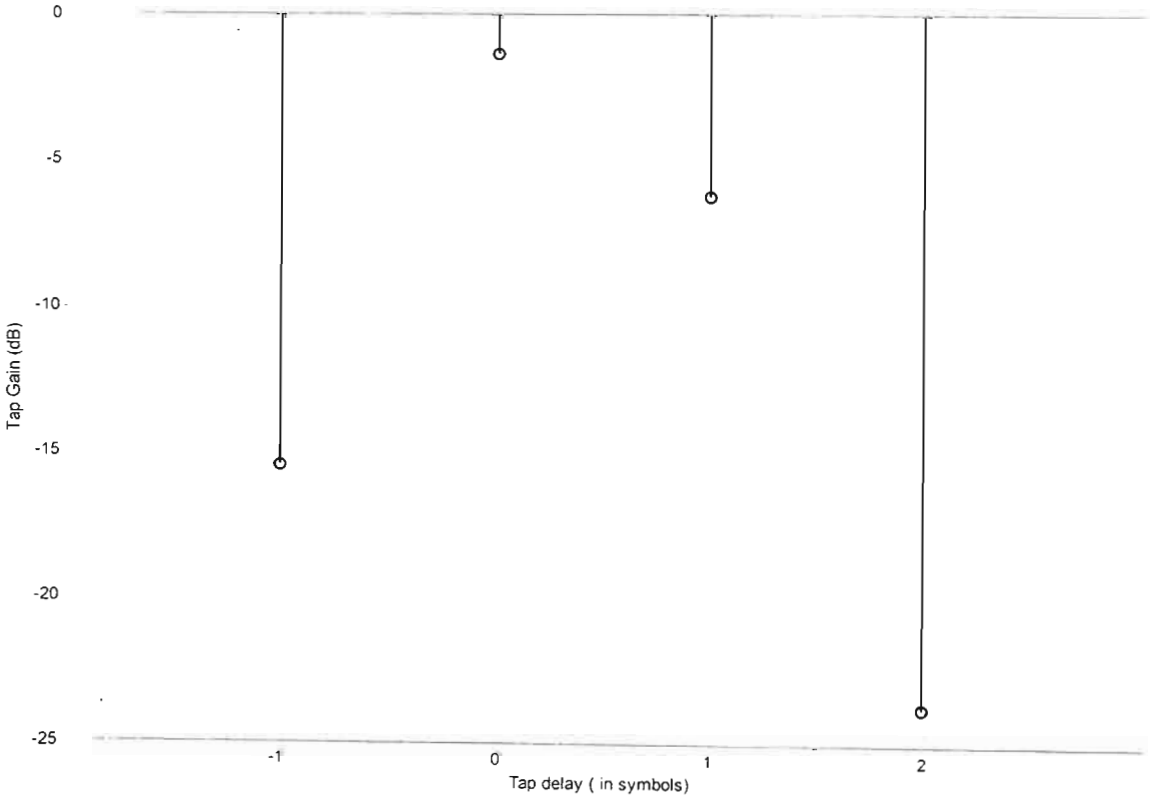

Fig. 3.2 Equivalent CIR for a TU channel with GMSK pulse shaping

The EDGE TU channel with 8-PSK modulation is considered. Equalization for EDGE poses a challenging problem due to the use of 8-PSK modulation unlike its predecessor that uses binary modulation in GSM. The TU channel impulse response generally has a non-minimum phase characteristic and the GMSK transmit filter used to combat this adds additional ISI. The delay profile of the TU channel given in [7, 8, 9] is presented in Table 3.1.

The transfer function for the GMSK filter is given by

$$h(t) = \frac{1}{\sqrt{2\pi\sigma T_s}} \exp\left[-\frac{1}{2\sigma^2} \left(\frac{1}{T_s} \right)^2 \right], \tag{3.24}$$

where a symbol duration of $T_s = 3.69\ \mu s$ and $\sigma = 0.3$ is proposed in 3rd generation TDMA cellular standard EDGE (2.5G). The overall TU channel impulse response (CIR) after GMSK pulse shaping is given is Fig. 3.2.

From Fig. 3.2, the overall channel has a length of four symbols and hence the channel memory is $L = 3$. All channels are assumed independent. The performance of the RLS algorithm is shown for different frequencies. The Jakes model is used to generate the Rayleigh fading coefficients. All taps are assumed independent and identically distributed (iid.) Gaussian.

3.5 Simulation Results

The main purpose of this section is to show a design tool that can be used to select various parameters for the RLS algorithm. Such a tool is not provided in [8]. Being consistent with the EGDE standard, each user has two transmit antennas with 8-PSK constellation. A data rate of 271kSymbol/sec is used. The effect of varying the Doppler frequency, re-training rate and block size are discussed in subsections 3.5.1 and 3.5.2. The forgetting factor, λ, is set to 0.95 for these two subsections. We use the same settings in [8] for the simulation to verify that our results match that in [8]. In 3.5.3, we investigate the effect of varying λ which is also not provided in [8].

3.5.1 The Effect of Doppler Frequency

Fig. 3.3 shows the performance of the RLS algorithm at different Doppler frequencies as compared to the system with perfect CSI. A data block size of 32 symbols plus three cyclic prefix symbols is used. The algorithm is re-trained after 50 data blocks. These are the same parameters that are used in [8,9]. Our simulation results are the same as the results presented in [8,9]. This also implies that the channel model described in section 3.4, and used for the simulations in [8] is correct.

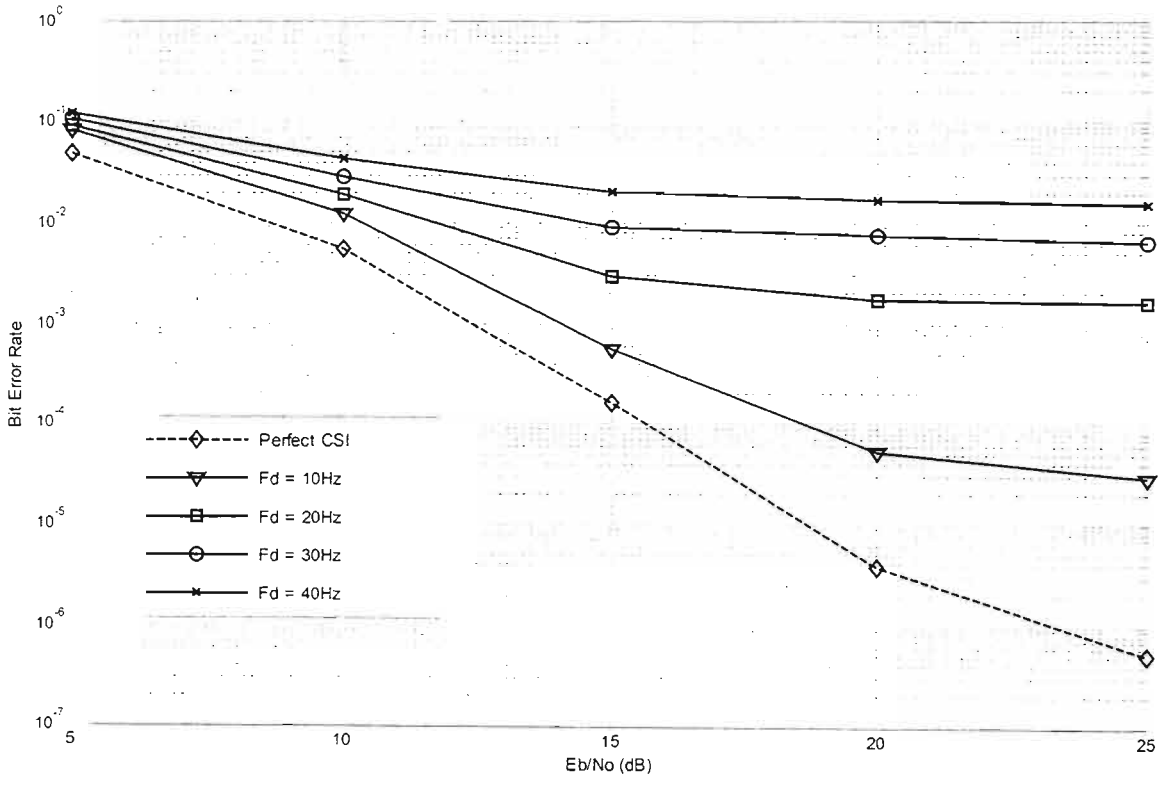

Fig. 3.3 Effect of Doppler frequency on the performance of RLS algorithm.

From Fig. 3.3 it is clear that the gap between the result for the algorithm and that of perfect CSI decreases as the Doppler frequency decreases. This shows that the algorithm suffers in channels with faster variations. For example, in Fig 3.3, the performance penalty when comparing a frequency of 40Hz and 10Hz is considerable and a more robust algorithm is clearly desired.

The RLS implementation of the linear MMSE receiver suffers from the following numerical problem [14]. The recursive estimates of $\Theta(i)$ and $\Omega(i)$ in (3.21) and (3.22),

respectively, contain the inversion square of the received data matrix $Y(i)$. From the two equations, the condition number is the square of the condition number of the received data matrix and hence twice the dynamic range is required in numerical computation. A solution to decrease the dependence on the condition number is described in chapter 5. The next subsection describes the effect of varying the retraining frequency and block size on the overall system performance.

3.5.2 The Effect of Re-training Interval and Block Size

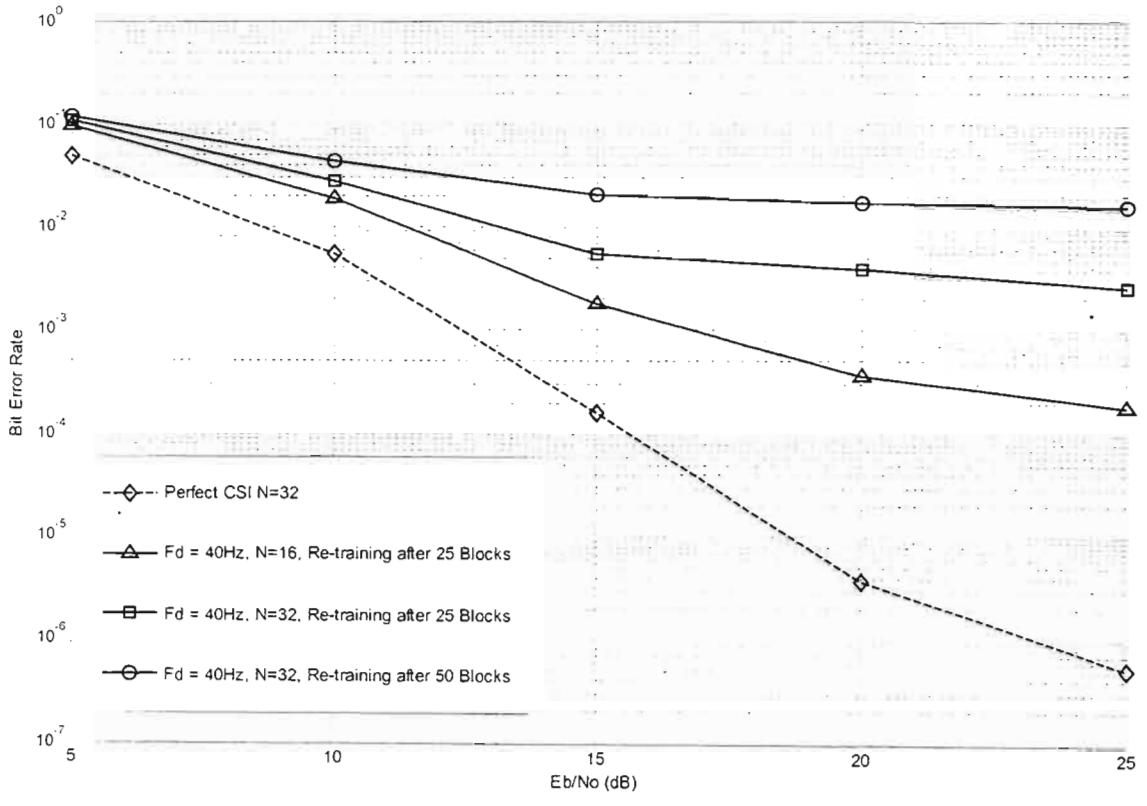

Fig. 3.4 Effect of block size and re-training interval

A smaller re-training interval implies that the pilot block is sent more frequently. This prevents the algorithm from converging and hence gives better performance. However, this also means that more bandwidth is used for the pilot blocks and this makes the system more bandwidth inefficient. A larger block length implies that the block is more prone to deep fades and hence degrades the performance of the system.

By decreasing the block length and decreasing the re-training interval, the performance of the adaptive receiver is improved drastically as shown in Fig. 3.4. With the Doppler

frequency set to 40 Hz, it can be seen that the performance gap of the RLS system and the perfect CSI system decreases as the re-training interval and the block size are decreased. Once again the same parameters as [8,9] are used to verify the simulation results.

It can be concluded that at higher channel variations a smaller block size with smaller re-training interval is required. Finally the effect of the forgetting factor, λ, that was not properly described in [8] is given in the next subsection.

3.5.3 The Effect of the Forgetting Factor

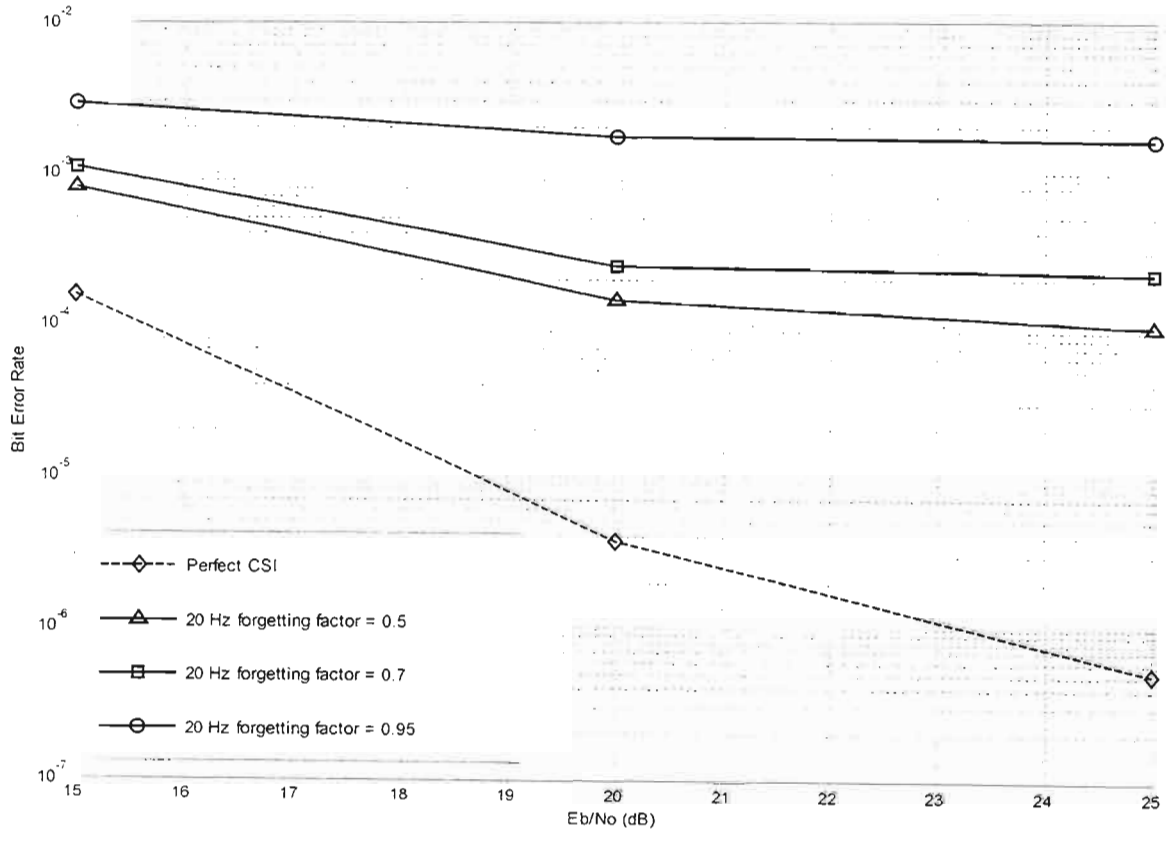

Fig. 3.5 Effect of forgetting factor

Fig. 3.5 shows the effect of varying the forgetting factor, λ. For the simulation, the block size and Doppler frequency was set to 32 symbols and 20 Hz, respectively. λ was varied between the values of 0.95, 0.7 and 0.5. It can be seen that there is a significant improvement when varying λ from 0.95 to 0.7. However the change in performance decreases significantly between 0.7 and 0.5. Furthermore, a smaller

forgetting factor causes numerical instability of the RLS algorithm and results in degraded performance in channels with larger variations [23]. This implies that a decrease in the forgetting factor at higher Doppler frequencies can result in degradation of performance.

3.6 Concluding Remarks

The adaptive receiver for space-time block–coded transmissions has been discussed for the single user case. The receiver does not require CSI. By using the system with perfect CSI as a bench mark, a method of optimizing various parameters such as block size, re-training frequency and forgetting factor has been shown. Therefore, depending on the channel variations present and performance required, values for these parameters can be designed using the perfect CSI result as a bench mark. Furthermore, the effect of varying the forgetting factor which is not provided in [8] is also given in 3.5.3.

From the results, there are two main problems associated with the RLS algorithm. As seen in section 3.5.2, it is clear that the RLS algorithm requires a smaller re-training interval to achieve better performance at the expense of additional bandwidth. In the next chapter, by using a linear predictor and assuming the knowledge of the Rayleigh autocorrelation function at the receiver, a new bandwidth efficient receiver is proposed. By decreasing the number of symbols required in the pilot block, better performance is achieved using the same effective pilot size. Simulation results also show that the performance penalty of the linear predictor is negligible.

As seen in section 3.5.1, the performance of the RLS receiver at higher Doppler frequencies motivates the need for a more robust algorithm. Added to the numerical problems of the RLS algorithm, the form of the recursive updates limits the parralism and pipelining that can be implemented for the system [14]. These problems are overcome using a rotation based QR receiver in chapter 5. This receiver provides a more robust solution.

CHAPTER 4

A NEW LINEAR PREDICTION BASED RLS RECEIVER FOR BETTER PERFORMANCE

4.1 Introduction

In wireless communications, the frequency spectrum is a limited resource and motivates the need to preserve this resource in an efficient manner. In chapter 3, the conservation of bandwidth by the RLS based adaptive receiver is achieved in annihilating the requirement of a preamble in every block transmission. Hence, this scheme has a clear advantage over other pilot-aided schemes that require pilot symbols in every block transmission.

However, during the so called training period, the adaptive receiver sends an entire block of pilot symbols before it switches to the direct-decision mode of the RLS algorithm. Provided that the re-training interval is sufficiently large, the bandwidth used up by the pilot block is not significant. The simulation results in chapter 3 shows that decreasing the re-training interval increases the performance of the receiver. Hence there is a trade-off between the performance gain required and the bandwidth available for the additional overhead.

This motivates the need to decrease the re-training interval of the receiver without the additional requirement of extra pilot symbols. In this chapter, we present a method to decrease the pilot symbols required during the re-training interval. This is based on a forward linear predictor algorithm that uses the autocorrelation function of the channel. The autocorrelation function for several channel models is well documented [18, 19] making such an algorithm a practical option. Using this knowledge, the predictor coefficients for the algorithm are derived. Using a forward prediction, the coefficients of the channel are then derived.

The rest of the chapter is organized as follows. Section 4.2 provides a brief survey on the various prediction algorithms that are available, and quantifies the selection of the linear predictor algorithm for our application. In section 4.3, we introduce the linear

predictor algorithm [15, 16] that is used to make a forward prediction on the channel coefficient values. We present the continuous time channel model and the Rayleigh fading autocorrelation function in terms of the Jakes model in section 4.4. The Wiener-Hopf equation is then derived. The solution to the Wiener-Hopf equation is the predictor coefficients that are used in the linear predictor algorithm. In section 4.5, the overall RLS receiver with linear prediction is described. The simulation results are given in section 4.6. We show that the addition of the linear prediction results in negligible performance penalty. It is also shown that, by using the same effective number of pilot symbols for the new system, the performance is improved. Finally conclusions are drawn in section 4.7.

4.2 Overview of Prediction Algorithms

For stationary inputs, the optimum solution to minimize the mean square error (MSE) of the error signal is known as the Wiener filter. The design of a Wiener filter requires a priori information about the statistics of the data to be processed. The optimum Wiener filter is derived only when the statistical characteristics of the input data match the a priori information on which the design of the filter is based. When this information is not known, the design of the filter may no longer be optimum. Under such conditions, an estimate and plug procedure is required [15]. This results in a two stage process where by the filter first estimates the statistical properties and then plugs the estimates into a non-recursive formula for computing the filter parameters.

The Levison-Durbin [15] recursion computes the prediction-error filter coefficients and prediction-error power by solving an augmented normal equation. The method is recursive in nature and makes particular use of the Toeplitz structure of the filter tap inputs correlation matrix. More specifically, explicit knowledge of the autocorrelation function of the input process and reflection coefficients [15] is required. The estimation of the reflection coefficients can be obtained directly from the autocorrelation function of the input process.

The Lattice predictor combines the forward and backward prediction-error filtering operations into a single structure. The lattice predictor consists of a number of stages connected in cascade, with each stage in the form of a lattice, hence, the name. The number of lattice stages in the filter corresponds to the order of the filter. Like the

Levison-Durbin recursion, this algorithm also computes the forward and backward error predictions recursively.

However, in context of the estimation problem, the initial forward samples of the channel coefficients can be obtained using a shortened pilot sequence at the start of the training block. In order to implement the above two algorithms, a post-amble at the end of the training block is required to perform the backward prediction. To reduce the post-amble requirement and algorithm complexity, we pursue a forward linear predictor algorithm by limiting the number of pilots sent in the same way as [19]. Provided that the autocorrelation function for the fading model is known, the linear predictor provides a good solution for the Wiener filter. The simulation results in section 4.6.1 show that the performance penalty is negligible and hence the performance improvement of using a more complex algorithm will be minimal.

4.3 Overview of Linear Prediction

4.3.1 Preliminary Definitions

This section provides a summary of the forward linear predictor algorithm [15], [16]. Consider the time sequence $\begin{bmatrix} h(0) & h(1) & \cdots & h(M-1) \end{bmatrix}$. The forward linear prediction of order (window size) M is given by:

$$\begin{aligned} \hat{h}(n) &= c_1 h(n-1) + c_2 h(n-2) + \cdots c_M h(n-M) \\ &= \sum_{k=1}^{M} c_k h(n-k) = \underline{c}^T \underline{h}(n-1), \end{aligned} \tag{4.1}$$

where $\underline{h}(n-1) \triangleq \begin{bmatrix} h(n-1) & h(n-2) & \cdots & h(n-M) \end{bmatrix}^T$ is the regression vector. The forward predictor vector of order M is given as

$$\underline{c} = \begin{bmatrix} c_1 & c_2 & \cdots & c_M \end{bmatrix}^T. \tag{4.2}$$

The forward prediction error is given by [15]

$$\begin{aligned} f_M(n) &= h(n) - \hat{h}(n) \\ &= h(n) - \underline{c}^T \underline{h}(n-1). \end{aligned} \tag{4.3}$$

If we let

$$\begin{aligned}\underline{a}_M &= \begin{bmatrix}1 & -c_1 & -c_2 & \cdots & -c_M\end{bmatrix}^T \\ &= \begin{bmatrix}a_{M,0} & a_{M,1} & a_{M,2} & \cdots & a_{M,M}\end{bmatrix}^T,\end{aligned} \tag{4.4}$$

then (4.3) can be written as

$$\begin{aligned}f_M(n) &= \underline{a}_M^T \begin{bmatrix} h(n) \\ \underline{h}(n-1)\end{bmatrix} \\ &= \underline{a}_M^T \underline{h}(n).\end{aligned} \tag{4.5}$$

The autocorrelation matrix is given by

$$\begin{aligned}R &= E\left[\underline{h}(n-1)\underline{h}^T(n-1)\right] \\ &= E\left[\begin{bmatrix} h(n-1) \\ h(n-2) \\ \vdots \\ h(n-M)\end{bmatrix}\begin{bmatrix}h(n-1) & h(n-2) & \cdots & h(n-M)\end{bmatrix}\right] \\ &= \begin{bmatrix} E[h(n-1)h(n-1)] & E[h(n-1)h(n-2)] & \cdots & E[h(n-1)h(n-M)] \\ E[h(n-2)h(n-1)] & E[h(n-2)h(n-2)] & \cdots & E[h(n-2)h(n-M)] \\ \vdots & \vdots & \ddots & \vdots \\ E[h(n-M)h(n-1)] & E[h(n-M)h(n-2)] & \cdots & E[h(n-M)h(n-M)]\end{bmatrix} \\ &= \begin{bmatrix} r(0) & r(1) & \cdots & r(M-1) \\ r(1) & r(0) & \cdots & r(M-2) \\ \vdots & \vdots & \vdots & \vdots \\ r(M-1) & r(M-2) & \cdots & r(0)\end{bmatrix}.\end{aligned} \tag{4.6}$$

The autocorrelation vector can hence be defined as

$$\begin{aligned}\underline{r} &\triangleq E\left[\underline{h}(n-1)h(n)\right] \\ &= \begin{bmatrix}r(0) & r(1) & r(2) & \cdots & r(M-1)\end{bmatrix}.\end{aligned} \tag{4.7}$$

Let $\underline{r}^B \triangleq \begin{bmatrix}r(M-1) & r(M-2) & r(M-3) & \cdots & r(0)\end{bmatrix}$. We will use this definition in the next section.

4.3.2 Optimal MMSE Forward Linear Prediction

If we define the prediction error of order M in (4.3), the optimality criterion for the linear predictor algorithm in a MMSE sense [15] is given by

$$J(\underline{c}) = E\left[\left|f_M(n)\right|^2\right] = E\left[\left|h(n) - \underline{c}^T \underline{h}(n-1)\right|^2\right]. \tag{4.8}$$

From this, we get the optimal solution for the predictor coefficients in (4.1) as

$$\underline{c}_0 = R^{-1}\underline{r}^B, \tag{4.9}$$

which is the solution to the Wiener-Hopf equation. In the next section, we give a brief explanation of the Rayleigh channel and provide the autocorrelation function for this model. We then apply this to the Wiener-Hopf equation in (4.9).

4.4 Continuous Time Channel Model

The received signal for the Rayleigh frequency-flat fading channel is modelled as:

$$r_c(t) = \mathrm{Re}\left\{v(t)h(t)\sqrt{2}\exp\{j2\pi f_c t\}\right\} + n_c(t), \tag{4.10}$$

where $v(t)$ is the transmitted low pass signal, $n_c(t)$ is the AWGN noise, $h(t)$ is the continuous-time fading process and f_c is the phase of the fading process. The fading process is modelled as a zero-mean, wide-sense stationary, complex Gaussian random process. The amplitude $|h(t)|$ has a Rayleigh distribution. The phase of the fading process, which represents the carrier phase error, is uniformly distributed over $[0, 2\pi)$. The fading process is a time variant process which makes the fading estimation problem a difficult one. Added to this is the fact that the amplitude, $|h(t)|$, can have a small value for extended periods of time (this represents a deep fade). Assuming the fading process is correlated in time, the autocorrelation function is given as:

$$\phi_{h'}(\Delta t) \triangleq \frac{1}{2}\mathbf{E}\left[h^*(t-\Delta t)h(t)\right]. \tag{4.11}$$

A commonly used model to represent the land mobile fading process is the Jakes model [18]. The autocorrelation function for this model is given as:

$$\phi_{h}(\Delta t) = \frac{1}{2} J_0(2\pi B_d \Delta t), \tag{4.12}$$

where $J_0(\cdot)$ is the order zero Bessel function of the first kind, and B_d is the Doppler spread of the channel. Other known models include the first and second-order Butterworth fading models [19].

4.5 Applying Linear Prediction to the RLS Algorithm

The M^{th}-order linear forward predictor for the channel coefficients is given by [19]:

$$\hat{h}_n \triangleq \frac{1}{\varepsilon_s} \sum_{n=0}^{M-1} c_n^* h_{n-1}, \tag{4.13}$$

where $\hat{h}_n$ is the channel coefficients, c_n is the predictor coefficients and ε_s is the normalized energy for the channel. The predictor coefficients are the solution to the Wiener-Hopf equation given by:

$$\begin{bmatrix} \varepsilon_s\phi_F(0) & \varepsilon_s\phi_F(1) & \cdots & \varepsilon_s\phi_F(N-1) \\ \varepsilon_s\phi_F(1) & \varepsilon_s\phi_F(0) & \cdots & \varepsilon_s\phi_F(N-2) \\ \vdots & \vdots & \ddots & \vdots \\ \varepsilon_s\phi_F(N-1) & \varepsilon_s\phi_F(N-2) & \cdots & \varepsilon_s\phi_F(0) \end{bmatrix} \cdot \begin{bmatrix} c_0 \\ c_1 \\ \vdots \\ c_{N-1} \end{bmatrix} = \begin{bmatrix} \varepsilon_s\phi_F(N) \\ \varepsilon_s\phi_F(N-1) \\ \vdots \\ \varepsilon_s\phi_F(1) \end{bmatrix}, \tag{4.14}$$

where and $\phi_F(n)$ is as defined in (4.12). The size of the window must be at least greater than or equal to the length of the channel. For each given tap, we need to get $L+1$ previous values. Hence we send a pilot sequence of at least length $L+1$. We consider the previously used example of two antennas and one receive antenna considered in chapters 2 and 3. Let the channel impulse response be given by:

$$\mathrm{H}_{\mu} = \begin{bmatrix} h_{1..\mu} & \cdots & h_{L-1..\mu} & 0 & 0 \\ 0 & \ddots & \cdots & \ddots & \vdots \\ 0 & \cdots & h_{1..\mu} & \cdots & h_{L-1..\mu} \end{bmatrix} \quad \forall\ \mu = 1,2. \tag{4.15}$$

The received sequence given in (3.2) can be re-written as

$$Y=\underbrace{\begin{bmatrix} x_1 & x_2 \\ -\mathbf{P}x_2^* & \mathbf{P}x_1^* \end{bmatrix}}_{X}\underbrace{\begin{bmatrix} H_1 \\ H_2 \end{bmatrix}}_{H}+\begin{bmatrix} n_1 \\ n_2 \end{bmatrix}. \tag{4.16}$$

In training mode, the algorithm proceeds as follows. Ignoring the noise components we get

$$Y=X\cdot H, \tag{4.17}$$

where X and H are as defined in (4.16). Since the pilot sequence is known, the matrix X is reconstructed at the receiver. The length of the pilot sequence corresponds to the window size of the linear predictor. If the channel length is given by L, then $M > L$. The zero forcing (ZF) solution for the two channels is given by [5]:

$$H=\begin{bmatrix} H_1 \\ H_2 \end{bmatrix}=\left(X\cdot X^H\right)^{-1}\cdot\left(X^H\right)\cdot Y. \tag{4.18}$$

It must be noted, that there are no DFT and IDFT operations for the training period. Hence, the tap components required for the initial window of the linear estimator are retrieved. The algorithm then switches to direct-decision mode which has the DFT and IDFT operations. We define the diagonal matrices as

$$\begin{aligned} \Lambda_1 &\triangleq F_N F_N^* \tilde{H}_1, \\ \Lambda_2 &\triangleq F_N F_N^* \tilde{H}_2, \\ \Lambda_0 &\triangleq (\Lambda_1\Lambda_1^* + \Lambda_2\Lambda_2^*), \end{aligned} \tag{4.19}$$

where $\tilde{H}_1$ and $\tilde{H}_2$ represent circulant channel matrices. The tap values, and hence the circulant matrices $\tilde{H}_1$ and $\tilde{H}_2$, are then estimated for the next block using (4.13), with the predictor coefficients for the previous window of size M already defined. The diagonal matrices are then derived using (4.19).

Using (3.11) in chapter 3, we can solve for the channel matrix entries B_1 and B_2, and hence solve for the channel vector $\mathbf{E}$ in (3.13).

To summarize, the algorithm is implemented as follows:

1. The shortened pilot stream is sent and using $H=[H_1 \quad H_2]=(X\cdot X^H)^{-1}\cdot(X^H)\cdot Y$ the initial estimates of the channel taps are updated.
2. The linear predictor then estimates the channel coefficients for the next block using (4.13). Hence we update H_1 and H_2.
3. By solving Λ_0 in (4.19) and B_1 and B_2 (3.11), the vector channel vector, **E** in (3.13), is updated. The values of $\Omega(i)$ and $T(i)$ in (3.22) and (3.20), respectively, are then updated.
4. The RLS algorithm then switches to direct decision mode, until it is re-trained again.

The pilot requirement for the system is therefore decreased to the predefined window size M. By doing this, the system performance can be improved in the following two ways:

- Provided that addition of the LP does not incur any performance loss, the new system has a greater throughput than the old system without linear prediction. This is because, although the frame error rate (FER) for the new system is the same as the old system, the decrease in pilot requirements increases the overall data sent. Such an improvement in performance is called bandwidth efficiency.

- It has already been proven in [7] that by decreasing the re-training interval for an adaptive algorithm, the overall performance in terms of FER improves. By decreasing the pilot required during each re-train, the re-training interval can be decreased to get the same number of pilots used up as the system without linear prediction. Hence the overall system performance in terms of FER is improved.

Next, we present the simulation results for the modified RLS algorithm that includes the linear predictor. The main objective of the simulations is to verify that there is no significant performance loss incurred by using the linear predictor. Provided that there is no performance loss, we are able to increase the re-training interval while still

maintaining the same effective number of pilot symbols. This is once again shown in the simulation results.

4.6 Simulation Results

For the simulations, the same EDGE simulation environment with GMSK pulse shaping and 8PSK constellation described in chapter 3 is used. The channel memory L is set to 3.

4.6.1 Performance Penalty

The initial set of simulation results are done to show if there is any performance loss incurred by using the new system with linear prediction. The original RLS receiver is set with frequencies of 10 Hz and 40 Hz. The block size of 32 symbols is used. The re-training interval is set to 50 blocks in both cases and the window size of the linear predictor, M, is set to 10 blocks. The new receiver with the linear predictor is also set with the same frequencies and re-training interval.

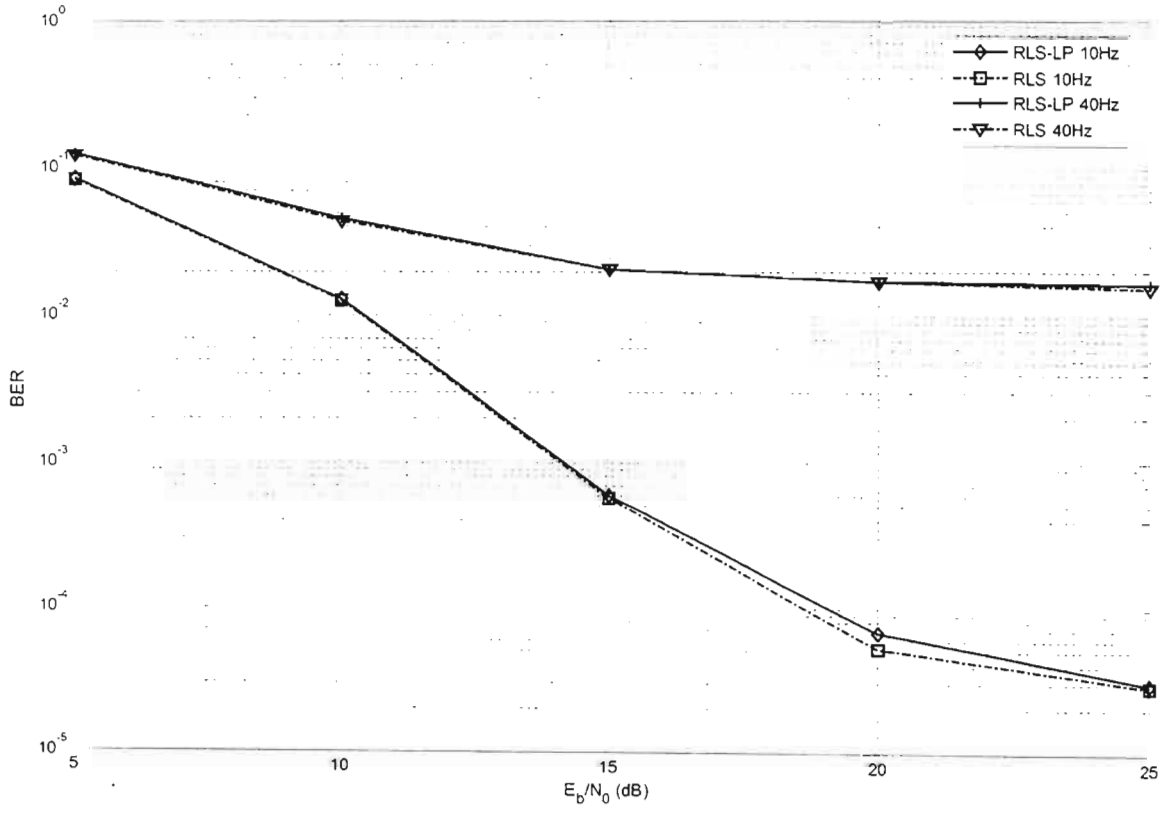

Fig. 4.1 Comparison of performance penalty with the linear predictor

Fig. 4.1 shows that the performance penalty incurred is negligible, hence making this an attractive method of improving the overall performance of the adaptive receiver. The autocorrelation function in (4.12) is an accurate model for the Rayleigh fading process used. It is shown in [16] that the forward linear predictor performance is dependant on accuracy of the autocorrelation function. This is the reason why the performance penalty is minimal.

4.6.2 Performance Using Equivalent Pilot Symbols

The linear predictor decreases the overhead required by the system during the training period of the algorithm. Fig. 4.2 shows the RLS algorithm with the training period that requires an entire block of pilot symbols as compared to the new receiver with linear prediction that shortens this requirement.

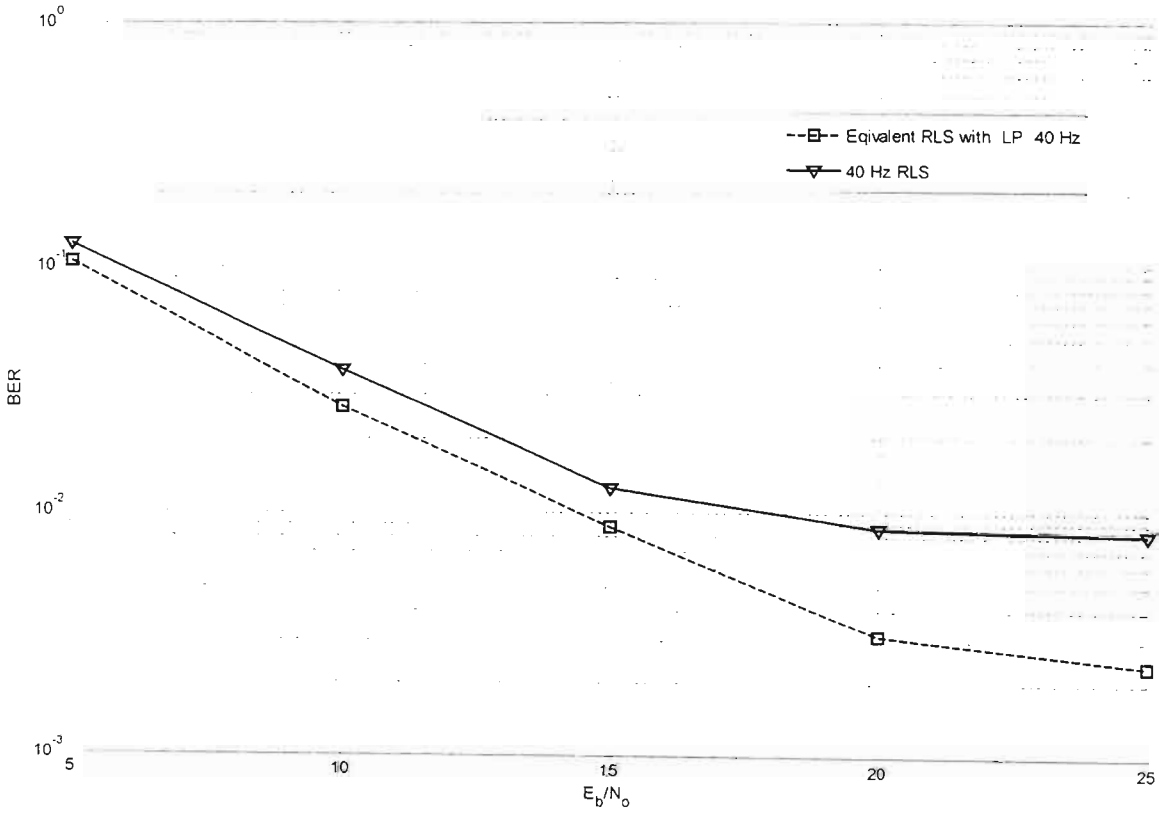

Fig.4.2 Performance of the linear predictor with equivalent number of pilot symbols

The block size of 40 symbols and Doppler frequency of 40Hz are used. The re-training interval is set to 40 blocks. The window size for the linear predictor is set to 10. In order to use the equivalent number of pilot symbols, the re-training interval is decreased to 10

blocks for the new system. From section 3.4 of chapter 3, it was concluded that increasing the retraining interval increases the overall system performance and this is demonstrated in the results shown in Fig. 4.2. Therefore, using the linear predictor improves the performance of the adaptive receiver without the additional bandwidth requirement. From these results, an adjustment of the window size for the linear predictor can result in better performance as the re-training interval can be decreased further. Since $M > L$, the knowledge of the channel length is required for this as it limits the window size that can be used.

4.7 Concluding Remarks

We have described a bandwidth efficient method of improving the overall system performance for the adaptive RLS receiver. The linear predictor decreases the number of pilot symbols that are required during the re-training period. Hence, the re-training interval can be decreased which results in the improved performance. The simulation results also show that there is no additional penalty when using the linear predictor making it an attractive scheme. The only requirement at the receiver is that the knowledge of the autocorrelation function for the channel is known. If the channel length can be estimated, as shown in [23], then the algorithm can be modified to adjust the window size of the linear predictor accordingly.

The robust property of the RLS algorithm with LP presented in this chapter is the same as the RLS receiver discussed in chapter 3. In the next chapter, we introduce a QR based approach that provides a more stable solution. By combining the QR based receiver with the linear predictor algorithm described in this chapter, a new bandwidth efficient and robust receiver is derived.

CHAPTER 5

QR-BASED RECEIVER WITH LINEAR PREDICTION FOR MORE ROBUST AND IMPROVED PERFORMANCE

5.1 Introduction

In the last two chapters, the adaptive receiver based on the recursive least squares (RLS) solution has been applied together with the unique quadtronic structure of space time codes to create a receiver capable of tracking a non-stationary (time-selective) and frequency selective channel. Although the original scheme proposed in [8] is bandwidth efficient in that it does not require the inclusion of pilot symbols in every block, the two key problems identified are as follows:

- There is still the requirement of an entire block of training data to initialize the RLS algorithm.
- The RLS algorithm is not robust particularly at high Doppler frequencies where there is a significant performance penalty. This is evident from the results given in chapter 3, section 3.5.1.

The size of the training data is drastically reduced by including the linear predictor (LP) discussed in chapter 4. The RLS algorithm achieves a good steady-state performance in a stationary environment as shown in [23]. However, when the system of equations is not sufficiently well conditioned, the performance of the algorithm deteriorates significantly [16]. This motivates the search for a more robust algorithm that is not affected to the same extend by the ill conditioned channel. The rest of this chapter is organized as follows:

Section 5.2 gives a brief literature survey on the various algorithms that are available. In section 5.3 we introduce the QR transformation and provide the properties of this algorithm that motivates its use in the adaptive receiver. In section 5.4, we provide a

brief description of the Givens rotation that is used to implement the QR decomposition (QRD). Section 5.5.1 describes how the QRD is used to modify the existing receiver to a more robust receiver. In section 5.5.2, the new proposed QRD receiver is combined with the linear predictor described in chapter 4. This increases the bandwidth efficiency of the QRD receiver. Section 5.6 provides simulation results. The results show the superior performance that the new QRD receiver has over the previous RLS based adaptive receiver at high Doppler frequencies. Finally conclusions are drawn is section 5.7. To aid the reader, we provide a few definitions that are used throughout this chapter next.

Key definitions:

Filtering: The extraction of information about a quantity of interest at time t by using data measured up to and including time t.

Wiener filter: For the stationary inputs, the optimum solution to minimize the MSE of the error signal is known as the Wiener filter.

Rate of convergence: The number of iterations required for the algorithm, in response to stationary input, to converge to the optimum Wiener solution.

Misadjustment/estimation error: This is the measure of the deviation of the final MSE for an algorithm from the MMSE that is produced by the Wiener filter.

Robustness: The ability of the algorithm to operate satisfactorily with ill conditioned input data.

Stationary process (wide sense): a random process where all of its statistical properties (mean, correlation) do not vary with time. Processes whose statistical properties do change are referred to as **non-stationary**.

Tracking/transient performance: Provides information about stability and convergence rate of an adaptive filter.

Steady-state performance: Provides information about the mean-square-error of the filter once it reaches steady state.

Ill-Conditioned matrix: Matrix that is close to be rank deficient.

Condition number: The condition number for a matrix A is defined as

$$\kappa(A) = \|A\|\|A^{-1}\|. \tag{5.1}$$

A large condition number implies the matrix is ill-conditioned.

Smoothing: When information about data at time t is not available, smoothing refers to the utilization of data later than time t to obtain this information.

5.2 Overview of Adaptive Algorithms

In [28], it is shown that the convergence behaviour of the RLS algorithm is faster than the least mean squares (LMS) algorithm and is not sensitive to variations in the eigenvalue spread of the input correlation matrix. However, in a non-stationary environment, the adaptive filter has the additional task of tracking statistical variations in the environmental conditions. The LMS algorithm exhibits better tracking behaviour than the RLS algorithm and in general, good convergence behaviour does not imply good tracking behaviour.

Although the RLS algorithm is a special case of the Kalman filter, with the latter being the optimal linear tracking device, the exponentially weighted RLS algorithm has not inherited this good tracking behaviour. It is stated in [28] that the reason for this lies in that fact that by incorporating the weighting function in the cost function, the transition matrix effectively becomes a constant which is not conducive in solving non-stationary problems.

In [27] the sign algorithm is shown to have several advantages over the RLS algorithm such as simplicity, high robustness and convenient tracking properties. An extended version of the RLS algorithm (ERLS) is also proposed in [28].

However, both of these adaptive techniques are designed for exponential a forgetting window which smoothes signal variations and thus allow low-complexity update at each step. However, this is only suitable for slowly varying signals.

The singular value decomposition (SVD) algorithm [16] is traditionally used for subspace estimation. In adaptive filtering, this algorithm usually leads to computationally demanding algorithms. In [29], a new sliding window adaptive SVD algorithm base on bi-orthogonal iteration approach is proposed. The complexity still remains demanding and the sliding window approach presented in [29] is not suitable for block level transmission.

The QR based decomposition is a well documented orthogonal transformation that is used in order to prevent a large dependence on the condition number. Such an algorithm provides a more stable solution at higher Doppler frequencies.

The conventional QR decomposition recursive least squares (QRD-RLS) method requires the order of $O(m^2)$ multiplications per output sample [15]. A number of fast QRD-RLS algorithms have been proposed in [22], [30] and [31]. The fast QR-RLS algorithms based on backward error, are well known for their good numerical behaviour and low complexity. These algorithms can be classified based on the type of triangularization applied to the input data matrix (upper or lower triangular) and type of error vector (a posteriori or a priori errors). However, once again the stacking/windowing operation that is shown in equations (3-5) of [22] becomes unrealistic in block level signal processing as each entry within the stack will represent a block of data.

In order to use the QR based decomposition for robust performance at high Doppler frequencies that can be implemented using block level signal processing, we pursue a QR solution based on the LMS problem. There is no stacking required for this algorithm. We will now describe the properties of the QRD that makes it a good solution in order to improve the overall robustness of the system.

5.3 Important Properties of QR Decomposition

In chapter 3, it was shown that the RLS algorithm achieves the best steady-state performance in a stationary environment. However, when the systems of equations are not sufficiently well conditioned, the performance of the algorithm deteriorates significantly. We therefore use the QRD to improve the system performance under such conditions. The most important application of QR is to the full rank least-squares problem which is defined as follows:

$$A\mathbf{x} = \mathbf{b}. \tag{5.2}$$

The solution $\hat{\mathbf{x}}$ that minimizes the performance index $\|A\hat{\mathbf{x}} - \mathbf{b}\|^2$ is given in [21] as:

$$\hat{\mathbf{x}} = \left(A^H A\right)^{-1} A^H \mathbf{b}. \tag{5.3}$$

However the condition number of $A^H A$ is the square of the condition number of A. Hence direct computation is usually not advisable. The advantage of using QRD lies in the fact that computing $A^H A$ requires a good dynamic range capability; essentially double the word size for a fixed-point representation in order not to be affected by an increase in the condition number. Next we define the Q and R in QR decomposition.

In QR decomposition, an $m \times n$ matrix A is written as

$$A = QR, \tag{5.4}$$

where Q is an $m \times m$ unitary matrix and R is upper triangular $m \times n$. The QR factorization divides the problem $A\mathbf{x} = \mathbf{b}$ into two sub-problems defined as:

$$\begin{aligned} Q\mathbf{y} &= \mathbf{b}, \\ R\mathbf{x} &= \mathbf{y}. \end{aligned} \tag{5.5}$$

Given that $\mathbf{y} = Q'\mathbf{b}$ and R is upper triangular, then both equations in (5.5) are solvable. Since Q is orthogonal, $\|Q\| = 1$ and $\|Q^{-1}\| = \|Q^T\| = 1$. This implies that $\text{cond}(Q) = 1$, for orthogonal matrices.

Since $\text{cond}(A) \geq 1$ for any matrix, this result implies that orthogonal transformations are more stable. Given that A is regular, then

$$\begin{aligned} \|A\| &= \|Q\|\|R\|, \\ \|A^{-1}\| &= \|R^{-1}\|\|Q^{T}\|. \end{aligned} \tag{5.6}$$

Hence,

$$\text{cond}(A) = \text{cond}(QR) = \text{cond}(R). \tag{5.7}$$

In summary, orthogonal transformations are stable and should be used whenever applicable. There are several ways of computing the QR factorization. These include the Gram-Schmidt algorithm, modified Gram-Schmidt algorithm, the Householder transformations and Givens Rotations [16]. The latter two algorithms are the most common methods [21]. The Householder transformation is a computationally faster algorithm. The Givens rotation is more accurate however and is hence used in our system. Next, a brief description of this algorithm is provided.

5.4 The Givens Rotation Algorithm

The Gram-Schmidt procedure is defined as the sequence of multiplications of A from the right by upper triangular matrices. However, this form of multiplication is not ideal to cater for the ill-conditioning problem. This is illustrated next. The Gram-Schmidt procedure is defined as

$$AR_1R_2 \cdots R_n = Q, \tag{5.8}$$

where R_i, $i = 1, \cdots n$ are the successive upper triangular matrices. Inverting the R_i matrices, we get

$$A = QR. \tag{5.9}$$

The condition number of the R matrices can be large, especially if A has a large condition number. Instead of multiplying A from the right by many unstable upper triangular matrices to bring it to an orthogonal form, we multiply from the left by a sequence of orthogonal matrices to bring it into an upper triangular form. i.e.

$$Q_1 Q_2 \cdots Q_n A = R. \tag{5.10}$$

Q_i, $i = 1, \cdots n$ are the successive orthogonal matrices. Hence, it can be concluded that if we invert and successively multiply with stable orthogonal matrices, the rounding errors will not get amplified.

The matrix that rotates any vector in the plane counterclockwise by θ, is defined as [15]

$$\begin{pmatrix} \cos\theta & -\sin\theta \\ \sin\theta & \cos\theta \end{pmatrix}. \tag{5.11}$$

By appropriately choosing θ a given vector can be rotated into a vector whose second entry is zero:

$$\begin{pmatrix} \cos\theta & -\sin\theta \\ \sin\theta & \cos\theta \end{pmatrix} \begin{pmatrix} x \\ y \end{pmatrix} = \begin{pmatrix} \sqrt{x^2 + y^2} \\ 0 \end{pmatrix}. \tag{5.12}$$

The solutions for the trigonometric functions are:

$$\cos\theta = \frac{x}{\sqrt{x^2 + y^2}}, \quad \sin\theta = \frac{-y}{\sqrt{x^2 + y^2}}. \tag{5.13}$$

Therefore, it is not necessary to explicitly compute the angle θ. (5.13) can be used instead. The rotations in n Euclidean space, $\mathbf{R}^n$, that rotate counterclockwise by θ in a specified coordinate plane is given by the following $n \times n$ matrix :

$$R(i, j, \theta) = \begin{pmatrix} 1 & 0 & \cdots & & & & & 0 \\ 0 & 1 & & & & & & \vdots \\ \vdots & & \ddots & & & & & \\ & & & \cos\theta & & -\sin\theta & & \\ & & & & \ddots & & & \\ & & & \sin\theta & & \cos\theta & & \\ & & & & & & \ddots & \\ & & & & & & 1 & 0 \\ 0 & \cdots & & & & & 0 & 1 \end{pmatrix}, \tag{5.14}$$

where the trigonometric functions are in the i-th row and j-th column and all other entries outside the main diagonal is zero. These are the so called Givens (Jacobi) rotations. $R(i,j,\theta)$ is an orthogonal matrix.

In summary, by multiplying A by $R(i,j,\theta)$, the off-diagonal elements of a_{ji} are zero if the θ is chosen as follows:

$$\cos\theta = \frac{a_{ii}}{\sqrt{a_{ii}^2 + a_{ij}^2}}, \quad \sin\theta = \frac{-a_{ji}}{\sqrt{a_{ii}^2 + a_{ij}^2}}. \tag{5.15}$$

In this manner one can eliminate all off-diagonal nonzero elements by sequence of Givens rotations. However, the zero elements may become nonzero again as a result of further rotations. If done in the proper order, one can eliminate all nonzero elements below the main diagonal. The order used follows the same format as in Gaussian elimination [21]. This format is described as follows:

Given a matrix A, start with the first column. Take the first non-zero element below the diagonal in the first column. Let us say this entry is in the k^{th} row. This entry is eliminated by left multiplying by $R(1,k,\theta)$. Then the algorithm proceeds to the next non-zero element in the first column.

Once the first column has only zeros below the diagonal, the algorithm moves to the second column and starts to eliminate the entries below the diagonal with matrices $R(2,k,\theta)$, with $k \geq 3$.

The zeros below the first column are preserved after the multiplications on the second column. In general, $R(i,j,\theta)$ changes only the i-th row and j-th column. Finally, an upper triangular matrix results by any such multiplications from the left by the Givens matrices. This is written as

$$G_N G_{N-1} \cdots G_2 G_1 A = R. \tag{5.16}$$

The maximum number of Givens matrices is

$$N_{\max} = (n-1)(n-2)/2, \tag{5.17}$$

for an $n \times n$ square matrix A. We finally have

$$A = QR, \tag{5.18}$$

where

$$Q = G_1^T G_2^T \cdots G_N^T. \tag{5.19}$$

To illustrate the steps for the Givens rotation we provide an example in Appendix B. Having described the QR rotation algorithm, we will now use this algorithm to modify the single carrier receiver to a more robust receiver. The error signal defined in 3.23 in chapter 3 is used to recursively update the new filter output values. Through simulation results, we then compare the performance of the receiver based on this new algorithm to that of the RLS based algorithm.

5.5 Modified QRD-based receiver

5.5.1 QRD receiver

We will first describe how the QR algorithm is used to solve the least squares problem. The least-squares estimator chooses the weight vector so as to minimize the index performance $\|\mathbf{A}\hat{\mathbf{x}} - \mathbf{b}\|^2$. One way of providing a numerically stable solution is by using the method of orthogonal triangularization just described. The estimation error is given by

$$\varepsilon(n) = d(n) - \mathrm{U}(n)w(n), \tag{5.20}$$

where $d(n)$, $\mathrm{U}(n)$ and $w(n)$ are the desired response, received observations and weight vector, respectively. The index n, represents the data index. The index performance, χ, can be rewritten [15] as

$$\chi = \|\mathbf{Q}(n)\varepsilon(n)\|^2, \tag{5.21}$$

where $\mathbf{Q}(n)$ is the unitary matrix. From (5.21), we have

$$\mathbf{Q}(n)\varepsilon(n) = \mathbf{Q}(n)d(n) - \mathbf{Q}(n)\mathrm{U}(n)w(n). \tag{5.22}$$

Given that

$$\mathbf{Q}(n)\mathrm{U}(n)=\begin{bmatrix}\mathbf{R}(n)\\0\end{bmatrix}, \tag{5.23}$$

where $\mathbf{R}(n)$ is upper triangular, then

$$\mathbf{Q}(n)\mathrm{U}(n)w(n)=\begin{bmatrix}\mathbf{R}(n)w(n)\\0\end{bmatrix}. \tag{5.24}$$

Now if we define

$$\mathbf{p}(n)\triangleq\mathbf{Q}(n)d(n), \tag{5.25}$$

then we get

$$\mathbf{Q}(n)\varepsilon(n)=\mathbf{p}(n)-\mathbf{R}(n)w(n). \tag{5.26}$$

Hence in order to optimize χ in (5.21), we have the condition for the optimal weight $\hat{w}(n)$ of $w(n)$ in (5.26) as [15]

$$\hat{w}(n)=\mathbf{R}^{-1}(n)\mathbf{p}(n). \tag{5.27}$$

This is the QR solution to the least squares problem. In order to apply the algorithm to our receiver, we first recall that the least squares problem in chapter 3 is given by

$$\begin{pmatrix}\hat{\mathrm{X}}_1(2i)\\ \hat{\mathrm{X}}_2^*(2i)\end{pmatrix}=\underbrace{\begin{pmatrix}\mathrm{diag}(\mathrm{Y}(2i)) & \mathrm{diag}(\mathrm{Y}^*(2i+1))\\ -\mathrm{diag}(\mathrm{Y}(2i+1)) & \mathrm{diag}(\mathrm{Y}^*(2i))\end{pmatrix}}_{\text{Quadtronic structure}}\cdot\begin{pmatrix}\mathrm{E}_1\\ \mathrm{E}_2\end{pmatrix}\triangleq\mathrm{U}(i)\mathbf{E}, \tag{5.28}$$

where $\mathbf{E}\triangleq\begin{bmatrix}\mathrm{E}_1 & \mathrm{E}_2\end{bmatrix}^T$ is the effective channel coefficient vector after the DFT operation and $\mathrm{U}(i)$ is the received observation sequence. Once again we define the desired response as

$$D(2i+2)=\begin{cases}\begin{pmatrix}X_1(2i+2)\\ X_2^*(2i+2)\end{pmatrix}, \text{for training}\\ \begin{pmatrix}\tilde{X}_1(2i+2)\\ \tilde{X}_2^*(2i+2)\end{pmatrix}, \text{for direct-decision tracking}\end{cases} \tag{5.29}$$

The algorithm proceeds as following four steps:

1. The channel response vector, $\mathbf{E}$, is initialized to zero
2. Perform QR decomposition of the U received sequence matrix in (5.28). Hence we get

$$Q(2i+2)R(2i+2)=U(2i+2), \tag{5.30}$$

which is computed using the Givens rotation described in the previous section.

3. As in chapter 3, the error signal is defined as

$$\mathbf{P}(2i+2)=\left[D(2i+2)-U(2i+2)\mathbf{E}(2i)\right]. \tag{5.31}$$

4. Finally, the recursive update is given as

$$\mathbf{E}(2i+2)=\mathbf{E}(2i)+R(2i+2)^{-1}Q(2i+2)\mathbf{P}(2i+2). \tag{5.32}$$

The overall block diagram for the QRD based receiver is shown in Fig. 5.1. The only modification to the receiver block diagram found in chapter 3 is the addition of the QRD block. In the next subsection, the linear predictor is added to the QR-based receiver in order to shorten the pilot requirement for the system.

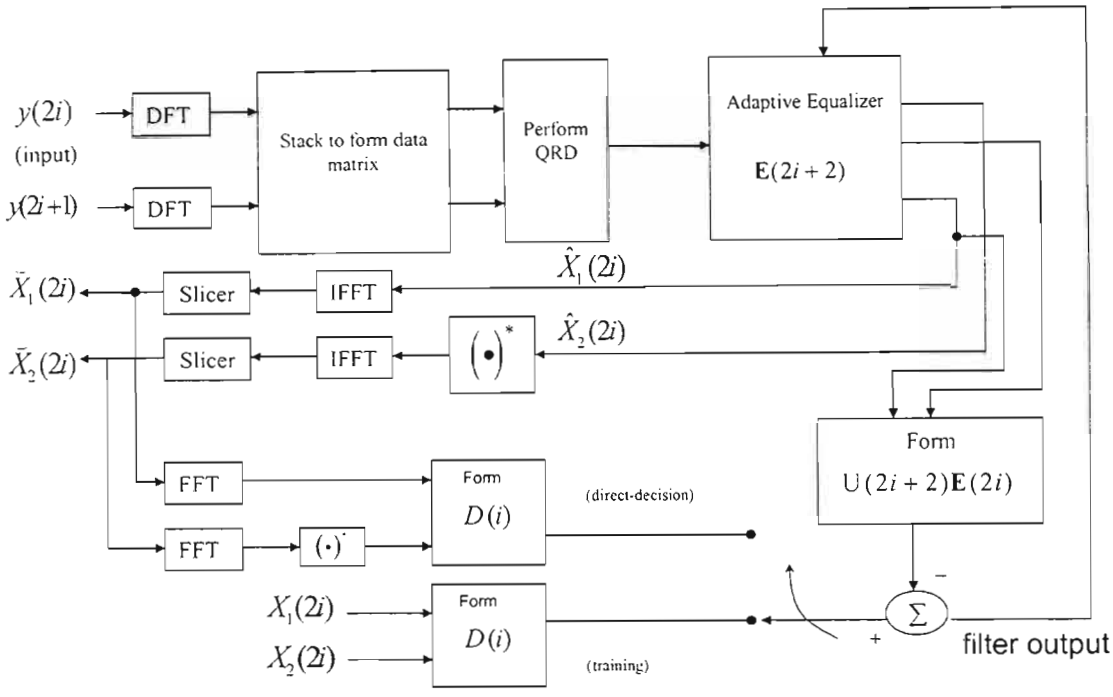

Fig. 5.1 Equivalent receiver model with the QRD

5.5.2 QRD receiver with LP

To incorporate the linear predictor, we pursue the exact same steps we described in section 4.4. Using (4.12)-(4.18), we estimate the initial values for the channel vector $\mathbf{E}$. The algorithm then switches to direct-decision mode and the values of $\mathbf{E}$ are then updated recursively using (5.30), (5.31) and (5.32).

This can be summarized as follows:

1. The shortened pilot stream is sent and using $\mathrm{H}=[\mathrm{H}_1 \quad \mathrm{H}_2]=\left(\mathrm{X}\cdot\mathrm{X}^H\right)^{-1}\cdot\left(\mathrm{X}^H\right)\cdot\mathrm{Y}$ the initial estimates of the channel taps are updated.
2. The linear predictor then estimates the channel coefficients for the next block using $\hat{h}_n \triangleq \frac{1}{\varepsilon_s}\sum_{n=0}^{M-1} c_n^* h_{n-1}$. Hence we update H_1 and H_2.
3. By solving Λ_0 in (4.11) and B_1 and B_2 (3.11), the vector channel vector, $\mathbf{E}$ in (3.13), is updated. The values of $\Omega(i)$ and $T(i)$ in (3.22) and (3.20), respectively, are then updated.
4. Proceed with steps 2-4 in section 5.5.1.

The overall block diagram for the QRD-based receiver with linear prediction (QRD-LP) is shown in Fig 5.2.

In non-stationary applications, conventional adaptive filters entail a trade off between the estimation errors (steady state analysis) and lag errors (tracking analysis). In effect, adaptive filters are designed to perform well in rapidly varying conditions, perform poorly when their environment is stationary and vice versa. The estimation error is a measure of how well the adaptive filter performs in a stationary environment, whereas the lag error measures the ability of the adaptive filter to respond to highly non-stationary environments. The total mean square error (MSE) is the sum of the above two parameters [23].

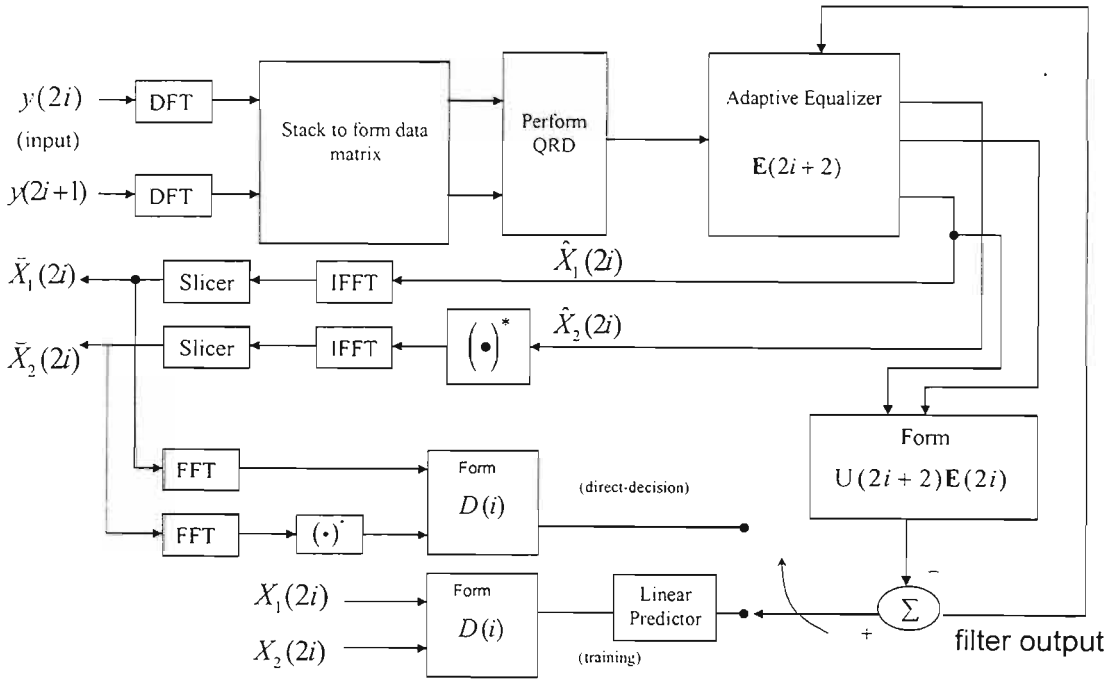

Fig. 5.2 Equivalent receiver model with the QRD and LP

In the next section, computer simulations are carried out to compare the performance of the QRD and RLS algorithms with respect to the tracking (non-stationary) and steady state (stationary) performance. We then verify through simulations that there is no significant performance loss when combining an QRD based receiver with the LP. Finally, we show results of the new QRD-LP receiver and compare this to the RLS receiver in [8]. These results summarize our achievements by showing how the new QRD-LP receiver outperforms the RLS receiver in terms of bandwidth efficiency and robustness at higher Doppler frequencies.

5.6 Simulation Results

The EDGE simulation environment that has been described throughout this dissertation is used once again. The main purpose of the simulation results is to investigate the following:

- Performance at high Doppler frequencies.
- Tracking and estimation error performance.
- Performance of the QR receiver with linear prediction.

5.6.1 Performance at High Doppler frequency

The main problem associated with the RLS algorithm is its lack of robustness particularly at high Doppler frequencies. To achieve better performance at higher Doppler frequencies, an adaptive QRD based receiver is derived in section 5.5.1.

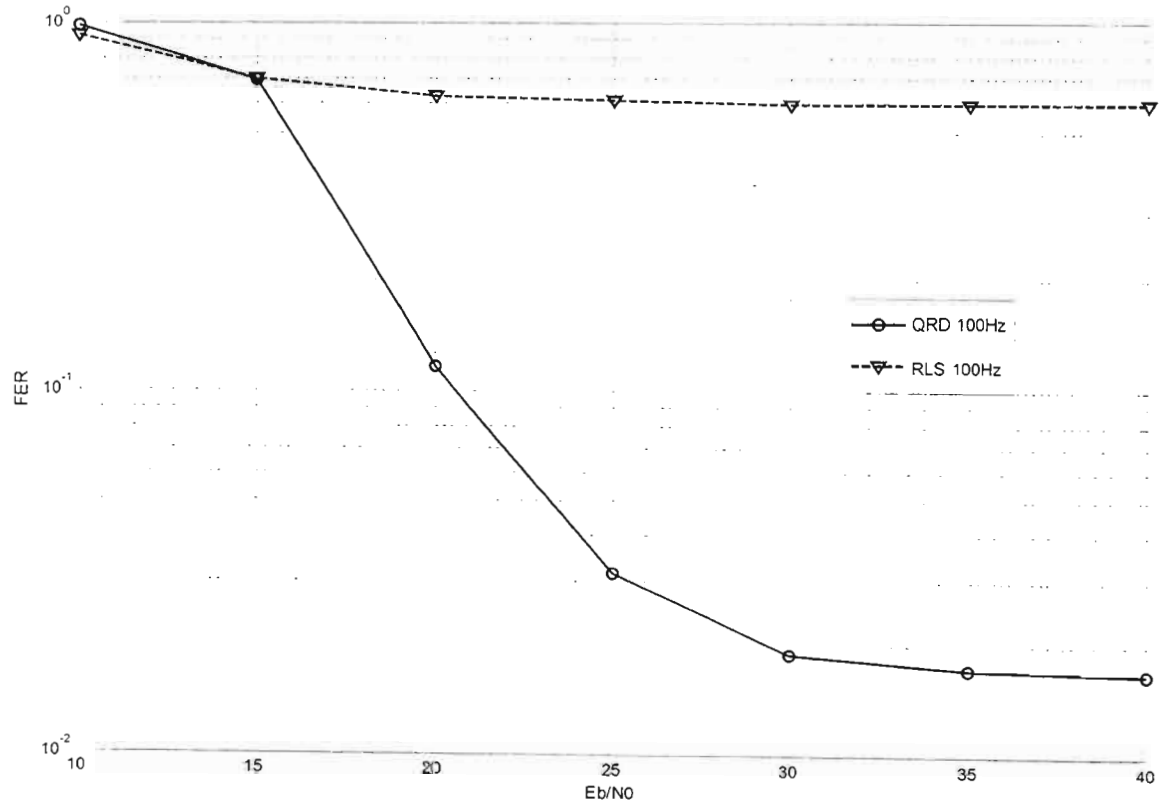

Fig. 5.3 Simulation results to verify the robust property of the QRD algorithm

Fig.5.3 shows the robust property of the new receiver as compared to the RLS based receiver. The Doppler frequency of 100 Hz is used. The block size and re-training interval is set to 96 blocks and 50 blocks, respectively.

Hence, by using the orthogonal transformation described in section 5.4, the extent to which the ill-conditioned problem affects the estimates is reduced and hence the overall performance at high user mobility is improved.

5.6.2 Tracking and Estimation Error Performance

The theoretical lag and estimation error expressions for the weighted RLS algorithm are shown in [23]. An approach similar to that shown in [25] can be used to derive the tracking expressions for the QR based receiver to prove theoretically that the QR algorithm has better tracking performance. However, this is not pursued in this dissertation. The purpose of the next set of results is to compare the tracking error and estimation error performance as the Doppler frequency is varied.

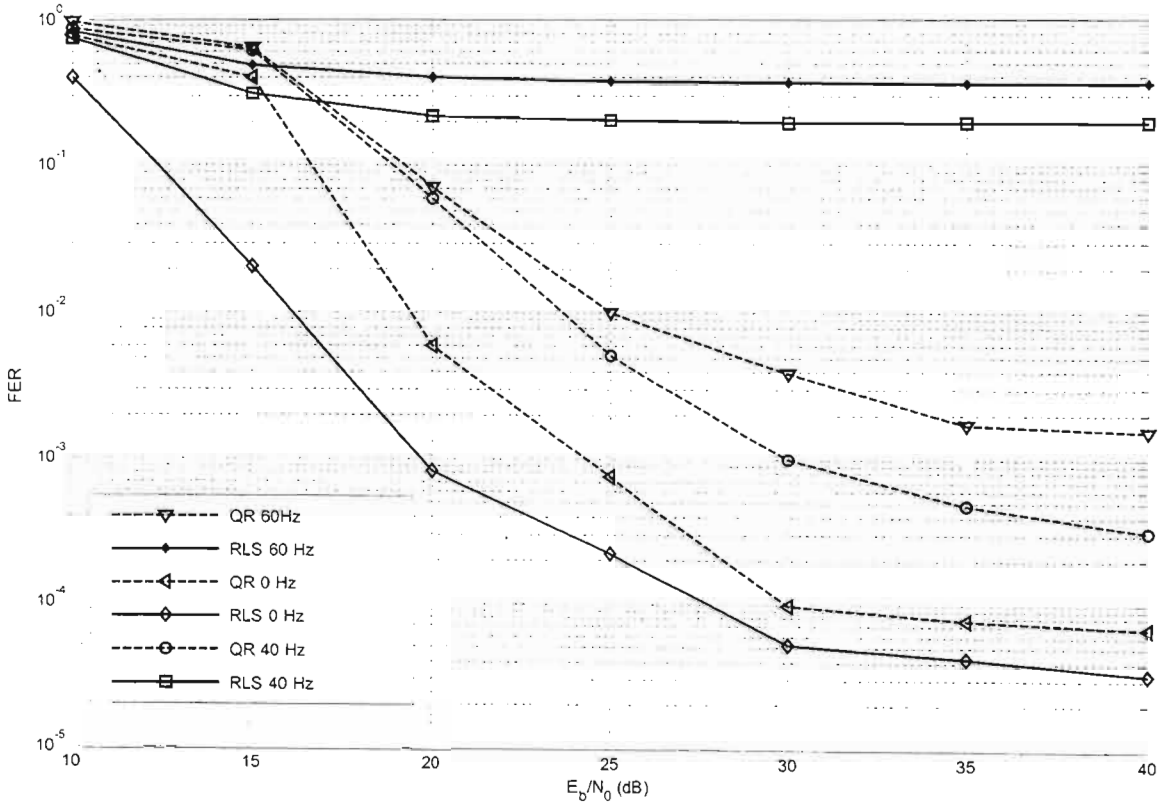

Fig. 5.4 Simulation results of the QRD and RLS algorithms for different Doppler frequencies

Fig. 5.4 shows the results at Doppler frequencies of 60 Hz, 40Hz and 0 Hz. We choose 60 Hz and 40 Hz to compare the tracking performance of the two algorithms at lower frequencies. The result at 0 Hz is used to compare the estimation error performance of the two algorithms. The block size and re-training interval is set to 96 bits and 50 blocks, respectively.

The QRD based receiver provides a more robust solution as shown in the results for the Doppler frequencies of 60 Hz and 40 Hz. The results imply that the QR based solution has a better lag error or tracking performance than the RLS based receiver. The results at 0 Hz for both algorithms also show that the estimation error or steady state performance of the RLS algorithm is better than that of the QR based algorithm.

The RLS algorithm provides a better steady state performance. Since there are no transformations involved in this algorithm, the estimate error for the RLS algorithm in a stationary environment is more accurate than the QRD based approach. This is shown in Fig 5.4 for the Doppler frequency of 0 Hz where the RLS algorithm outperforms the QRD based receiver.

In order to further improve the performance of the receiver, the linear predictor is combined with the QR based algorithm. The performance improvement can be achieved in two ways, namely the bandwidth efficiency and the FER performance as mentioned in section 4.3.

The next sub-section presents the simulation results that show these two performance improvements.

5.6.3 Performance of the QRD-LP

For the first set of simulations, the block size is set to 96 bits. The Doppler frequency of 60 Hz is used. The re-training interval is set to 50 blocks. The channel model and signal constellation is the same as before. The result in Fig. 5.5 shows that the addition of LP does not affect or hamper the performance to a significant extent. This emphasizes that the LP is an attractive method to shorten the preamble system requirements.

In order to verify this, we compare the QR receiver with fixed pilot symbols, and the QR-LP receiver with equivalent number of fixed pilot symbols.

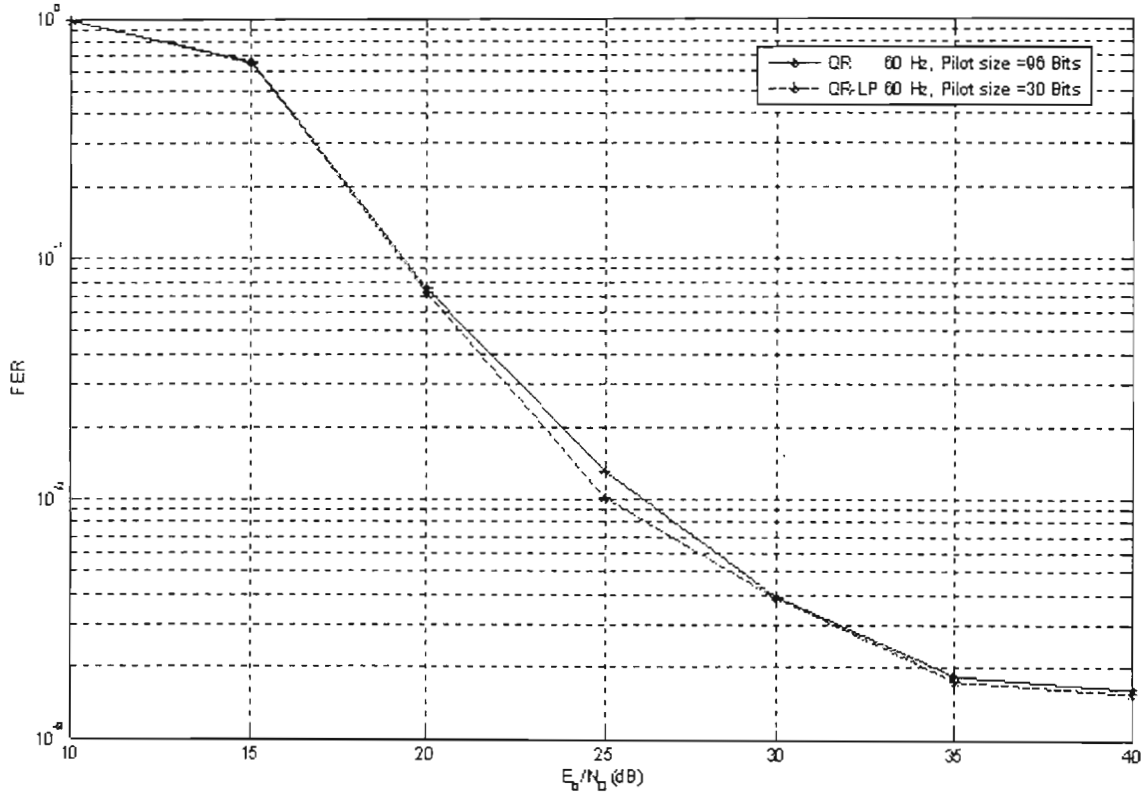

Fig. 5.5 Comparison of QRD and QRD with LP at 60 Hz

For the second set of computer simulations, the block size and Doppler frequency is set to 120 bits and 60 Hz, respectively. The re-training interval is set to 40 blocks for the RLS and QR algorithms. The window size for the linear predictor is set to 40 bits and hence the equivalent re-training interval for the QR-LP is set to 10 blocks.

As opposed to its RLS predecessor, the new QR based receiver provides a more robust solution at higher frequencies. Combining the linear predictor with the QRD based receiver results in decreasing the preamble requirements. This in-turn allows the system re-training interval to be decreased, hence increasing the overall receiver performance as shown in Fig.5.6. Hence the results show a superior performance improvement for the new QRD-LP receiver when compared to its RLS counterpart.

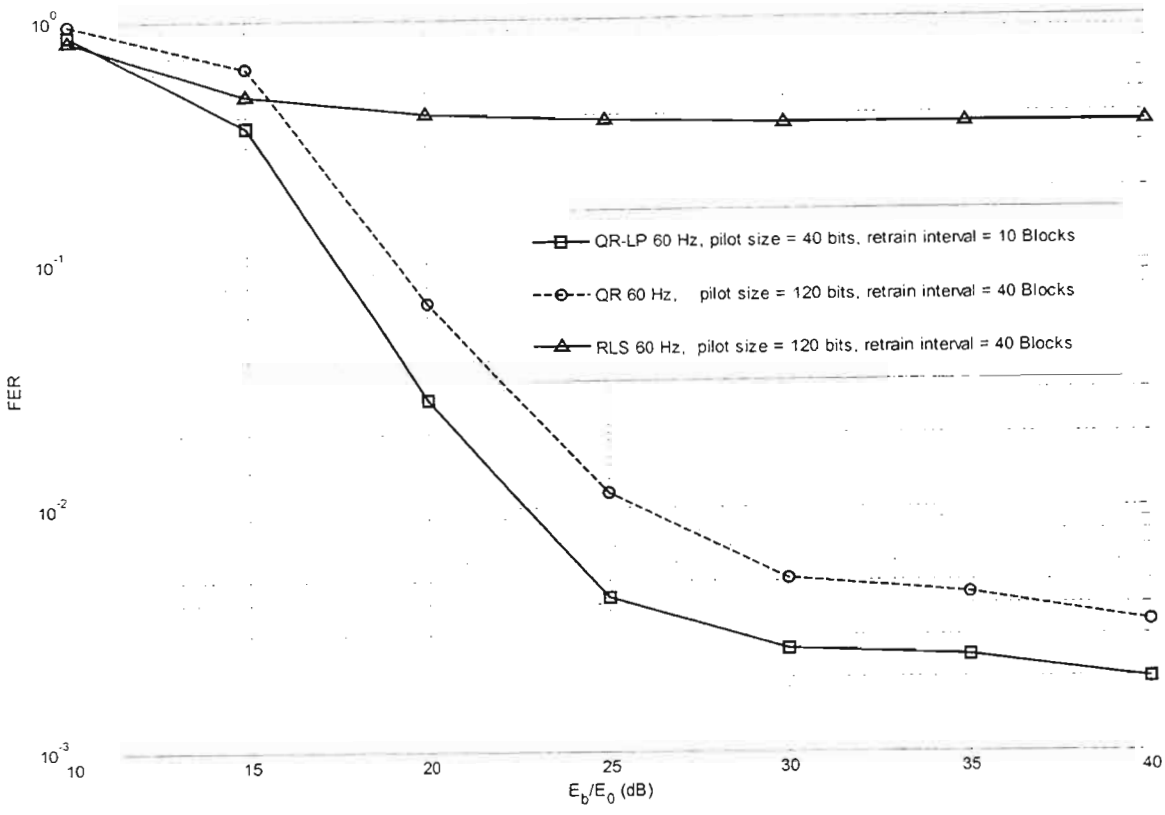

Fig. 5.6 Overall modified QRD-LP receiver versus RLS receiver

5.7 Concluding Remarks

The emphasis of this chapter is to provide a more robust alternative algorithm for the adaptive receiver in [8] to perform joint interference and equalization at high Doppler frequencies. This is achieved by using a new algorithm based on QR orthogonal transformation.

The second part of this chapter combines the QRD based receiver with the linear predictor derived in chapter 4 to increase the overall system performance by decreasing the re-training interval of the adaptive algorithm. This results in a receiver that offers stable performance at high frequencies and better overall performance as opposed to its RLS counterpart.

While the RLS based receiver provides an approach that does not require CSI estimation and hence reduces system overhead, the new QRD-LP based receiver provides a more robust solution while further decreasing the overhead requirements.

CHAPTER 6

CONCLUSION

6.1 Concluding Remarks

This dissertation focuses on the single carrier frequency domain (SC-FD) transmission schemes that exploit the space time block code (STBC) structure to provide computationally cost efficient receivers in terms of equalization and channel estimation. This scheme provides a coded transmit antenna diversity to improve the performance and capacity of single and multiple users in a wireless communications system without sacrificing system power or bandwidth. As shown in [38], [37] and [13], SC-FD STBC can be combined with DS-CDMA to provide a powerful downlink scheme that enables maximum antenna and spatial diversity.

Antenna diversity can improve system reliability without added system power or bandwidth requirements. The use of such diversity is particularly useful in downlink for cellular systems where receive diversity is not effective.

In chapter 1, under literature survey, the importance of CDMA, which is employed in the current 3G standard, is mentioned. The main problems highlighted for the current CDMA standard includes multi-user interference (MUI), fading and multi-path propagation. This motivates the extension of the original SC-FC to the multi-user environment in order to investigate the MUI effects for this scheme. Furthermore, the problem of time and frequency selective fading is further aggravated in high mobility and high data rate users. Hence an adaptive receiver that is able to track such variations without sacrificing the complexity, bandwidth and power requirements is clearly desired.

In Chapter 2, we have derived the single carrier block transmission for a multiple access channel. In section 2.7, it was proven that the multi-user system does not incur any performance loss in terms of diversity and SNR. The simulation results provided shows that this is also valid for a sub-optimal algorithm such as the MMSE. Hence, we prove

that the SC-FD STBC is suitable for extension to the multi-user system. This is an important result because such an extension improves the data rate for the overall system.

Chapter 3 describes the adaptive receiver for STBC transmission. This is done for the single user case. This receiver does not require channel state information (CSI). By using the system with perfect CSI as a bench mark, a method of optimizing various parameters such as block size, re-training frequency and forgetting factor is described. Therefore, depending on the channel variations present and performance required, values for these parameters can be designed using this method. Such a method is not provided in [8]. Furthermore, the effect of varying the forgetting factor is given in the simulation results.

From the simulation results, two main problems associated with the RLS algorithm are identified, namely:

- The excess bandwidth requirement during the training period.
- The poor robust property of the RLS algorithm at higher Doppler frequencies.

Therefore, in chapter 4, we described a bandwidth efficient method of improving the overall system performance for the adaptive RLS receiver. The linear predictor decreases the number of pilot symbols that are required during the re-training period. Hence, the re-training interval can be decreased which results in the improved performance. The simulation results verify that there is no additional penalty when using the linear predictor making it an attractive scheme. The only requirement at the receiver is that the knowledge of the autocorrelation function for the channel is available.

The emphasis of chapter 5 was to provide a more robust alternative algorithm for the adaptive receiver to perform joint interference and equalization at high Doppler frequencies. From the results obtained through computer simulations, the new QR based algorithm is more robust than the RLS algorithm. This is particularly evident in the results at high frequencies such as 100 Hz. The second part of chapter 5 involves combining the QR receiver with the linear predictor to provide a overall bandwidth efficient receiver. The simulation results verify that there is no performance loss

suffered through this modification. Hence a new bandwidth efficient and more robust receiver to the RLS receiver is proposed in this dissertation. Although the Givens rotation described in chapter 5 has a complexity of order $O(m^2)$, the so called fast QR algorithms of order $O(m)$ have been proposed in [22]. Furthermore in order to cater for high-speed real-time applications, pipelined and parallel algorithms for QR decomposition are necessary. Coordinate rotation digital computation (CORDIC) rotations provide a method for pipeline implementation without the requirement of computing trigonometric functions or square roots [16].

The linear prediction (LP) method described in this dissertation can be added to any system that requires overhead. Provided that the autocorrelation function for the channel model is known, the system overhead can be reduced. This is proven in chapters 4 and 5, when we combined the LP with the RLS and QR algorithms, respectively and the simulation results show that there is no performance loss in both cases.

6.2 Future work

The focus of this dissertation has primarily been on providing low complexity and bandwidth efficient receivers. In particular, the channel estimation problem is tackled using semi-blind approach to avoid to high complexity of the blind channel estimation approaches while still limiting the pre-amble requirements as apposed to the training-based approaches. Another alternative is to use a time-domain differential space-time transmit-diversity scheme that guarantees blind channel identifiably from second-order statistics [44]. Such non-coherent schemes are becoming attractive alternatives in-order to prevent the increased cost of channel estimation and degradation of tracking quality. The channel identification problem can be solved using standard factorization procedures.

The two algorithms described in this dissertation are the RLS algorithm and the QR-based algorithm. Two areas that need further work are as follows:

- In a practical sense, fixing the forgetting factor for the RLS algorithm does not cater for the variable channel conditions. A variable forgetting factor algorithm [20,23] that caters for the non-stationary effects is a more realistic approach.

Hence the performance of the RLS algorithm with variable Doppler frequencies using such an algorithm is an interesting topic.

- In order to quantify the performance of an adaptive algorithm, steady-state and tracking analysis of the algorithm must be presented [25]. We have compared the performance of the two algorithms using computer simulations in chapter 5. By using the analysis of the RLS algorithm in [23], and by using the approach presented in [25] to derive the analyses for the QR algorithm, the performance of the two algorithms can be compared. This would further justify the results obtained in the simulation results in chapter 5.

The linear predictor is proven to be an efficient method of decreasing the pilot requirements during the training period. It is shown that the widow size for this algorithm is dependant on the length of the channel. If the channel length can be estimated, such the system shown in [23], then the algorithm can be modified to adjust the window size of the linear predictor accordingly.

Lastly, the core of this dissertation has been focused on the use of multiple antennas in order to provide diversity and hence increase the overall capacity of the communications link. However, many wireless applications are limited by the size available and hence the provision of multiple antennas in such devices may not be possible. Recently [48], a new class of methods, know as cooperation communications, enable single antenna mobile units in a multi-user environment to share their antennas and hence produce a virtual multi-antenna system. Hence in this way the transmit diversity can be achieved. The treatment of joint equalization and interference suppression techniques in such a scheme has not been discussed and this could be an interesting topic to pursue.

APPENDIX A

CIRCULANT MATRICES PROPERTIES

(Adapted from [5])

P.1 Circulant matrices can be diagonalized by the FFT operation.

$$\begin{aligned}\tilde{\mathbf{H}}_{\mu} &= \mathbf{F}_J^H D(\tilde{h}_{\mu})\mathbf{F}_J \\ \tilde{\mathbf{H}}_{\mu}^H &= \mathbf{F}_J^H D(\tilde{h}_{\mu}^*)\mathbf{F}_J\end{aligned} \tag{A.1}$$

P.2 Pre- and post multiplying $\tilde{\mathbf{H}}_{\mu}$ by $\mathbf{P}$ yields $\tilde{\mathbf{H}}_{\mu}^T$.

$$\begin{aligned}\mathbf{P}\tilde{\mathbf{H}}_{\mu}\mathbf{P} &= \tilde{\mathbf{H}}_{\mu}^T \\ \mathbf{P}\tilde{\mathbf{H}}_{\mu}^*\mathbf{P} &= \tilde{\mathbf{H}}_{\mu}^H\end{aligned} \tag{A.2}$$

P.3 Given the following matrix containing the diagonized channel matrices as defined in **P.1**

$$\begin{aligned}\mathbf{D} &\triangleq \begin{bmatrix} D_1 & D_2 \\ D_2^* & -D_1^* \end{bmatrix} \\ \bar{\mathbf{D}}_{12} &\triangleq \left[D_1^* D_1 + D_2^* D_2 \right]^{1/2}\end{aligned} \tag{A.3}$$

it can be verified that $D^H D = I_2 \otimes \bar{\mathbf{D}}_{12}^2$. The symbol $\otimes$ stands for Kronecker product. Defining the unitary operator $U \triangleq D\left[I_2 \otimes (\bar{\mathbf{D}}_{12})^{-1} \right]$, independent on whether $\bar{\mathbf{D}}_{12}$ is invertible, the unitary operator can be constructed to satisfy the following two conditions.

$$\begin{aligned}U^H U &= \mathbf{I}_{2R} \\ U^H D &= \mathbf{I}_2 \otimes \bar{\mathbf{D}}_{12}\end{aligned} \tag{A.4}$$

APPENDIX B

AN EXAMPLE OF THE GIVENS ROTATION

(Adapted from [21])

We show the steps for a 4×3 general matrix i.e.

$$A=\begin{pmatrix} * & * & * \\ \underline{*} & * & * \\ * & * & * \\ * & * & * \end{pmatrix}. \tag{B.1}$$

Let us define $s \triangleq \sin e$ and $c \triangleq \cos ine$. Assuming that the first non-zero entries in the first column is the underlined element, we can define the Givens matrix $R(1,2,\theta)$ as:

$$G_1=\begin{pmatrix} c & -s & & \\ s & c & & \\ & & 1 & \\ & & & 1 \end{pmatrix}, \tag{B.2}$$

where

$$c=\frac{a_{11}}{\sqrt{a_{11}^2+a_{21}^2}} \quad s=\frac{-a_{21}}{\sqrt{a_{11}^2+a_{21}^2}} \tag{B.3}$$

Hence we get

$$A_1=G_1A=\begin{pmatrix} c & -s & & \\ s & c & & \\ & & 1 & \\ & & & 1 \end{pmatrix}\begin{pmatrix} * & * & * \\ \underline{*} & * & * \\ * & * & * \\ * & * & * \end{pmatrix}=\begin{pmatrix} * & * & * \\ 0 & * & * \\ \underline{*} & * & * \\ * & * & * \end{pmatrix} \tag{B.4}$$

Next, we eliminate the next underlined element in A_1 using a new rotation matrix $G_2=R(1,3,\theta')$:

$$A_2=G_2A_1=\begin{pmatrix} c' & & -s' & \\ & 1 & & \\ s' & & c' & \\ & & & 1 \end{pmatrix}\begin{pmatrix} * & * & * \\ 0 & * & * \\ * & * & * \\ * & * & * \end{pmatrix}=\begin{pmatrix} * & * & * \\ 0 & * & * \\ 0 & * & * \\ \underline{*} & * & * \end{pmatrix} \tag{B.5}$$

Finally, by defining $G_3 = R(1,4,\theta'')$, the last entry is eliminated as follows:

$$A_3 = G_3 A_2 = \begin{pmatrix} c'' & & & -s'' \\ & 1 & & \\ & & 1 & \\ s'' & & & c'' \end{pmatrix} \begin{pmatrix} * & * & * \\ 0 & * & * \\ 0 & * & * \\ * & * & * \end{pmatrix} = \begin{pmatrix} * & * & * \\ 0 & * & * \\ 0 & \pm & * \\ 0 & * & * \end{pmatrix} \tag{B.6}$$

We continue with the second column. Defining $G_4 = R(2,3,\tilde{\theta})$

$$A_4 = G_4 A_3 = \begin{pmatrix} 1 & & & \\ & \tilde{c} & -\tilde{s} & \\ & \tilde{s} & \tilde{c} & \\ & & & 1 \end{pmatrix} \begin{pmatrix} * & * & * \\ 0 & * & * \\ 0 & \pm & * \\ 0 & * & * \end{pmatrix} = \begin{pmatrix} * & * & * \\ 0 & * & * \\ 0 & 0 & * \\ 0 & \pm & * \end{pmatrix} \tag{B.8}$$

Finally we eliminate the last nonzero element under the diagonal in A_4 by defining the matrix $G_5 = R(2,4,\hat{\theta})$. We get

$$A_5 = G_5 A_4 = \begin{pmatrix} 1 & & & \\ & \hat{c} & & -\hat{s} \\ & & 1 & \\ & \hat{s} & & \hat{c} \end{pmatrix} \begin{pmatrix} * & * & * \\ 0 & * & * \\ 0 & 0 & * \\ 0 & \pm & * \end{pmatrix} = \begin{pmatrix} * & * & * \\ 0 & * & * \\ 0 & 0 & * \\ 0 & 0 & * \end{pmatrix} \tag{B.9}$$

where the last matrix is the upper triangular R matrix.

Finally, we have $G_5 G_4 G_3 G_2 G_1 A = R$, hence $A = QR$ with

$$Q = G_1^T G_2^T G_3^T G_4^T G_5^T \tag{B.10}$$

REFERENCES

[1] S.M. Alamouti, "A simple transmit diversity technique for wireless communications," *IEEE Journal on Selected Areas in Communications*, vol. 16, no. 8, pp.744-765, 1998.

[2] V. Tarokh, N. Seshadri, and A.R. Calderbank, "Space-time codes for high data rate wireless communication: performance criterion and code construction," *IEEE Transactions on Information Theory*, vol. 44, no. 2, pp. 744-765, 1998.

[3] Lindskog E. and A. Paulraj, "A transmit diversity scheme for channels with inter-symbol interference," *in Proceedings Globecom*, vol. 1, pp. 307-311, New Orleans, La, USA, June 2000.

[4] S. Zhou and G.B Giannakis, "Space-time coding with maximum diversity gains over frequency-selective fading channels," *IEEE Signal Processing Letters*, vol. 8, no. 10, pp. 269-272, 2001.

[5] S. Zhou and G.B Giannakis, "Single-carrier space-time block coded transmissions over frequency-selective fading channels," *IEEE Transactions on Information Theory*, vol. 49, no.1, pp. 164-179, 2003.

[6] S.N. Diggavi, N.Al-Dhadhir, "Algebraic Properties of space-time block codes in intersymbol interference multiple-access channels," *IEEE Transactions on Information Theory*, vol. 49, no. 10, pp.2403-2411, 2003.

[7] N.Al-Dhadhir, "Single-carrier frequency domain equalization for space time block coded transmission over frequency selective fading channels," *IEEE Communication Letters*, vol. 5, pp. 304-306, July 2001.

[8] Waleed M. Younis et al, "Efficient adaptive receivers for joint equalization and interference cancellation in multi-user space-time block-coded systems", *IEEE Trans. Signal Processing*, vol. 51, no.11. pp 2849-2861, 2003.

[9] Waleed M. Younis "Efficient receivers for space time block coded transmission over broadband channels", PhD Thesis, UCLA, USA, 2004.

[10] Larsson, E. and Stoica, P. "Space time block coding for wireless communications" University Press, Cambridge, 2003.

[11] H.H. Zheng and L. Tong "Blind channel estimation using second order statistics: algorithms" *IEEE Trans. Signal Processing*, vol. 45, no.8. pp 1919-1930, 1997.

[12] S. Perreau and L. Tong "Multichannel blind identification: from subspace to maximum likelihood methods" *Proceedings of the IEEE*, vol.86, no.10, pp 1951-1967, 1998.

[13] G. Leus, F. Petre and Marc Moonen "Space-time chip equalization for maximum diversity space-time block coded DS-CDMA downlink transmission" *EURASIP Journ. on Applied Signal Processing*, pp 740-750, 2004 .

[14] Wang, X. and Poor, H.V. "Wireless communications systems" Prentice Hall, 2004.

[15] Haykin, S, "Adaptive filter theory", Prentice Hall, 1986.

[16] Moon, T.K and Stirling, W.C. "Mathematical methods and algorithms" Prentice Hall, 2000.

[17] N.Al-Dhadhir, "Overview and comparision of equalization schemes for space-time-coded signals with application to EDGE", *IEEE Trans. Signal Processing*, vol. 50, no.10. pp. 2477-2488, 2002.

[18] William C. Jakes "Microwave mobile communications" Wiley, NY,1974..

[19] Ian. D. Marsland "Iterative noncoherent detection of differentially encoded M-PSK", PhD Thesis, University of British Colombia , Canada, 1999.

[20] W. Zhuang, "RLS algorithm with variable forgetting factor for equalizing time-variant fading channels", Proc. 18th B. Symp. Commun., pp. 231-234, Kingston, June 2-5, 1996.

[21] Erwin Kreyszig, "Advanced engineering mathematics" Seventh Edition, John Wiley & Sons, 1993.

[22] J. A. Apolinario Jr., Paulo S.R. Diniz, "A new fast QR algorithm based in apriori errors", *IEEE Signal Processing Letters*, vol. 4, no. 11, 1997.

[23] S. D. Peters and Andreas Antoniou, "A parallel adaptation algorithm for recursive-least-squares adaptive filters in nonstationary environments", *IEEE Trans. Signal Processing*, vol. 43, no.11. pp 2484-2495, 1995.

[24] Ali Sayed. Fundamentals of Adaptive filtering, Wiley, NY, 2003.

[25] Nabil R. Yosef and Ali H. Sayed, "Nabil R. Yosef and Ali H. Sayed, "A unified approach to steady state and tracking analysis ", *IEEE Signal Processing Letters*, vol.49, no.2, pp.314-324, Feb 2001.

[26] D. J. Young et al, "A quantitative evaluation of generation methods for correlated rayeigh random variates" *in Proceedings Globecom* 1998, vol. 6.

[27] E. Eweda, Comparison of RLS, LMS, and sign algorithms for tracking randomly time-varying channels, *IEEE Trans. Signal Process.*, vol.42, no. 11, pp. 2937-2944, November 1994.

[28] S. Haykin, A. H. Sayed, J. Zeidler, P. Wei, and P. Yee, "Adaptive tracking of linear time-variant systems by extended RLS algorithms," *IEEE Transactions on Signal Processing*, vol. 45, no. 5, pp. 1118-1128, May 1997.

[29] Roland Badeeau et al, "Sliding window adaptive SVD algorithms," *IEEE Transactions on Signal Processing*, vol. 52, no. 1, pp. 1-10, January 2004.

[30] P. A. Regalia and M. G. Bellanger, "On the duality between fast QR methods and lattice methods in least squares adaptive filtering," *IEEE Transactions on Signal Processing*, vol. 39, pp. 879-891, April 1991.

[31] M.D. Miranda and M. Gerken, "A hybrid QR-lattice least squares algorithm using a priori errors," *in Proceedings of the 38 Midwest Symposium on Circuits and Systems*, pp. 982-986, Rio de Janerio, RJ, Brazil, August, 1995.

[32] S. Verdu. "Multi-user detection", Cambridge press, 1998.

[33] Shengli Zhou, "Multiple access over time and frequency selective channels", Phd Thesis, Unversity Minnesota, USA, 2003.

[34] M. K Varansi and B. Aazhang, "Multi-user detection in asynchronous code-division multiple access communications", *IEEE Trans in Comm.* , vol. 38, no. 4, pp. 509-519, April 1990.

[35] A. Duel-Hallen, "Decorrelating decision feedback multi-user detection for synchronous code division multiple access channel", *IEEE Trans. in Comm.*, vol. 41, no. 2, pp 285-290, Feb 1993.

[36] U. Mitra and H.V Poor, " Adaptive receiver algorithms of near far resistant CDMA", *IEEE Trans. on Comm.*, vol. 43, no. 2, pp. 1713-1724, April 1995.

[37] G. Leus, F. Petre L. Deneire and Marc Moonen "Downlink frequency-chip equalization for single carrier block transmission DS-CDMA with known symbol padding", *in Proc. Of Global Telecommunications Conference*, 2002.

[38] G. Leus, F. Petre L. Deneire and Marc Moonen "Downlink frequency-chip equalization for space time block coded single carrier block transmission DS-CDMA", in Proc. Of Global Telecommunications Conference, 2002.

[39] L. Tong and S. Perreau, "Multichannel blind identification: from subspace to maximum likelihood methods," *Proceedings of the IEEE*, vol. 86, no. 10, Oct 1998.

[40] H. Holma and A. Toskala, "WCDMA for UMTS: Radio Access for third generation mobile communications, John Wiley & Sons, NY, USA, 2001.

[41] Z. Ding and Z. Mao, "Knowledge based identification of fractionally sampled channels", in *Proc. of ICASSP '95*, Detroit, U.S.A, pp. 1996-1999, May 1995.

[42] M. Torlak and G. Xu, "Blind multiuser channel estimation on asynchronous CDMA systems", *IEEE Trans. Signal Processing*, vol. 45, pp. 137-147, Jan. 1997.

[43] L. Tong, G. Xu and T. Kailath, "Blind identification and equalization based on second order statistics: a time domain approach", *IEEE Trans. Inform. Theory*, vol. 40, pp. 340-349, Mar. 1994.

[44] S.N Diggavi et al, "Differential Space-time coding for frequency-selective channels", *IEEE Trans. Signal Processing*, vol. 6, no.6, pp.253-255, June 2002.

[45] Claude Berrou and Alain Glavieux, "Near optimum error correcting coding and decoding: turbo-codes", *IEEE Trans. on Comms.*, vol.44, no. 10, Oct 1996.

[46] Tapan K. Sarkar, Michael C. Wicks, Magdalena Salazar-Palma, Robert J. Bonneau, "Smart antennas", May 2003, Wiley-IEEE Press.

[47] G. J. Foshini, "Layered space time architecture for wireless communications in a fading environment when using multiple antennas," *Bell Labs Technical Journal*, vol. 1, no.2, pp. 41-59, 1996.

[48] Aria Nosratinia et al, "Cooperative communications in wireless networks", *IEEE Communications Magazine,* pp. 74-80, Oct 2004.